

EFFECTS OF POLARIZATION IN A DISTRIBUTED RAMAN FIBRE AMPLIFIER

By

Kennedy Mwaura Muguro

Submitted in fulfilment of the requirements for the degree of

PHILOSOPHIAE DOCTOR

in the Faculty of Science at the
Nelson Mandela Metropolitan University

December 2011

Promoter: **Prof A. W. R. Leitch**

The bursary assistance of the NMMU research office and the African Laser Centre (ALC) toward this research is hereby acknowledged. Opinions expressed and conclusions arrived at are those of the author and not attributed to any persons or organisation.

DECLARATION

I, KENNEDY MWAURA MUGURO

Student Number: S208028818

hereby declare that the treatise/dissertation/thesis for PHILOSOPHIAE DOCTOR is my own work and that it has not previously been submitted for assessment or completion of any postgraduate to another University or for another qualification.

Signature: _____

Date: _____

Unto Him who is able to do
exceeding abundantly above all that we ask or think
be the glory.

Acknowledgement

First I would like to appreciate the people and organisations whose contribution and involvement made this work a success and hitch free. In this regard I particularly thank my promoter professor A.W.R Leitch for his great contribution to this work and for giving me an opportunity to learn under him, and acquire skills in this field, thereby moulding my future in a very special way. I thank Dr Lorinda Wu for introducing me into the field of optical fibre and for her wise management of the optical fibre laboratory. I appreciate Dr T. B Gibbon for assistance in the laboratory, many encouragements and discussions that generated new ideas and perceptions toward this work. I specially acknowledge Dr D. W. Waswa for being resourceful and helpful in a profound way during these studies. I extend my appreciation to R. Gamatham for willingly assisting me to familiarize with the optical fibre measurement equipment in my first days. Special thanks to Mrs Alta Beer for coordinating and efficiently executing every administrative task in regard to the smooth running of this program. I thank all friends and members of Nelson Mandela Metropolitan University (NMMU) physics department. I also appreciate the Telkom South Africa staff at Sidwell, Port Elizabeth for their kindness and allowing us to use the Telkom facilities for the field measurements. I specially am grateful to the Telkom Centre of Excellence at Nelson Mandela Metropolitan University, for creating an enabling environment for this project. I thank all our supporters who include Telkom S.A. Ltd, Ingoma Communications Services (Pty) Ltd, Hezeki Contracting (Pty) Ltd, Dartcom1 (Pty) Ltd and THRIP, well as the NRF, NLC and the ALC.

Finally I convey gratitude to all the members of our family for the moral support they have accorded to me during this period. Particularly I appreciate great encouragements and prayers from my Dad. Many thanks to my dear wife Anne and our children Faith and Favour, for being very supportive, focus and patient all along.

Table of Contents

Abstract.....	vi
Abbreviation	vii
Chapter One.....	1
Chapter Two.....	6
2.0 Introduction	6
2.1 Polarization states of light representation	6
2.1.1 Degenerate polarization states.....	8
2.1.2 Poincaré sphere	8
2.1.3 Stokes polarization parameters	9
2.1.4 Mueller and Jones matrix.....	10
2.2 Polarization mode dispersion	11
2.2.1 Birefringence.....	11
2.2.2 Polarization mode coupling	13
2.3 PSP and PMD bandwidth	13
2.4 Power dependent birefringence	14
2.5 Polarization dependent loss.....	15
2.5.1 Definition and effects of PDL	15
2.6 Cascaded PDL and PDL evolution.....	16
2.7 PDL in the presence of PMD	17
2.8 Statistics of PDL.....	18
Chapter Three	19
3.0 Introduction	19
3.1 Origin of Raman scattering	19
3.1.2 Stimulated Raman scattering.....	20
3.1.3 Raman Gain spectrum in optical fibres.....	21
3.4 Characteristics of Raman fibre amplifier	21
3.5 Pumping techniques	22
3.6 Polarized Raman fibre amplifier	23
3.6.1 Average Raman gain	24
3.6.2 Raman PDG and on-off gain.....	25
3.7 Amplified spontaneous Emission noise	25
3.7.1 OSNR and bit error ratio	27

Chapter Four	28
4.1 Introduction	28
4.2 Experimental and simulation setup	29
4.3 Raman gain and pump power	30
4.3.1 Raman gain dependence on fibre length.....	31
4.3.2 Gain and input signal power	32
4.3.3 Raman gain and concatenated fibres	34
4.3.4 Gain variation with wavelength.....	35
4.4 Influence of signal input states of polarization on Raman amplification gain in single mode fibres.....	37
4.4.1 Low PMD fibre.....	37
4.4.2 High PMD fibre.....	38
4.4.3 Effect of fibre length on SOPs dependent gain.....	39
4.4.4 Gain variation with arbitrary SOPs.....	41
4.5 PMD effects and optical noise	42
4.5.1 Impact of ASE noise on system performance	43
4.5.2 Effects of ASE noise on the eye diagram.....	45
Chapter Five	48
5.1 Introduction	48
5.2 Statistics of net gain	49
5.3 Experimental setup	52
5.4 Effects of polarization scrambling technique	53
5.5 Raman on-off gain distribution	55
5.5.1 Short fibre length	55
5.5.2 Standard length fibre	56
5.5.3 Long length fibre	58
5.6 Dependence of PDG and signal gain fluctuation on fibre PMD	59
5.6.1 Field measurements for high PMD fibre.....	60
5.7 Signal power distribution	63
5.8 Raman gain and PMD characterization of fibre.....	65
5.8.1 Relation between PDG and on-off gain	66
5.8.2 Determination of fibre PMD parameter	66
5.8.3 Effects of PDL and SNR.....	69
5.9 Forward and backward pumped Raman PDG.....	71

Chapter Six	73
6.0 Introduction	73
6.1 Measurement setup.....	74
6.2 Statistics of RFA gain in the presence of PDL.....	76
6.3 Simulation of PDL/PDG interaction in the presence of PMD.....	78
6.3.1 Wavelength dependence of RFA gain in the presence of PDL.....	80
Chapter Seven	83
7.0 Introduction	83
7.1 Measurement setup.....	85
7.1.1 Effects of scrambled pump on signal pulling	85
7.2 Pump-signal orientation on the Poincaré sphere	87
7.3 Effects of fibre length and PMD on polarization pulling.....	90
7.3.1 Dependence of pulling on signal wavelength	92
7.4 Limitations of Raman polarization pulling in fibre	93
Chapter Eight	96
Appendix I	100
PDG-PDL interaction in the presence of PMD	100
Appendix II	101
Pump and signal SOPs variation with pump power	101
Appendix III	102
Equipment and components used in experimental work.....	102
Appendix IV	103
Polarization of light representation	103
Appendix V	104
Appendix VI	105
Appendix VII	106
Research outputs of the author	106
References	108

Abstract

The need to exploit the large fibre bandwidth and increase the reach has seen the application of the Raman fibre amplifier (RFA) become indispensable in modern light wave systems. The success and resilience of RFAs in optical communication is deeply rooted in their unique optical properties and new technologies which have allowed the amplifier to come of age. However, the full potential of RFAs in optical communication and other applications are yet to be realized. More so are its polarization properties which still remain largely unexploited and have not been fully understood. In this work, fundamental issues regarding distributed RFA have been investigated with the aim of acquiring a better understanding of the amplifier polarization characteristics which have potential applications. In particular the effects of polarization mode dispersion (PMD) and polarization dependent loss (PDL) have been demonstrated both by simulation and experiment. The possibility of Raman polarization pulling in single mode fibres (SMFs) has also been addressed. Polarization sensitivity of RFA has been known for a long time but the clear manifestation of it has become evident in the advent of modern low PMD fibre. Unlike EDFAs which make use of special doped fibre, RFAs require no special fibre for operation. Besides, RFA uses a very long length of fibre and as such the fibre polarization characteristics come into play during amplification.

In the demonstrations presented in this thesis a fibre of PMD coefficient $< 0.05 \text{ pskm}^{-1/2}$ was regarded as low PMD fibre while one having coefficient $\geq 0.05 \text{ pskm}^{-1/2}$ was categorized to have high PMD unless otherwise stated. Several experiments were performed to evaluate the RFA gain characteristics with respect to fibre PMD and the system performance in the presence of noise emanating from amplified spontaneous emission (ASE). Analysis of Raman gain statistics was done for fibres of low and high PMD coefficients. The statistics of PDG and on-off gain were eventually used to demonstrate the extraction of PMD coefficients of fibres between 0.01- 0.1 $\text{pskm}^{-1/2}$ using a forward pumping configuration. It was found that, at increasing pump power a linear relationship exists between forward and backward signal gain on a dB scale. The interaction of PDL and Raman PDG in the presence of PMD were observed at very fundamental level. It was found the presence of PDL serves to reduce the available on-off gain. It was also established that the presence of PMD mediates the interaction between PDG/PDL. When PMD is high it reduces PDG but the presence of PDL introduces a wavelength dependent gain tilting for WDM channels. Further analysis revealed that signal polarization is influenced by the pump SOP due to the pulling effect which is present even at moderate pump power.

Abbreviation

ASE – amplified spontaneous emission

BER – bit error ratio

CD – chromatic dispersion

DCF – dispersion compensating fibre

DGD – differential group delay

DOP – degree of polarization

DRBS – double Rayleigh backscattering noise

DSF – dispersion shifted fibre

DWDM – dense wavelength division multiplexing

EDFA – erbium doped fibre amplifier

FWHM – full width at half maximum

FWM – four wave mixing

JME – Jones matrix eigenanalysis

MPI – multipath interference

NRZ – non-return to zero

NZDSF – non-zero dispersion shifted fibre

OSA – optical spectrum analyzer

OSNR – optical signal to noise ratio

PDG – polarization dependent gain

PDL – polarization dependent loss

PMD – polarization mode dispersion

PON – passive optical network

PSP – principal state of polarization

RFA – Raman fibre amplifier

SBS – stimulated Brillouin scattering

SSMF – standard single mode fibre

SOP – state of polarization

SPM – self phase modulation

SRS – stimulated Raman scattering

XPM- cross phase modulation

Chapter One

Introduction

Optical fibre communications success story is traceable in the concurrent research and development of its four basic elements. These are: the optical source (Laser), modulation, transmission medium (fibre) and optical detector. The development of optical fibre and other facets in communications has been motivated by the demand for long haul applications, high speed data communications and transmission capacity. The demand for bandwidth is increasing due to among other things the growing internet traffic coupled with new applications. Social networking which is one of the new applications has taken the centre stage and was the theme of year 2011 Southern African Telecommunication Networks and Applications Conference (SATNAC 2011).

Although the concept of propagation of light by total internal reflection was known for centuries with many demonstrations of the idea, it was not until the late 1950s when the first practical glass fibre was fabricated (Hecht, 1999). Even so the fibre had high loss due to light absorption and attenuation and could not be used for optical communications. The advent of low loss optical fibre in the 1970's paved the way for optical fibre communications as well as the fabrication of nonlinear optical devices. The first optical communications systems operated in the 850 nm transmission window and were limited in capacity due to high loss and intermodal dispersion (Keiser, 2000). With further development of optical sources transmission was shifted to the 1310 nm transmission window where attenuation is ~ 0.5 dB/km. This window has the advantage of zero dispersion but because of its relatively high signal loss and also the presence of water peak (impurities) at the vicinity, it was abandoned since it could not conveniently accommodate the transmission of wavelength division multiplex (WDM) channels. Further development of laser sources resulted in migration to the 1550 nm transmission window where attenuation is a low ~ 0.2 dB/km. Despite the diverse achievements made so far in advancing and maturing the state-of-the-art of optical systems, many issues concerning the future of the system in regard to efficiency and the ever increasing demand for capacity still need to be addressed. In particular, the interactions between linear and nonlinear polarization effects in optical fibre which manifest at high optical power is still a subject of great concern. More attention is required in addressing this

issue because as more wavelengths are introduced in the fibre, the more the average optical power will increase in the fibre.

Although modern fibres have low attenuation of ≤ 0.2 dB/km, the value is still large enough to limit the distance of transmission to a few hundred kilometres. The problem of attenuation was initially addressed using optoelectronics repeaters in long-haul systems (Tricker, 2002). However, signal regeneration was a major drawback due to the low speed of electronics involved and the numerous repeaters required in the system. The development of optical amplifiers in the early 90's was a major boost to fibre communication and resulted in elimination of repeater systems and the birth of all-optical systems with increased capacity. Optical amplifiers are characterized by large amplification bandwidth which has enabled the application of dense wavelength division multiplexed (DWDM) transmission. Indeed, the DWDM technique owes its success to the introduction of optical amplifiers and has resulted in increased capacity and span. There is also the technique of optical time division multiplexing (OTDM) which has been proposed as an alternative method for increasing the fibre transmission capacity (Spirit, 1994).

Erbium-doped fibre amplifier (EDFA) is one of the most popular and widely used only by demand and capacity but also by its high performance coupled with a stable dynamic behaviour. As a result EDFA has been exploited close to its theoretical limits such that its lowest noise figure is close to the quantum limit of 3 dB. This noise figure is a limitation to the near future systems. The high power associated with the EDFA amplified WDM system is a source of nonlinear signal impairments which are known to affect the performance of optical devices such as compensators (Bononi *et al*, 2003). These nonlinearities are caused by induced nonlinear refractive index which occurs when a fibre is subjected to a high intensity beam (Agrawal, 2007).

The other limitation of EDFA is its relatively narrow bandwidth compared to the available fibre bandwidth. Modern fibre technology has virtually eliminated the water attenuation peak around 1400 nm in conventional single –mode fibres and has effectively opened the region between the second and third transmission window (Keiser, 2000). This implies that there is more bandwidth in such fibres which is usable for transmission. Example is AllWaveTM fibre which was designed for metro networks applications.

Research on Raman amplification in optical fibre started the 1970's but the first demonstration of the use of the Raman fibre amplifier (RFA) was in 1999, approximately ten

years after commercialization of the EDFA (Bromage, 2004). The deployment of a highly competitive and seemingly sufficient EDFA was a major blow to RFA. Other factors that attributed to delay in the development and implementation of RFA included its low efficiency and also the unavailability of high power pump lasers that could provide the appropriate pumping wavelengths. However, due to its great potential in extending fibre bandwidth and now the availability of high power lasers, RFA could not be left out in the upgrading of existing networks and in the deployment of modern fibre networks (Islam, 2002). For example RFA has found applications in hybrid optical systems such as Raman/ EDFA, where it is used to increase amplifier spacing thus reducing the number of cascaded amplifiers in the system (H. Masuda, 2004). It has also been tested for metro application in extending the bandwidth in passive optical networks (PONs) (Kjaer *et al*, 2007). The potentials of RFA are yet to be fully exploited and may not be limited to optical communications but with new applications as well.

Polarization effects in optical fibre are significant in regard to the operation and stability of optical communication systems as well as optical devices and can be classified as linear and nonlinear. Ideally a fibre is a circular dielectric waveguide designed to confine light inside the core during its propagation. Due to intrinsic and extrinsic perturbations on the fibre the core isotropic property is lost resulting in a linear birefringence. This birefringence is nonuniform and changes in magnitude and orientation all along the fibre length. When light is coupled into a single mode fibre it split into two modes which propagate along the slow and the fast axes of the fibre. There is also mode coupling where the two axes change orientation. These phenomena lead to polarization mode dispersion (PMD) which is a linear effect and has its counterpart second order polarization mode dispersion (SOPMD). Another linear effect is polarization dependent loss (PDL) which is present in optical devices incorporated in a fibre optic system. Optical devices such as couplers, beam splitters, isolators, multiplexers, etc all behave like partial polarizers. They have an axis of maximum and minimum transmission such that when polarized light passes through them it can be attenuated depending on device orientation. This loss leads to signal distortion and decreases the system signal to noise ratio (SNR) at the receiver.

Single mode fibres have a tiny core with diameter ranging from 4 μm to 10 μm which is surrounded by a cladding of diameter 125 μm and having slightly lower refractive index than the core. As a result of high mode confinement, optical intensity in the core can be very high especially in an optical system employing WDM techniques and optical amplifiers. In this

case, the intense optical field can cause anharmonic motion of the bound electrons of silica and induce a power dependent refractive index. The resulting nonlinear effects are elastic and are collectively known as the Kerr effect. A high power channel will induce a nonlinear phase shift upon itself otherwise known as self-phase modulation (SPM). When two wavelengths are co-propagating they can impose a power dependent nonlinear phase shift on each other in which case the effect is known as cross-phase modulation (XPM). If three or four high intensity beams propagate simultaneously in a fibre they can induce Kerr nonlinearities by their beating which is known as four-wave mixing. Although Kerr nonlinearities cause limitations in optical communication systems they have found applications in the fabrication of optical devices. Similarly, some optical devices operate on a principle governed by these nonlinearities (Agrawal, 2008).

There is also an inelastic nonlinear effect which is the cause of stimulated Brillouin scattering (SBS) and stimulated Raman scattering (SRS). The phenomenon of SBS is caused by resonance of optical waves with acoustic phonons while SRS is caused by the beating of two waves with a vibration mode of molecules involving optical phonons. SRS is the phenomenon behind Raman amplification in fibres and results in polarization dependent gain (PDG). This PDG, though detrimental in optical communication can also be exploited in other applications such as polarization pulling. (Martinelli *et al*, 2009). It is therefore significant to cultivate a good understanding regarding polarization effects in RFA which would enable new applications of this amplifier, thereby realizing its full potential.

This thesis constitutes three goals, the first of which is to bring forth a clear understanding of how linear polarization effects influence the performance of RFA in modern fibres. The next goal is to bridge the gap between previous work that has been carried out using other types of fibres such as DCF and DSF and compare different pumping schemes using SSMF of low and high PMD. The third goal is to develop an experimental feedback which can be used to improve and support the existing theories of RFA. The small residue birefringence still existing in modern fibres is of great concern to the fibre industry. Increasing transmission span and capacity would introduce more optical power into the fibre resulting in the power dependent nonlinear birefringence. Investigating the behaviour and performance of RFA in the presence of linear and nonlinear birefringence would be highly significant. In most cases the fibre with appropriate parameters may not be available, thus one would resort to a simulation approach.

The work presented in this thesis is organized as follows: Chapter 2 consists of a brief explanation of theory with a focus on polarization of light as well as polarization effects in optical fibre. In particular the chapter addresses the various aspects of PMD and PDL effects with the aim of laying the required foundation toward the understanding of their manifestation in fibres. Chapter 3 deals with Raman amplification in fibres and considers the various facets of Raman gain. The chapter introduces the parameters that determine Raman gain and the contribution of amplified spontaneous emission (ASE) in the degradation of the amplifier optical signal to noise ratio (OSNR). Chapter 4 presents simulations and experimental results showing the gain characteristics of RFA in the presence of high and low fibre PMD. The RFA which was used in the measurement was newly acquired and assembled in our laboratory, thus becoming necessary to study its PMD characteristics. The chapter concludes by evaluating the system performance in the presence of ASE noise when a fibre of low and high PMD is employed in the amplification. Chapter 5 investigate the statistics of RFA due to PMD for different lengths of fibre and compares the three pumping schemes of Raman amplification. The chapter underscores the issue of extracting the fibre PMD parameter simply by analysing the gain statistics of a forward pumped RFA. Chapter 6 considers the effects of PDL on Raman gain in the presence of PMD and shows the effects on the gain due to PDL positioning in the RFA system. Chapter 7 presents results on Raman polarization pulling showing the effect of fibre PMD, fibre length and pump power. Chapter 8 bears the concluding remarks and unifies the findings of this work.

Chapter Two

Polarization effects in optical fibre

2.0 Introduction

Polarization phenomena in optical fibre were cited as early as 1961 (Snitzer and Osterberg) but became significant only in the later stages of development of fibre communication. In the absence of chromatic dispersion (CD) polarization effects emerged to be the next hurdle in the advancement of the modern lightwave system. The significance of polarization effects in optical fibres have been attributed to major developments on the system which include increasing bit rate and the introduction of WDM channels in the fibre. Polarization effects have further been boosted by the introduction of optical amplifiers and increasing optical components in the system. In this chapter we start by reviewing some mathematical tools which are relevant for understanding and analysing polarization in single mode fibre. Later we discuss two linear polarization phenomena occurring in optical communication namely PMD and PDL.

2.1 Polarization states of light representation

Light is an electromagnetic wave that satisfies Maxwell's equations. When a transverse electromagnetic wave propagates longitudinally in free space or vacuum its electric and magnetic components are orthogonal and its polarization state is defined by the direction of Electric field vector \mathbf{E} . A transverse electromagnetic wave $\mathbf{E}(z,t)$, moving in a vacuum in the z -direction is composed of two independent plane polarized components (fig 2.1a) which are orthogonal to each other. In the right hand Cartesian coordinate, $\mathbf{E}(z,t)$ can be written in terms of its two sinusoidal components in the form:

$$\mathbf{E}(z, t) = \mathbf{E}_x(z, t) + \mathbf{E}_y(z, t) \quad 2.0$$

$$\mathbf{E}_x(z, t) = E_{0x} \cos(\omega t - kz + \delta_x) \quad 2.1$$

$$\mathbf{E}_y(z, t) = E_{0y} \cos(\omega t - kz + \delta_y) \quad 2.2$$

where E_{0x} and E_{0y} are the amplitudes of each component, δ_x and δ_y are the corresponding phases and $\omega t - kz$ is the wave propagator.

The nature and behaviour of polarized light can be understood if we eliminate the wave propagator between the two components $\mathbf{E}_x(z,t)$ and $\mathbf{E}_y(z,t)$ to get the equation:

$$\frac{E_x^2(z,t)}{E_{0x}^2} + \frac{E_y^2(z,t)}{E_{0y}^2} - \frac{2E_x(z,t)E_y(z,t)}{E_{0x}E_{0y}} \cos \delta = \sin^2 \delta \quad 2.3$$

where $\delta = \delta_y - \delta_x$ is the phase difference. The end point of the electric vector as seen by an observer looking into the source traces an ellipse as the wave propagates in the z-direction (fig 2.1b). This concept is popularly known as polarization ellipse and provides the most basic and convenient way of representing polarized light.

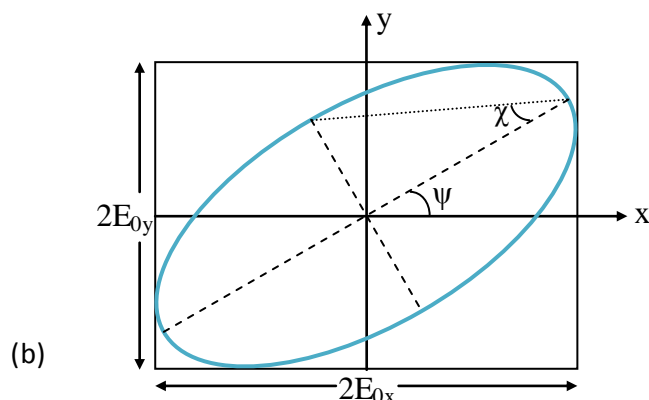
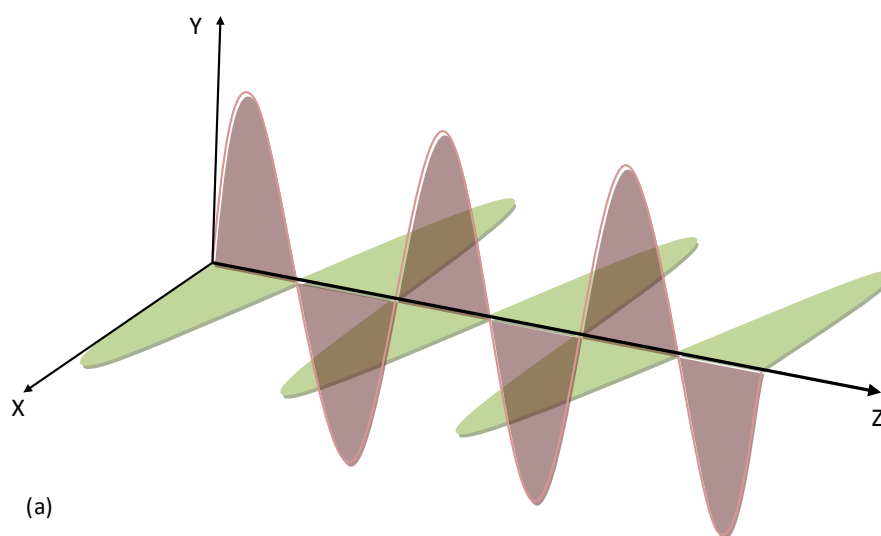


Figure 2.1: (a) Illustration of a transverse electromagnetic wave propagating in z-direction and (b) Polarization ellipse.

The rotation angle ψ and ellipticity χ can be expressed in terms of optical field amplitudes and the phase difference.

$$\tan 2\psi = \frac{2E_{0x}E_{0y}}{E_{0x}^2 - E_{0y}^2} \cos \delta \quad 0 \leq \psi < \pi \quad 2.4$$

$$\sin 2\chi = \frac{2E_{0x}E_{0y}}{E_{0x}^2 + E_{0y}^2} \sin \delta \quad \pi/4 \leq \chi < \pi/4 \text{ and } 0 \leq \delta < 2\pi \quad 2.5$$

2.1.1 Degenerate polarization states

There are six unique polarization states which are mostly used in the study of polarized light because they can be easily created in a laboratory environment. These states can easily be derived from the polarization ellipse by defining E_{0x} , E_{0y} and δ .

If E_{0y} or $E_{0x}=0$ the resulting polarization states are known as linear horizontal polarization (LHP) and linear vertical polarization (LVP) respectively. When $E_{0x}=E_{0y}$ and $\delta = 0$ or π the states are known as linear - 45 (L- 45P) and linear + 45 (L+45P) respectively. If $E_{0x}= E_{0y}$ and $\delta = \pi/2$ or $3\pi/2$ the states are known as right circular polarization (RCP) and left circular polarization (LCP) respectively. We use right handed convention to define the direction of rotation of the \mathbf{E} -vector as the wave propagates. In this case for right circular polarization the vector rotates clockwise while for left circular polarization the vector rotates counter clockwise.

2.1.2 Poincaré sphere

Polarization ellipse is a powerful tool of representing and visualizing any state of completely polarized light but the method becomes more complex when applied to changing polarization states. In any polarizing medium such as optical fibre the state of polarization of light keeps on changing as light propagates from one end to the other. The behaviour can be extremely difficult to visualize by the analysis of a polarization ellipse. A more practical method of representing polarized light is the Poincaré sphere (fig 2.2) which was suggested and named after a German astronomer H. Poincaré in 1892. In the Poincaré sphere representation the polarization ellipse, which is characterized by orientation ψ and ellipticity χ , is mapped onto a point P on the sphere. If the state of polarization (SOP) of light changes as light propagates through a medium the new state is represented by another point on the sphere. That is, each point on the sphere represents a specific SOP of completely polarized light. Poincaré sphere whose theory was presented in 1954 by H. G. Jerrard is now used extensively in research activities related to fibre optics.

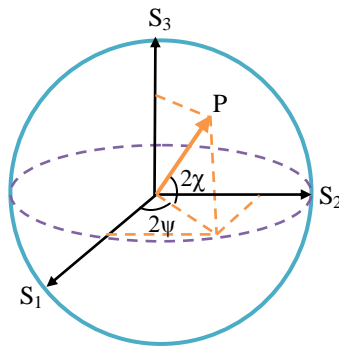


Figure 2.2: Poincaré sphere representation of light

2.1.3 Stokes polarization parameters

In its original presentation the Poincaré sphere was not practical because the amplitudes E_{0x} and E_{0y} of the field components are not observable. The period of light is very small ($\sim 10^{-15}$ sec) and therefore it is practically impossible to observe the elliptical behaviour of light as it propagates in a cycle. In addition polarization mapping cannot be used to represent partially polarized and unpolarized light which are also equally important aspects of light. G.G. Stokes (1852) introduced into optics the measurable or observables of polarization ellipse which are now known as Stokes parameters (vectors). Stokes parameters can be derived after rewriting the amplitudes of equation 2.1 and 2.2 in terms of complex amplitudes. That is,

$$E_x(t) = E_{0x} \exp j(\omega t + \delta_x) \quad 2.6$$

$$E_y(t) = E_{0y} \exp j(\omega t + \delta_y). \quad 2.7$$

The kz term was dropped because only the time average of polarization ellipse (i.e. intensity) is of interest. Now Stokes parameters are defined by the relations:

$$S_0 = E_x E_x^* + E_y E_y^* = E_{0x}^2 + E_{0y}^2 \quad 2.8$$

$$S_1 = E_x E_x^* - E_y E_y^* = E_{0x}^2 - E_{0y}^2 \quad 2.9$$

$$S_2 = E_x E_y^* + E_y E_x^* = 2E_{0x} E_{0y} \cos \delta \quad 2.10$$

$$S_3 = j(E_x E_y^* - E_y E_x^*) = 2E_{0x} E_{0y} \sin \delta \quad 2.11$$

where $E_{i=(x,y)}^*$ are the complex conjugates of the E-fields. The interpretation of the four Stokes parameter S_0, S_1, S_2, S_3 is as follows: S_0 is the total intensity of the optical beam, S_1 signifies the difference between the intensity of horizontally polarized and vertically polarized beam,

S_2 represents the difference between the intensity of linear+ 45 polarized and linear- 45 polarized light, while S_3 describes the difference in intensity of right circularly polarized and left circularly polarized beam.

The Stokes parameters are commonly arranged in column matrix known as Stokes vectors. In the Poincaré representation the Stokes vectors are normalized and can conveniently be expressed in terms of rotation ψ and ellipticity χ angles as;

$$\begin{pmatrix} S_1 \\ S_2 \\ S_3 \end{pmatrix} = \frac{1}{s_0} \begin{pmatrix} S_1 \\ S_2 \\ S_3 \end{pmatrix} = \begin{pmatrix} \cos 2\chi \cos 2\psi \\ \cos 2\chi \sin 2\psi \\ \sin 2\chi \end{pmatrix}. \quad 2.12$$

All linear polarization states are represented at the equator of the sphere while right circular polarized light and left circular polarized light are represented at the north Pole and south Pole of the sphere respectively. All other points on the surface of the Poincaré sphere represent elliptically polarized light. The origin of the sphere represents completely unpolarized light while points inside the sphere represent partially polarized light.

The degree of polarization (DOP) of light is given by:

$$\text{DOP} = \frac{1}{s_0} \sqrt{S_1^2 + S_2^2 + S_3^2} \quad 0 \leq \text{DOP} \leq 1 \quad 2.13$$

The DOP of partially polarized light is less than unity while the DOP of completely polarized light and unpolarized light is one and zero respectively.

2.1.4 Mueller and Jones matrix

When light propagates in a polarizing medium the state of polarization at the output varies from the input polarization. H.Mueller and R.C Jones in the 1940s separately developed the Mueller and the Jones formulations as alternative mathematical tools to the Poincaré sphere approach for solving polarization problems. These matrices are mathematical relations that describe the transmission characteristics of an optical device and have been successfully applied in polarization studies. However the Poincaré sphere still remains a powerful tool for visualization of the behaviour of polarized light as it passes through polarizing medium.

In the Mueller matrix formulation the input Stokes vectors $S(s_0, s_1, s_2, s_3)$ representing the beam intensity and polarization at the input of a device are related to the output Stokes vectors $\hat{S}(\hat{s}_0, \hat{s}_1, \hat{s}_2, \hat{s}_3)$ of the beam such that:

$$\hat{S} = M. S \quad 2.14$$

where M is the Mueller 4x4 matrix whose elements are real quantities.

Similarly, the Jones matrix relates the components of the incident field to the emergent components of the field of completely polarized light. In the Jones formulation a 2x1 column vector whose elements are the instantaneous E-field components represents any polarization state and a 2x2 Jones matrix describes the characteristics of the polarizing device. Thus the transmission of any beam of polarized light in Jones space is described by the relation:

$$\begin{bmatrix} E_x \\ E_y \end{bmatrix} = \begin{bmatrix} j_{xx} & j_{xy} \\ j_{yx} & j_{yy} \end{bmatrix} \begin{bmatrix} E_{0x} e^{i\delta_x} \\ E_{0y} e^{i\delta_y} \end{bmatrix} \quad 2.15$$

where E_{0x} and E_{0y} are the field amplitudes and δ_x , δ_y are the phases. Unlike Mueller matrix representation, the Jones technique is limited to completely polarized light and cannot describe partially polarized light and unpolarized light. A complete and more elaborate treatment of polarization optics can be found in (O'Neill, 2004; Collet, 2003).

2.2 Polarization mode dispersion

Polarization mode dispersion (PMD) in optical fibres is an impairment caused by polarization dependent delays in propagation of a signal pulse resulting in pulse spreading. At high bit rates (>10 Gb/s) PMD causes intersymbol interference which limits the transmission capacity of the fibre. This effect was introduced by several authors and observed in fibres as early as mid 1970's. However, a modern description of PMD was achieved by Poole and Wagner, (1986) and the mathematical formulation unified by Gordon and Kogelnik (2002). In single mode fibres PMD emanates from the fact that at a given wavelength the fibre supports two orthogonally polarized modes (Buck, 1995). In an ideal fibre the two modes are degenerate such that if we excite only one mode at the fibre input no signal energy coupling takes place between the modes and during propagation. Real fibres are generally anisotropic and the core is asymmetric all along the length of the fibre. As a result the two modes exhibit a difference in the phase and group velocities commonly known as birefringence (Rashleigh, 1983). The loss of degeneracy also results in a mixing of the two polarization states which is known as mode coupling. Both the birefringence and mode coupling define the PMD of a fibre.

2.2.1 Birefringence

The small difference in refractive index exhibited by the two modes as the pulse propagates through the fibre (fig 2.3a) and optic fibre components is a measure of birefringence. In single mode fibre birefringence originates from loss of core circularity due to internal and external perturbations (Poole and Nagel, 1997). Internal perturbations are inherent to the fibre

manufacturing process while external perturbations are induced into the core during cabling and deployment of fibre. Since these perturbations are nonuniformly distributed on the fibre transverse and longitudinal dimensions, the birefringence varies in strength from one fibre section to the other. Fibre birefringence is also sensitive to environmental conditions such as change in temperature. Mathematically we can define birefringence if we consider a fibre to be made up of small sections each having a uniform birefringence (Poole and Nagel 1997). Over a short fibre length which is characterized by birefringence uniformity, the difference between the propagation constants of the slow and fast modes is given as:

$$\Delta\beta = \beta_s - \beta_f = \frac{\omega n_s}{c} - \frac{\omega n_f}{c} = \frac{\omega \Delta n}{c} = \frac{2\pi \Delta n}{\lambda} \quad 2.16$$

where ω is the frequency, c is the speed of light, $\Delta n = n_s - n_f$ is the differential effective refractive index between slow (s) and fast (f) modes.

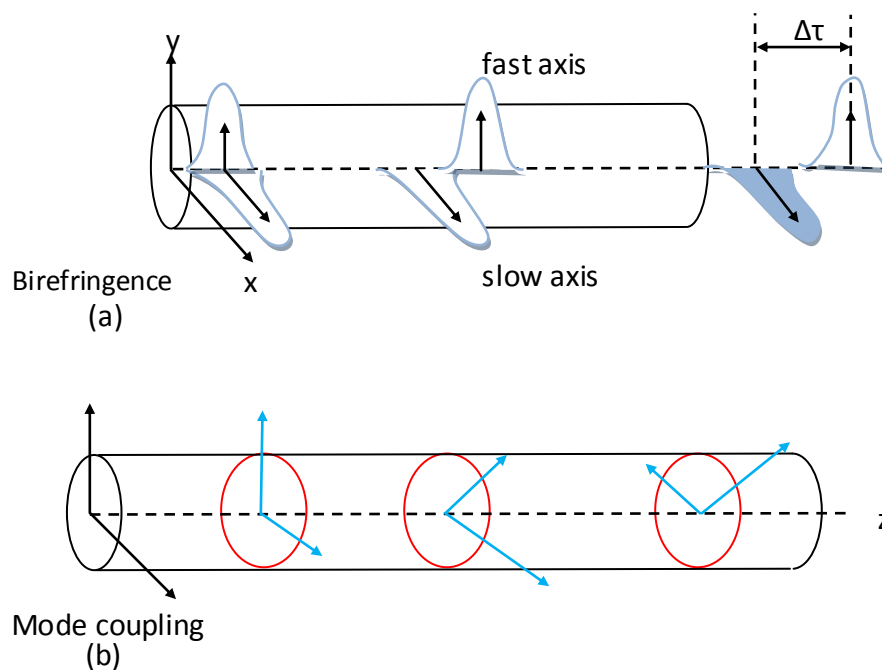


Figure 2.3: Illustration of the (a) effect of fibre birefringence on an optical pulse which is propagating along its length (b) mode-coupling sites where the birefringence changes orientation.

The birefringence causes the state of polarization (SOP) of the input light to rotate in a cyclic manner as it propagates in the fibre. In a short fibre length, the beat length L_b is defined as the fibre length over which the polarization rotates through a full cycle or in the frequency domain it is the propagation length for which a 2π phase difference accumulates between the two modes. That is

$$L_b = \frac{\lambda}{\Delta n} = \frac{2\pi c}{\omega \Delta n} \quad 2.17$$

The group-delay difference between the slow and fast modes is known as differential group delay (DGD).

2.2.2 Polarization mode coupling

In long fibre spans such as used in terrestrial and submarine transmission systems the birefringence orientation changes (fig 2.3b) in a random fashion all along the cable length. To understand the mode coupling in fibre we consider the fibre as a concatenation of small segments whose birefringence axes (and strength) are randomly oriented along the fibre (Poole and Wagner, 1986). At the coupling site where the birefringence changes orientation, the fast and slow polarization modes from one segment decompose into both the fast and slow modes of the next segment. As a result of mode coupling the birefringence of each segment may add to or subtract from the total birefringence. It has been shown that due to mode coupling the DGD accumulates with the square root of distance (Poole 1988, Poole and Nagel 1997). Mode coupling in fibre can be intentionally induced during fibre drawing (spun fibres) or unintentionally during spooling, cabling and deployment. Due to mode coupling and the statistical nature of PMD two fibre regimes (short and long length) are defined and are characterized by a parameter called correlation length L_c (Poole and Nagel 1997). In this classification a fibre is short if, $L \ll L_c$ and as such DGD increases linearly with distance. For a long fibre, $L \gg L_c$ the mean DGD increases with the square root of distance. That is, $\langle DGD \rangle = \overline{\Delta\tau} = D_p \sqrt{L}$, where D_p is the PMD coefficient of the fibre.

2.3 PSP and PMD bandwidth

Manifestation of PMD in optical fibre can be described in both the time domain and frequency domain (Gordon and Kogelnik, 2000). The principal states model which was first developed by Poole and Wagner, (1986) applies equally well in both domains. In the frequency domain, the states model implies that, there exists for every frequency a special pair of polarization states called the principal states of polarization (PSP). A PSP is that input polarization for which when light is launched the output SOP remains independent of frequency to first order. That is, in a small frequency range $\Delta\omega$, light launched in the PSP does not change polarization at the output. In the time domain, a light pulse launched into the PSPs will experience maximum differential group delay (DGD). In the absence of polarization dependent loss (PDL), the PSPs are orthogonal and for short fibre ($L \ll L_c$) they correspond to the fast and slow modes.

In the Stokes space, the principal states model can easily be used to characterize PMD in randomly birefringent fibres. In particular the PMD vector $\vec{\tau}$ is defined as:

$$\vec{\tau} = \Delta\tau\hat{p} \quad 2.18$$

where $\Delta\tau$ is the instantaneous DGD and \hat{p} is a unit vector pointing in the direction of the slower PSP (Kogelnik *et al.* 2002). The unit vector $-\hat{p}$ denotes the fast PSP such that the two unit vectors are antiparallel (180°) in Stokes space. For a fixed input SOP the output SOP \hat{s} precesses about the PSP \hat{p} at a rate equal to the DGD or the magnitude of the PMD vector as frequency changes. For a small frequency range the output SOP precession is of the form:

$$\frac{d\hat{s}}{d\omega} = \vec{\tau} \times \hat{s} \quad 2.19$$

The PMD vector is stationary only over a small frequency bandwidth. The change of the PMD vector with frequency ω can be understood by determining the bandwidth of the principal states. That is, the bandwidth over which the PMD vector is constant. The concept of PSP bandwidth is important and has been used in the frequency domain measurement of PMD vectors and the measurement of PMD statistics (Kogelnik *et al.* 2002). It can also be applied in understanding of the PMD behaviour when more than one wavelength is launched into a fibre. One such example is Raman amplification, where the pump and signal propagate simultaneously in the fibre. Betti *et al.*, (1991) and Bruyere, (1996) reported varying constants of PMD bandwidth ($\Delta\omega_{PSP}$) while Jopson *et al.*, (1999) provided the practical estimate given by the relation:

$$\Delta\omega_{PSP} \cdot \overline{\Delta\tau} = \pi/4 \quad 2.20$$

where $\overline{\Delta\tau}$ is the mean DGD of the fibre. When the mean DGD is expressed in picosecond (ps) we can rewrite the above relation in terms of frequency band $\Delta\nu_{PSP}$:

$$\Delta\nu_{PSP} = 125/\overline{\Delta\tau} \quad 2.21$$

Note that for the PMD vector, a variation with frequency also leads to higher order PMD, which is a subject outside the scope of this work

2.4 Power dependent birefringence

The fibre birefringence discussed in section 2.2 is commonly known as linear or modal birefringence. When optical power increases in the fibre, the associated optical field induces a power dependent refractive index whose magnitude depends on the field intensity. This

nonlinear refractive index which is also the cause of Kerr effects in fibre, results in polarization dependent nonlinear birefringence (Agrawal, 2007). In the absence of linear birefringence the nonlinear birefringence manifests as a rotation of the polarization ellipse for a continuous wave propagating in the fibre (Maker *et al.* 1964). Interaction of linear (\mathbf{W}_L) and nonlinear birefringence (\mathbf{W}_{NL}) leads to complex motion of the SOP which can be described for continuous wave CW as:

$$\frac{d\mathbf{S}}{dz} = \mathbf{W} \times \mathbf{S} \quad 2.22$$

where $\mathbf{W} = \mathbf{W}_L + \mathbf{W}_{NL}$. In WDM systems where PMD compensation is achievable on a channel to channel basis, the nonlinear birefringence enhances SOP scrambling of channels making optical based PMD compensation difficult (Collings and Boivin, 2000). A more detailed analysis of nonlinear birefringence can be found in chapter six of the text by Agrawal, (2007).

2.5 Polarization dependent loss

Polarization dependent loss in fibre optic systems comes from the fibre and optical components interleaved with the fibre. However, the PDL of fibre is negligibly small and is due to imperfections and bends along the fibre. With the introduction of dense WDM technique as well as the application of optical amplifiers in the modern optical system, the number of optical devices in the system has greatly increased. Each of these devices has an associated small insertion loss which depends on the polarization state of incident light. When a signal is transmitted in an amplified fibre link or in passive optical networks (PONs) it encounters many of these optical components whose cumulative loss can lead to signal impairment. Optical components such as isolators, couplers, filters, splitters, fibre grating etc exhibit polarization dependent loss (PDL). When these components are incorporated in the system their PDL become random and time varying because of polarization evolution as light propagates over long distances in fibre. This random variation of PDL causes power fluctuations which affect the performance of a system (Yamamoto *et al.* 1993; Lichtman 1995).

2.5.1 Definition and effects of PDL

Polarization dependent loss PDL is defined as the difference between maximum and minimum power transmitted by an optical component or device as the input SOP is varied over all possible polarization states (Ding *et al.*, 2007). The causes of PDL include dichroism (the unequal spectral absorption of orthogonal components), fibre bending, angled optical

interfaces and oblique reflections. An element exhibiting PDL is characterized by its orientation vector and the transmission coefficient which are defined in relation to the maximum T_{\max} and the minimum T_{\min} transmission axes. The SOPs corresponding to T_{\max} and T_{\min} axes of the PDL element are not necessarily linear but are orthogonal in Stokes space (Gisin, 1995). Light launched along the PDL axis is transmitted unaltered and undiminished while light launched along the orthogonal axis is unaltered in state but suffers loss.

According to international standards (TIA and IEC), PDL is defined for completely polarized light, in decibel unit as:

$$\rho_{dB} = 10 \log_{10} \left(\frac{T_{\max}}{T_{\min}} \right) \quad 2.22$$

where T_{\max} and T_{\min} are the maximum and minimum power transmitted through the PDL element. An incident light having arbitrary polarization that is not aligned with either of the axes will suffer loss and polarization change on traversing a PDL element.

If unpolarized light is incident on a PDL element it emerges partially polarized and the element becomes a partial polarizer. Depolarized light can be treated as a mixture of two orthogonal polarization states (Gisin, 1995), so that the transmission coefficient T_{depol} in this case is given by:

$$T_{\text{depol}} = \frac{T_{\max} + T_{\min}}{2} \quad 2.23$$

from which the statistical definition of PDL is given by:

$$\Gamma = \frac{T_{\max} - T_{\min}}{T_{\max} + T_{\min}} \quad 2.24$$

where Γ is the length of a global PDL vector $\vec{\Gamma}$. Therefore, the decibel expression of PDL has the form:

$$\rho_{dB} = 10 \log_{10} \left(\frac{1+\Gamma}{1-\Gamma} \right). \quad 2.25$$

PDL decreases as the degree of polarization of incident light decreases (Ding *et al.* 2007).

2.6 Cascaded PDL and PDL evolution

In a fibre network where many PDL components are cascaded, their transmission coefficients do not multiply. This is because the polarization sensitive axes of each PDL element in the cascade are not aligned and each element has its own orientation $\hat{\alpha}$ which is different from

the other elements in the chain. Besides, PDL orientation fluctuates with time due to PMD, causing PDL to manifest the wavelength dependent nature. Thus, each element changes the SOP incident to it and a cascade will exhibit multiple polarization alteration along its length (Gisin, 1995; Damask, 2005). The implication is that the global PDL requires statistical treatment (Amari *et al*, 1998).

In the Stokes space the global PDL vector $\vec{\Gamma}$ is cumulative and always tries to track the local PDL $\vec{\alpha}$ vector but it can be decorrelated if the cascaded elements have low PDL and random orientation. For a chain of PDL elements having arbitrary orientation, the evolution of the PDL vector $\vec{\Gamma}$ has been derived using a different approach (N Gisin *et al* 1997; B. Huttner *et al*, 2000; A. Mecozzi and M. Shtaif, 2004) and has the form:

$$\frac{d\vec{\Gamma}}{dz} = \vec{\alpha} - (\vec{\alpha} \cdot \vec{\Gamma})\vec{\Gamma}. \quad 2.26$$

The implication of this equation is that the magnitude of $\vec{\Gamma}$ may increase or decrease in a cascade but is always less than $\vec{\alpha}$. The equation has been thoroughly discussed in the text by Damask, 2005.

2.7 PDL in the presence of PMD

In real systems the fibre and optical components are interleaved along the link, resulting in the interaction between the PDL of the components and the fibre PMD. This interaction has many anomalous effects which are more severe than individual effects of PMD or PDL. Firstly, PDL elements exhibit wavelength dependence in the presence of PMD. This is because the SOP incident onto a PDL element depends on the source wavelength. This implies that in a WDM system each channel will experience a different PDL resulting in unequal power in the channels. Second, the principal states of polarization lose their orthogonality and are no longer the fast and the slow axis (Gisin and Huttner, 1997). The evolution of the output SOP with frequency is complex and the simple precession motion (equation 2.19) is no longer valid (Frigo, 1986; Eyal and Tur, 1998) Other implications of PDL and PMD interaction include increased DGD (B. Huttner and N. Gisin, 1997) and increase in higher order PMD (C. Xie *et al*, 2003) which leads to pulse spreading even at zero DGD (B. Huttner *et al*, 1999).

In the presence of PDL the modified PMD vector \vec{W} has a complex form and is given by:

$$\vec{W}(\omega) = \Omega_R(\omega) + i\vec{\Lambda}(\omega) \quad 2.27$$

where $\Omega_R(\omega)$ and $i\vec{\Lambda}(\omega)$ are the real and the imaginary components of the complex PMD vector. Consequently the motion of SOPs on the Poincaré sphere as the frequency changes is also complex and is of the form:

$$\frac{d\vec{S}}{d\omega} = \vec{\Omega} \times \vec{S} - (\vec{\Lambda} \times \vec{S}) \times \vec{S} \quad 2.28$$

2.8 Statistics of PDL

The stochastic nature of PDL is caused by time dependent orientation of the PDL vector. There exist different views in the literature in regard to the statistics of global PDL involving two or more elements. The global PDL in the absence of PMD is stated to have a Gaussian form of distribution (Gisin, 1995). Numerical simulations showed that the PDF of the decibel global PDL in the presence of small DGD take the form of Rayleigh distribution (Lu *et al*, 2001). A Maxwellian-distribution has been reported for global PDL (dB) and was shown to be independent of the amount of PMD present in the system (Mecozzi and Shtaif 2002, A. Steinkamp et al, 2004). The Maxwellian distribution has been validated for a rather high mean cumulative PDL (~25dB) (Galtarossa and Palmieri; 2003).

Chapter Three

Raman amplification in optical fibres

3.0 Introduction

Raman amplification in optical fibres has been applied in optical communication to overcome signal attenuation and to increase the usable fibre bandwidth. The Raman nonlinear effect was first observed in 1928 (Raman, 1928) but attracted limited interest until 1962 (Woodbury and Ng, 1962) when the phenomenon of stimulated Raman scattering was discovered. The success of Raman amplification in optical communication was prompted by the fabrication of low loss fibres and high power laser sources. This chapter highlights the basics of Raman scattering in optical fibres and explains relevant parameters that influence Raman gain and performance of the amplifier in communication systems. No attempt has been made to exemplify the subject because detailed texts bearing the relevant topics are readily available.

3.1 Origin of Raman scattering

Raman scattering of light is a phenomenon that is due to inelastic nonlinear behaviour of a dielectric medium, such as fibre when subjected to a high intensity optical beam. In this case the effect is known as spontaneous Raman scattering. In the quantum mechanical description (figure 3.1), Raman scattering is most easily understood and involves photon-optical phonon interaction. Raman scattering is different from Brillouin scattering which involves acoustic phonons. Optical photons are inelastically scattered by quantized molecular vibrations called optical phonons (Ashcroft and Mermin, 1976). The photons lose or gain energy to the molecular lattice resulting in scattered light of lower or higher frequency. The lower frequencies ω_s of scattered light are the Stokes-shift (fig 3.1a) and the higher frequencies ω_p are called anti-Stokes shift (fig 3.1b). The anti-Stokes process is very weak in fibres and plays no role in Raman fibre amplifiers. This is because the occurrence of the anti-Stokes shift requires a population inversion in the vibration states, a process which cannot be easily achieved (Boyd, 1992; Singh, 2007).

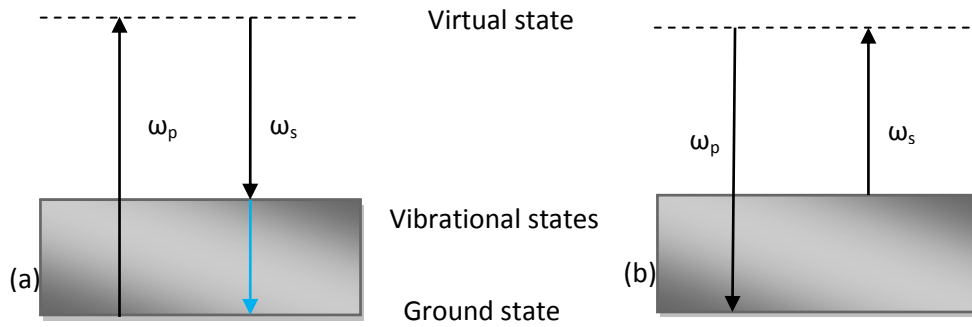


Figure 3.1: (a) Stokes scattering and (b) Anti Stokes scattering process

3.1.2 Stimulated Raman scattering

Stimulated Raman scattering (SRS) occurs when signal light in the Stokes frequencies and a high power pump are coherently coupled by the Raman process. This nonlinear process results in the transfer of power from the pump to the signal and can turn optical fibres into broadband amplifiers. SRS was first observed in fibres by Stolen, (1972) and was initially considered a detrimental nonlinear effect in WDM systems where it can transfer power from a high frequency channel to a low frequency channel causing signal crosstalk (Zhou and Magill, 2004). It is important to note that SRS is polarization dependent and results in polarization dependent gain (PDG) where the gain is maximum when the pump and signal are parallel and minimum if both are orthogonal. The SRS process can be described quantum mechanically in a similar way as the spontaneous Raman scattering. In this case a pump photon is converted to a second signal photon that is an exact replica of the first and the remaining energy is converted into an optical phonon. The virtual state is due to the fact that Raman scattering is non-resonant and is therefore a very fast process (Stolen *et al*, 1989). The continuum nature of molecular vibration states is due to the amorphous nature of silica.

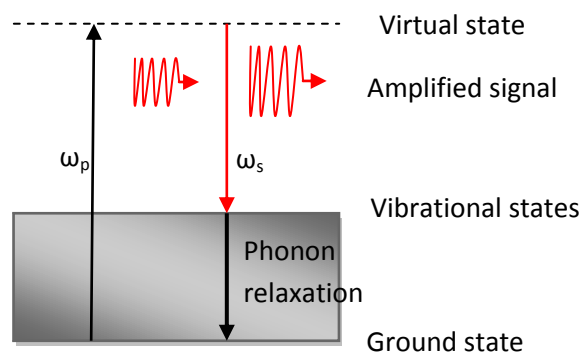


Figure 3.2 Quantum representation of Stimulated Raman scattering

3.1.3 Raman Gain spectrum in optical fibres

The Raman gain spectrum in optical fibres is very broad and extends over a range beyond 40THz as shown in figure 3.3. The broadband gain is a manifestation of the continuum nature of the vibrational states of silica corresponding to different transition states. The frequency difference between the pump and the signal is the Stokes shift or pump –signal detuning. The peak of the Raman gain curve for standard single mode fibres occurs at Stokes shift of about 13.2 THz which is approximately 100 nm bandwidth. The Raman fibre amplifier RFA gain can be flattened for dense WDM application, by employing multiple pumps of slightly different wavelengths (Rottwitt, and Kidorf, 1998; Emori *et al*, 1999). All signals whose wavelengths are within the Stokes shift are amplified via the SRS process.

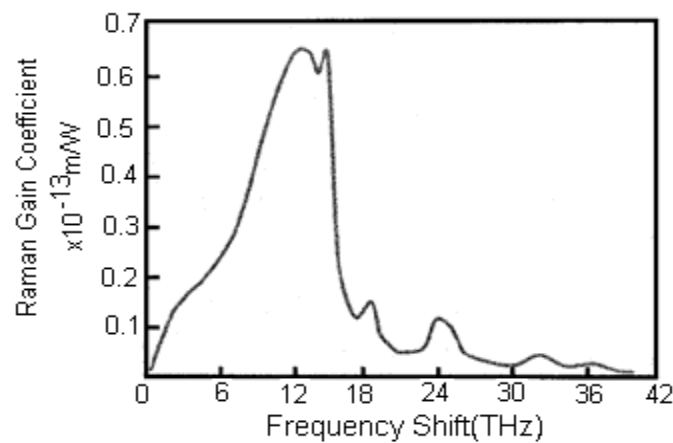


Figure 3 3: Raman gain spectrum in fused silica fibre for co-polarized pump-signal light (After H. Stolen and Ippen, 1973).

The Raman gain coefficient g_R is a function of frequency shift Ω and is the most important parameter for characterizing the Raman amplifier. It is also referred to as the Raman gain efficiency which is the ratio of a nonlinear coefficient $\gamma_R(\Omega)$ and effective area A_{eff} of the fibre. The gain efficiency varies for different types of optical fibres depending on fibre effective area and the level of GeO_2 doping. A standard single mode fibre SSMF has the lowest Raman gain efficiency while dispersion compensating fibre DCF has relatively high gain efficiency (Bromage; 2004). The gain efficiency increases with decreasing pump wavelength (Cordina and Fludger, 2002; Newbury, 2003) which is an added advantage when pumping on the high attenuation frequencies.

3.4 Characteristics of Raman fibre amplifier

The Raman fibre amplifier has several advantages which make it a potential candidate for application in passive optical networks (PONs) (Kjær *et al*; 2007, I. T. Monroy *et al*; 2008). It

is a broad-band amplifier with a bandwidth $> 6\text{THz}$ at full-wave half-maximum (FWHM) and the gain is relatively flat over a wide wavelength range. (Islam, 2002). Unlike the EDFA which requires a specially fabricated fibre, SRS occurs in any fibre and amplification can be achieved at any signal wavelength by choosing the pump wavelength appropriately. This implies that RFA can extend the usable bandwidth of a fibre enabling transmission in the S-band, L and C-band. Beside, the RFA has a lower noise figure and higher gain saturation than the EDFA. The fact that amplification is distributed in RFA greatly reduces the Kerr nonlinear penalty in long haul transmission because the channel's average power remains moderately low (Islam, 2002).

The nonlinear SRS is polarization dependent and depends on the orientation of pump and signal (Stolen, 1997; Dougherty *et al*, 1995). This implies that Raman gain is polarization dependent and is maximum when pump and signal are copolarized and minimum when both are orthogonally polarized. In optical fibres polarization cannot be maintained during signal amplification. This is because polarization mode dispersion PMD present in fibres rotates the pump and signal SOPs at different rates thus changing the pump-signal orientation as both propagate through the fibre. Raman polarization dependent gain PDG is mitigated by depolarizing using the pump. This can be accomplished by using polarization multiplexing of two pumps of same wavelength (Emori *et al*, 2000; Tokura *et al*, 2002), fibre Lyot depolarizers (Böhm *et al*, 1983; Wang *et al*, 1999) and PMD fibre depolarizers (Tokura *et al*, 2006). This unfortunately reduces the Raman gain efficiency by half of the polarized pump (Toge *et al*, 2002) which implies that more pump power is required to compensate for the lost gain.

3.5 Pumping techniques

Raman gain is independent of the relative direction of propagation of a pump and signal. The photon-optical phonon momentum conservation is always achieved irrespective of the relative direction of pump and signal photons (Ashcroft and Mermin, 1976). There are three basic pumping schemes which are popularly used in the research on Raman amplification in optical fibres. The pump and the signal can copropagate in which case the method is called forward pumping. When the pump propagates through the fibre in the opposite direction to the signal, the scheme is called counter pumping or backward pumping. We also have bidirectional pumping where two pumps are employed simultaneously at opposite ends of the fibre during amplification. When pumping is done on the actual transmission fibre linking two points, the setup is referred as a distributed Raman amplifier (Hansen *et al*, 1997). If the

amplifier is pumping a localized DCF in the transmission system (Lewis, 2000) or is placed near the transmitter or receiver end, the system is called a discrete Raman amplifier. The performance of RFA depends on the pumping scheme applied. However, each of these pumping configurations has advantages which make them equally competitive. Forward pumping scheme provides a high optical to signal ratio (OSNR) while bidirectional pumping is appropriate in reducing noise transfer between pump and signal. Backward pumping greatly reduces PDG because of gain averaging as signal and pump traverse each other. The choice of which scheme to adapt can only be determined using performance criteria of a particular RFA design (Kim *et al*, 2007). A thorough treatment of Raman amplification in fibres can be found in the two volumes (Headley and Agrawal, 2005; Islam, 2004).

3.6 Polarized Raman fibre amplifier

Polarization properties of the Raman fibre amplifier (RFA) are related to the imaginary part of the third-order nonlinear polarization in silica (Hellwarth *et al* 1975; Hellwarth, 1977). To understand the amplification process we consider the case for continuous wave CW where a single pump amplifies a signal as both propagate in the fibre. We assume the pump-signal configuration where the signal propagates forward and the pump propagates forward or backward. In Stokes space, the two coupled equations governing the dynamics of pump \mathbf{P} and signal \mathbf{S} are of the form (Lin and Agrawal 2002):

$$\xi \frac{d\mathbf{P}}{dz} = -\frac{\omega_p g_R}{2\omega_s} [\mathbf{P}_s \mathbf{P} + \mathbf{P}_p \mathbf{S}] - \alpha_p \mathbf{P} + (\omega_p \beta + \gamma_p \mathbf{W}_p) \times \mathbf{P} \quad 3.1$$

and

$$\frac{d\mathbf{S}}{dz} = +\frac{g_R}{2} [\mathbf{P}_p \mathbf{S} + \mathbf{P}_s \mathbf{P}] - \alpha_s \mathbf{S} + (\omega_s \beta + \gamma_s \mathbf{W}_s) \times \mathbf{S} \quad 3.2$$

where $\xi = \pm 1$, in the forward and backward pumping configurations respectively, \mathbf{P}_j , α_j and $\gamma_j = n_2 \omega_j / c A_{\text{eff}}$ ($j=p,s$) account for input pump and signal power, fibre losses and nonlinearities at pump and signal frequencies, ω_j is the pump and signal frequencies, A_{eff} is the effective core area of the fibre, $g_R = (\gamma_R / A_{\text{eff}})$ is the Raman gain efficiency, $\alpha_{(p,s)}$ represent the pump and signal attenuation, β is the linear birefringence vector, \mathbf{W}_p and \mathbf{W}_s account for the SPM and XPM induced nonlinear polarization rotation. The boldface symbols imply vector representation of quantities in Stokes space.

The terms in the equations 3.1 and 3.2 can be explained as follows; the first term on the right side of equation 3.1 represents the pump depletion, the second term pump loss and the third

term accounts for the effect of linear and nonlinear birefringence on the pump. Similarly, the first term on the right side of equation 3.2 represents the signal gain, the second term the signal loss and the third term represents the linear and nonlinear birefringence effects on the signal. The pump and signal SOPs rotate as both propagate in the fibre and their motion is governed by the linear birefringence vector β in Stokes space (Ciprut *et al*, 1998). The nonlinear birefringence whose magnitude is intensity dependent induces a nonlinear rotation of polarization ellipse (Maker *et al*, 1964). The equations can be simplified depending on the quantities of interest one would like to investigate and detailed treatment of these equations can be found in chapter two of Headley and Agrawal, (2005).

3.6.1 Average Raman gain

In the small-signal analysis the pump depletion is negligible because the signal power is usually low. The output signal power fluctuates with time due to pump-signal misalignment mostly caused by time variation of birefringence in the fibre. The average gain of the signal is defined as:

$$G_{av} = \frac{\langle P_s(L) \rangle}{P_s(0)} \quad 3.3$$

where $\langle P_s(L) \rangle$, is the average power of the amplified signal at the output end of fibre of length L and $P_s(0)$ is the power at fibre input. The variance of the signal power fluctuation has the form:

$$\sigma_s^2 = \frac{\langle P_s^2(L) \rangle}{\langle P_s(L) \rangle^2} - 1. \quad 3.4$$

Integrating equation 3.2 and using equation 3.3, the average gain G_{av} which is also the net gain can be expressed in the form (C. Headley and G. P. Agrawal, 2005):

$$G_{av} = \exp \left[\frac{1}{2} g_R P_{in} L_{eff} - \alpha_s L \right] \quad 3.5$$

where P_{in} is the input pump power, L_{eff} is the Raman effective length which is defined as the length of a lossless fibre that would achieve the same Raman gain as the actual fibre. In the expression for G_{av} it is assumed that $L_{eff} \gg L_d$, where L_d is the PMD diffusion length which is the length at which the SOPs of the pump and signal are decorrelated. Fibre diffusion length is given by:

$$L_d = 3/D_p^2 \Omega_R^2 \quad 3.6$$

where D_p is the fibre PMD coefficient and $\Omega_R = \omega_p - \omega_s$ is the frequency shift. The fibre effective length L_{eff} is given by:

$$L_{\text{eff}} = \frac{1}{\alpha_p} (1 - e^{-\alpha_p L}). \quad 3.7$$

For a typical transmission fibre the pump attenuation coefficient α_p is ~ 0.25 dB/km and when $\alpha_p L \gg 1$, then L_{eff} is approximately 20km (Rottwitt and Stentz, 2002)

A quantity of importance is the Raman on-off gain G_A which is the ratio of signal power at the output with the pump switched on to the signal power when the pump is off. Alternatively, the on-off gain is equal to Raman average gain minus the fibre loss. That is:

$$G_A = \exp \left[\frac{1}{2} g_R P_{\text{in}} L_{\text{eff}} \right]. \quad 3.8$$

If RFA is operated in the saturation mode, the gain reduces and the above sets of equations do not hold.

3.6.2 Raman PDG and on-off gain

As mentioned in section 3.1.2 Raman gain is polarization dependent and therefore depends on pump-signal orientation. Polarization dependent gain (PDG) is defined as the difference between the maximum and the minimum Raman gain. It has been shown analytically (Q. Lin and G.P. Agrawal, 2003) that when $L_{\text{eff}} \gg L_d$, the average PDG_{dB} in the forward pumping configuration is given by:

$$\langle \Delta \rangle = \frac{4 a g_R P_{\text{in}}}{\sqrt{\pi} D_p |\Omega_R|} \left[L_{\text{eff}} (1 - \alpha_p L_{\text{eff}} / 2) \right]^{1/2} \quad 3.9$$

where $a = 10/\ln 10 \approx 4.343$, P_{in} is pump input power, and D_p is the fibre PMD coefficient.

3.7 Amplified spontaneous Emission noise

An amplified light signal always suffers from optical noise which is generated during amplification. The amplified spontaneous emission (ASE) is an inherent noise which is present in all optical amplifiers. In RFA the ASE is generated by spontaneous Raman scattering which is due to phonon population in the vibration states of silica. Phonon excitation is temperature dependent, thus the ASE noise increases with the temperature of the amplifying fibre (Ashcroft and Mermin 1976). Due to its random phases the ASE is generated in all directions in the fibre but in practice it exists only in the amplifier bandwidth.

The ASE noise performance of a RFA can be describe in terms of a quantity known as optical-signal-to-noise ratio (OSNR) which is defined as the ratio of the signal optical power to the power of the ASE with respect to a given reference bandwidth centred about the signal wavelength. The OSNR is often referenced to 0.1 nm bandwidth when measured with the optical spectrum analyser (OSA). The system OSNR can be improved by filtering the ASE at the amplifier output i.e. by placing an optical filter just before the receiver photo-detector. The OSNR at the amplifier output is defined as:

$$\text{OSNR} = \frac{G_L P_{\text{in}}}{P_{\text{ASE}}} = \frac{P_{\text{in}}}{2n_{\text{sp}} h \nu B_m} \quad 3.10$$

where G_L is amplifier gain, P_{in} is the input signal power, P_{ASE} is the unpolarized ASE noise power, n_{sp} is the spontaneous-scattering parameter also known as population inversion parameter, h is Planck's constant, ν is the optical frequency of noise and B_m is the measurement bandwidth. The factor of 2 in the equation accounts for the two fibre polarization modes. However, if ASE is partially polarized as would happen in the case of pump polarized RFA the P_{ASE} factor takes a value of one because only the component of ASE copolarized with the signal contributes to the ASE noise. (Sun *et al*, 2003).

At the receiver, the photo-detector converts optical power to electrical current in a process that gives rise to mixing between the optical signal power and the optical noise power (Olsson, 1989; Steele, 1991). The detector current contains the signal-spontaneous beat noise which is the dominant noise occurring when signal light interferes with copolarized ASE which is propagating in the same direction. The detector current also includes a spontaneous-spontaneous beating noise term but this noise contribution to current fluctuation is insignificant. This noise terms causes fluctuation of the detector current which may lead to erroneous bit recognition in digital systems.

Beside ASE generation in RFA other effects can also contribute to amplifier noise depending on operating conditions. The main noise factors which can impair the RFA include, the multipath interference noise MPI which is mainly caused by double Rayleigh back scattering (DRBS) and the relative intensity noise (RIN) which is due to pump power fluctuations. Details of generation of these noises in RFA and their control can be found in literature (Bromage, 2004 and Bromage *et al*, 2003).

3.7.1 OSNR and bit error ratio

Optical amplifiers are meant to improve the OSNR of the system but can also degrade the system performance if their noise level is high (Bromage *et al*, 2003). According to equation 3.10 OSNR at the output of the amplifier is degraded if the system noise increases. The bit error ratio (BER) is one of the parameters used to characterize the performance of the system at the receiver end. The system BER is the ratio of the number of bits which are erroneously detected to the total number of bits transmitted in a specified time. For example a BER of 10^{-9} imply that one error can occur for every one billion bits transmitted. BER is related to system quality factor Q, which is the ratio of the difference between the mean powers of digital states and the sum of the standard deviations of the states. The BER can be calculated with respect to system Q using a simplified but valid approximation (Essiambre *et al* 2007; Winzer and Essiambre, 2008). That is;

$$\text{BER} = \frac{1}{Q\sqrt{2\pi}} \exp\left(-\frac{Q^2}{2}\right). \quad 3.11$$

In an amplified fibre optic system where the dominant noise is due to spontaneous emission the system Q can be related to OSNR at the receiver end. That is;

$$Q = \sqrt{\text{OSNR}} \sqrt{\frac{B_o}{B_e}} \quad 3.12$$

where B_o and B_e are the optical and electrical bandwidths respectively. This Q approximation assumes negligible receiver noise (thermal and shot noise) and that other effects such as dispersion, nonlinearities, PMD virtually contribute to the eye closure. Therefore the above equation is only applicable in numerical modelling of receiver responses to amplifier noise. More detailed analysis of BER can be found in (Matera and Settembre, 1996; Iannone *et al.*, 1998).

Chapter Four

PMD effects characterization in Raman fibre amplifier

This chapter investigates the effects of polarization mode dispersion (PMD) in the distributed Raman fibre amplifier (RFA). We focus on the consequences of polarization when single mode fibres of low PMD coefficients are employed in the design of the forward and backward pumped RFA. Using experimental setups as well as simulations we demonstrate the various aspects of PMD effects and quantify the behaviour of RFA gain. Finally we demonstrate the impact of ASE generated noise in distributed Raman amplification based on low PMD fibre.

4.1 Introduction

In fibre optic communication polarization mode dispersion (PMD) effects become significant when light pulses are transmitted over long distances. In high bit rate (>10 Gb/s) optical systems PMD becomes a problem causing inter symbol interference of the transmitted signal (Kogelnik *et al*, 2002). In these cases the effects of PMD on the propagating pulse are described using the concept of DGD. PMD effects can also be observed when a continuous wave (CW) propagates through the fibre. In the frequency domain PMD manifests as a change in the output SOP when the source SOP is fixed at the input and the frequency is varied. This variation in output SOP forms the basis for several PMD measurement techniques (Hernday, 1998). When two wavelengths propagate in the fibre the frequency dependent birefringence rotates their SOPs at difference speeds (Gordon and Kogelnik, 2000). In RFA the effects of PMD can be quantified using the concept of Raman PDG (Headley and Agrawal, 2005). According to their theoretical analysis, PDG in a Raman amplifier behaves in a similar way to PDL and is inversely proportional to fibre PMD. Investigations by Mahgerefteh *et al*, (1997) while using two 2 km spools of randomly birefringent fibre revealed that the length over which Raman gain for copropagating pump and signal becomes independent of the input polarization is determined by the fibre PMD. In another numerical analysis Ebrahimi *et al*, (2001), while investigating the statistics of RFA, found that PDG decreases as the fibre PMD coefficient increases. Similar experimental results were observed by Popov *et al*, (2002) using two dispersion compensated fibres of

different PMD coefficients. Theoretical analysis by Lin and Agrawal, 2003 showed that PMD effects in the backward pumped RFA are far less compared to the forward pumping. Further analysis by Galtarossa *et al*, (2006) revealed that these effects largely depend on the PMD regime under consideration and can be more than previously predicted for backward polarized RFA. While the effects of PMD in RFA have been observed experimentally and analysed theoretically there is the need to review and compare previous results that were based on moderately high PMD fibre with findings based on modern low PMD fibre. When a low PMD fibre is subjected to high optical power such as used with RFA, the resulting nonlinear birefringence may not be negligible and will interact with linear birefringence (Agrawal, 2007). We also find that much of the optical amplifier characterization is based on the EDFA (Derickson, 1998; Desurvire, 2002) which is rarely affected by the fibre characteristics. On the other hand RFA makes use of transmission fibre as the gain media and their characteristics are affected by parameters such as variation in span length, attenuation and the type of fibre (Evans *et al*, 2002). This chapter highlights some issues which are often assumed in the evaluation of PMD effects in RFA.

4.2 Experimental and simulation setup

The schematic shown in figure 4.1 is that of a distributed RFA which was used in performing simulations and experiments. Measurements were obtained for both the forward and backward pumping schemes. Two signal sources namely: a WDM source and a tunable laser were used in the experiments and the choice of a source depended on the particular measurement. In the simulations, commercially available *VPI 8.6 software* was used and has the capability to configure any type of optical device. The signal and the pump were coupled into the fibre using an input WDM coupler while the output coupler was used to couple the backward pump and also separate the signal from excess forward pump. The signal was then filtered of noise before measurement using either the OSA or power meter.

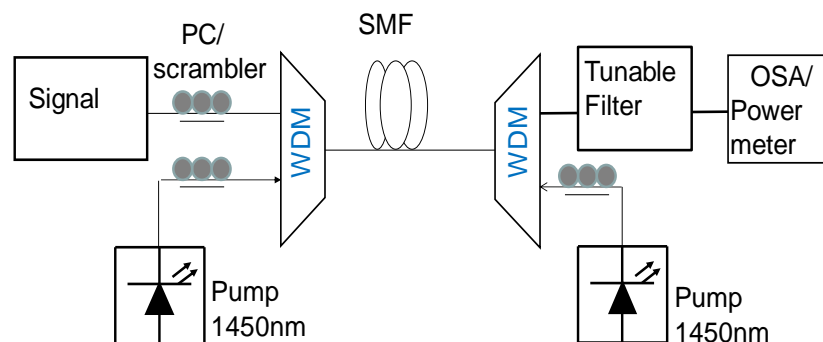


Figure 4.1: Schematic diagram of RFA used in the measurement

4.3 Raman gain and pump power

The dependence of Raman gain with pump power is one of the basic steps we used to characterize PMD effects during Raman amplification. This step served a twofold purpose: firstly, we were able to determine the range of possible pump powers to use in other experiments. Second, we obtained an understanding of how Raman PDG can be managed by choosing an appropriate pump power. This step also enabled us to characterize the newly acquired Raman pump for our optical fibre research unit. In the simulations a 1 mW signal transmitted at a wavelength of 1550 nm and a pump of variable power operating at a wavelength of 1450 nm were propagated through a 25 km single mode fibre (SMF). The pump power was varied over a range of values while different fibres were simulated by varying the PMD parameter. The amplified signal was filtered and detected using the power meter before obtaining the Raman on-off gain. In the experiment, two fibres each of length 24.06 km and PMD coefficients 0.011 pskm^{-1/2} and 0.113 pskm^{-1/2} were used.

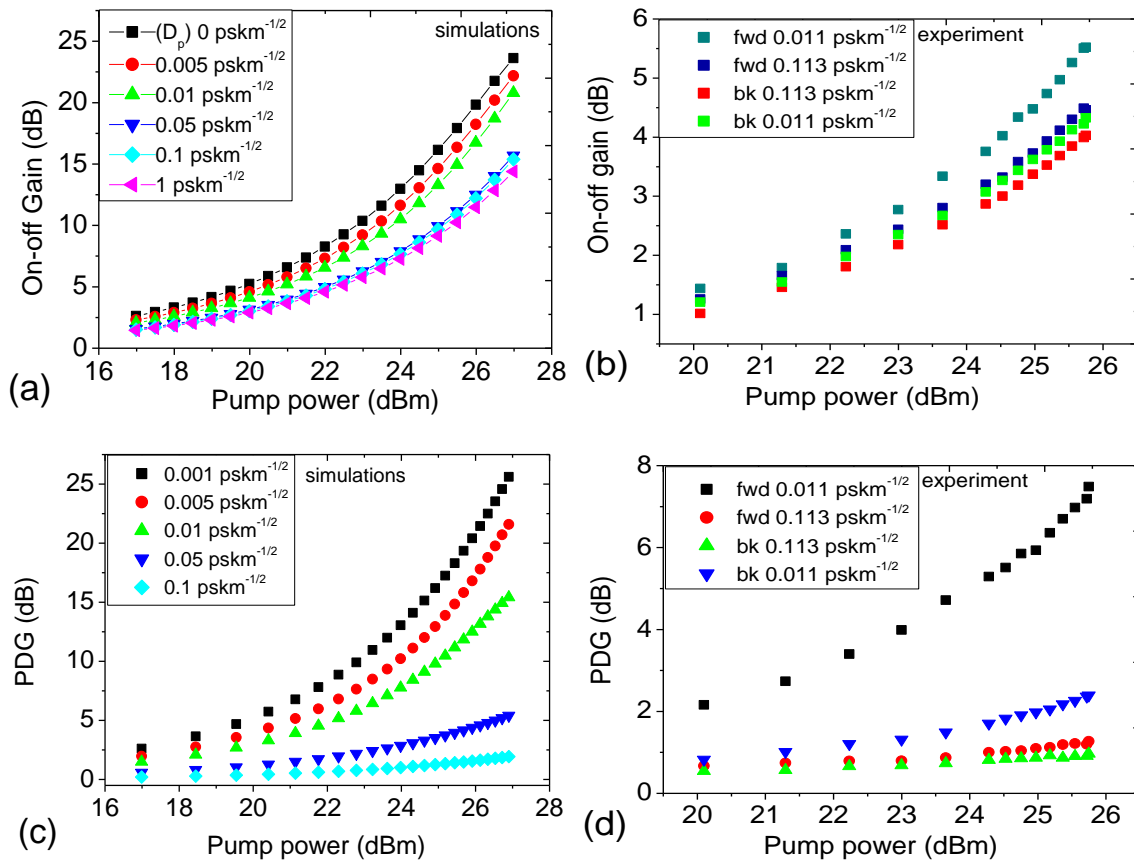


Figure 4.2: Raman on-off gain and PDG variation with pump power for fibres of different PMD coefficients; (a), (c) simulations and (b), (d) experiment (fwd-forward pumping, bk-back pumping).

The signal power was set at -10 dBm while the pump power remained the same as in the simulation. Using the IQS- 1722X high performance power meter the Raman PDG and on-off gain were measured after filtering.

As can be seen in figure 4.2, the experimental results are in agreement with the simulations. However the gains obtained in the experiment are lower because of losses at the splices, and connectors which are not present in the simulations. In addition the fibre attenuation coefficients for pump and signal were assumed to be the same at 0.2 dB/km. In a separate measurement the loss coefficient at pump wavelength was found to be 0.27 dB/km. The Raman gain coefficient g_R of the fibre used in the experiment was found to have a value $0.53 \text{ W}^{-1}\text{km}^{-1}$, at signal wavelength of 1550 nm. This value of g_R is less than the one used in the simulations which is approximately $0.6\text{-}0.7 \text{ W}^{-1}\text{km}^{-1}$ (Dougherty *et al*, 1995; Namiki and Emori, 2001). Simulation results in figure 4.2a were obtained for the forward pumped distributed RFA and show that Raman on-off gain increases exponentially with pump power for different values of the fibre PMD coefficients. The same behaviour was confirmed by experiment (fig 4.2b) using a pump of a maximum output power of 375 mW. As the pump power decreased (<20 dBm) the Raman on-off gain showed least dependence on the pumping scheme employed. The decrease in gain as PMD increased is clearly notable at high pump power as can be seen for power values >24 dBm. Figure 4.2c and 4.2d show the simulations and experimental results which were obtained for Raman PDG. These results show similar behaviour as in the case of on-off gain. In both the simulations and experiment it is observed that PDG reduces drastically even for high pump power if the fibre PMD coefficient is $> 0.01 \text{ pskm}^{-1/2}$. Figure 4.2c presents the gain behaviour of a forward pumped RFA and shows that PDG reduces greatly for PMD coefficients $> 0.05 \text{ pskm}^{-1/2}$, even for high pump power. Figure 4.2d shows that PMD reduces the Raman PDG in a similar way as when counter pumping is used. However, there is a great dependence of PDG with pump power when PMD is very low as can be seen for the fibre of PMD coefficient $\leq 0.01 \text{ pskm}^{-1/2}$. Again, the values of PDG obtained by simulations differ from the experiment due to the same reasons that affected the on-off gain.

4.3.1 Raman gain dependence on fibre length

In the simulation setup the fibre parameter for length was varied between 0-40 km. The pump power was fixed at 200 mW and the signal at 1 mW. With the signal wavelength set at 1550nm the on-off gain and the net gain were determined at each fibre length.

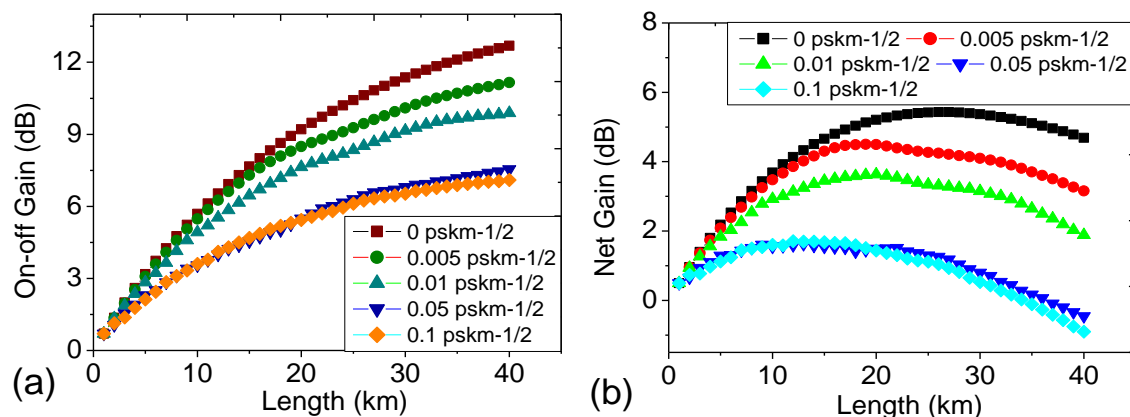


Figure 4.3 Variation of Raman (a) on-off gain and (b) net gain as a function of length.

Figure 4.3 illustrates the results obtained by simulation showing the dependence of Raman on-off gain and net gain on the fibre length in the forward pumping configuration. Raman net gain is different from on-off gain for a given fibre length because the net gain includes signal losses due to fibre attenuation (Headley and Agrawal 2005). That is, the on-off gain is the ratio of output signal power with the pump on to the output power with pump off. Since the signal experiences losses even when the pump is switched on, the ratio eliminates the effect of attenuation in the fibre. In practice there are other causes that would result in signal losses as can occur at the fibre connectors, mid coupler and splices all of which affect the RFA net gain. The net gain can be negative as is the case for the fibres of PMD coefficient $>0.05 \text{ pskm}^{-1/2}$. This is because fibre attenuation or losses increase linearly with length decreasing the power of the pump and signal. When the length L of the fibre is such that $L \gg L_{\text{eff}}$, pump power becomes very low and amplification ceases causing the signal to experience a net loss (equation 3.5). It is evident that both gains increase up to a maximum as fibre length increases. We also observe that the gains have little dependence on fibre PMD, for coefficients $>0.05 \text{ pskm}^{-1/2}$ and depend entirely on fibre length.

4.3.2 Gain and input signal power

In this case the gain was characterized as a function of input signal power. The length of the fibre used in the simulation was 25 km while three fibres, two of which were standard single mode fibre (SSMF) of length 24.06 km and a none zero dispersion shifted fibre (NZDSF) of length 24.7 km, were used in the experiment. The pump power was set at constant value of 200 mW in the simulations and experiment. The source wavelength was set at 1550 nm while the signal power was varied over a range of values. A similar setup was used to perform field measurements of Raman gain on a 28.8 km of buried fibre cable.

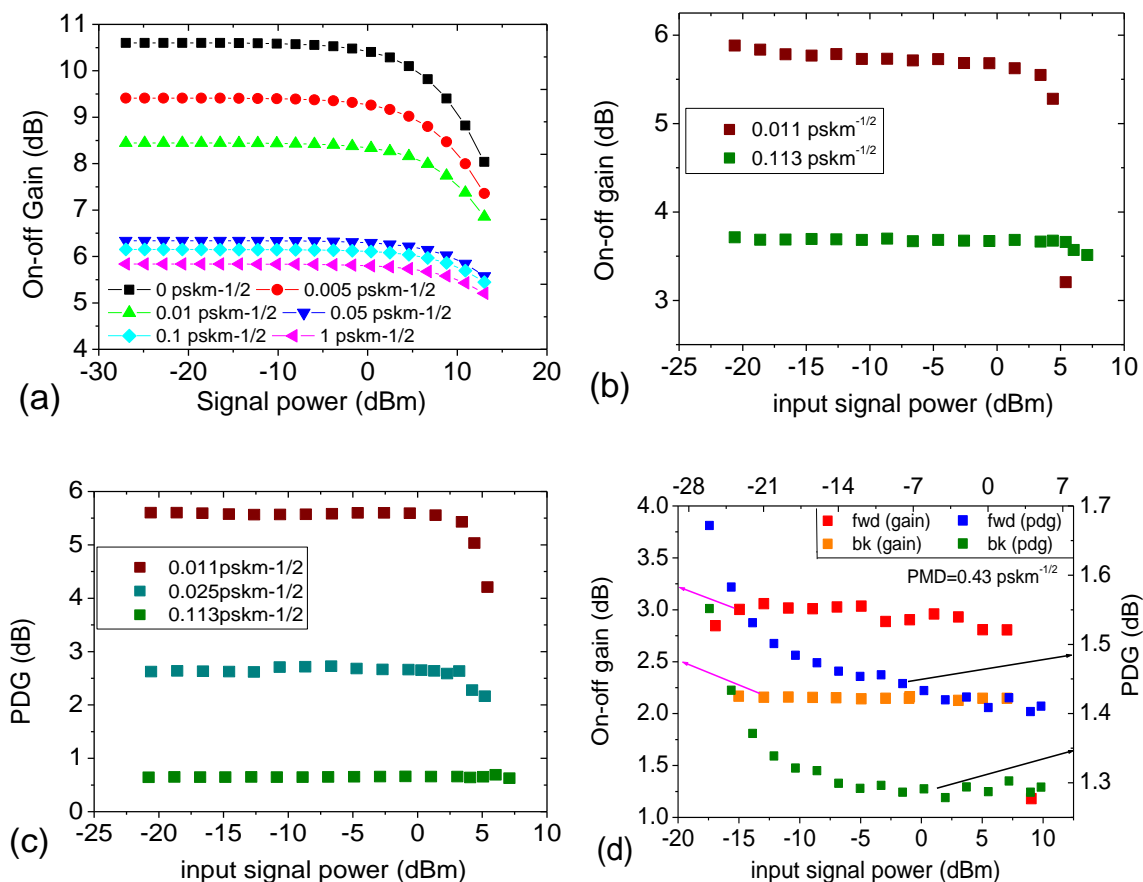


Figure 4.4 Raman on-off gain and PDG as a function of input signal power for different fibre PMD coefficients. (a) simulations, (b),(c) experiments and (d) field measurements at Sidwell TelkomSA exchange at Port Elizabeth (fwd-forward, bk-backward).

Simulation results in figure 4.4a indicate that, the Raman on-off gain is fairly uniform over a wide range of input signal power. The gain saturates as the input signal power increases beyond 0 dBm. As can be seen the signal power at the ‘knee’ (where the amplifier begins to saturate) depends on the fibre PMD coefficient. When the fibre PMD coefficient is low the RFA gain is high and the gain is less if the amplifying fibre has high PMD. Thus the RFA enters into saturation at a lower signal power if the gain is high while saturation occurs at a higher signal power if the gain is low (Ikeda, 1981). This behaviour was confirmed by experimental results in figure 4.4b using two fibres of PMD coefficients, 0.011 pskm^{-1/2} and 0.113 pskm^{-1/2}. These results can be very significant in the design of a RFA for WDM applications where the total power is a function of the number of channels. In this case the total average power of the channels should not exceed the maximum (‘knee’) value if the RFA is designed to operate in the small-signal region. Experimental results in figure 4.4c show the PDG behaviour of three fibres and are similar to those of the Raman on-off gain.

The fibre of PMD coefficient $0.025 \text{ pskm}^{-1/2}$ is a spooled none zero dispersion shifted fibre NZDSF of length 24.7 km. It is important to emphasize the fact that the input signal power has a lower limit below which the gain is no longer uniform. This can be seen in field measurements of figure 4.4d where a deployed cable of length 28.8 km was tested for on-off gain and PDG in both forward and backward pumping configurations. The non uniformity of PDG as the signal power decreases was observed for input powers below -15 dBm. This is because as the signal power decreases the OSNR also decreases and the signal become susceptible to the noise. Similar results have been obtained with EDFA (Desurvire, 1994). The key advantage of RFA is the improvement in noise figure (Islam, 2002) so that lower signal powers can be used in longer transmission distances.

4.3.3 Raman gain and concatenated fibres

Fibre links comprise of several short fibre segments which have been spliced together in cables. It is of interest to evaluate the RFA gain when the PMD of such segments differ slightly. Besides, old deployed fibre has been found to often consist of sections of high and low PMD. (Ehrhardt *et al*, 2008). In this step of characterization two fibres each of length 12.03 km having PMD coefficients of $0.011 \text{ pskm}^{-1/2}$ and $0.162 \text{ pskm}^{-1/2}$ respectively were spliced to make a concatenate of low-high (high-low) PMD fibre of length 24.06 km. The fibre ends were arranged in such a way that would enable the signal coupling from high-low (or low-high) PMD section. The Raman on-off gain and PDG was evaluated in both the forward (fwd) and backward (bk) pumping configurations.

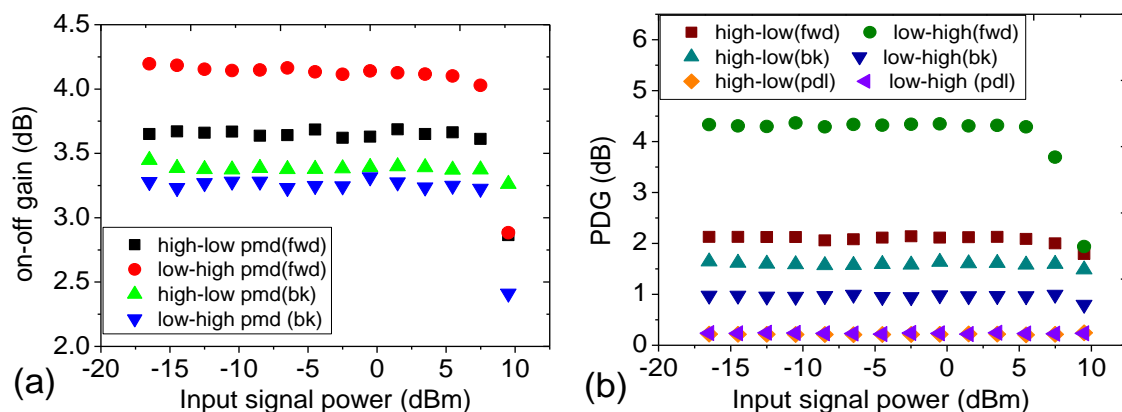


Figure 4.5: (a) Raman on-off gain and (b) PDG as a function of input signal power. The amplifying fibre was obtained by splicing two equal fibres of high and low PMD coefficients.

As is evident in figure 4.5a the on-off gain depends on the end from which the signal is coupled into the fibre. The gain is lower in the forward pumping configuration when the

coupling is from high-low and is high if the coupling is from low-high PMD section of the fibre. In the backward pumping case the gain difference is small with the high-low coupling showing a slightly higher gain. These results can be easily understood by noting that the fibre with low PMD has a higher gain than the one with high PMD. When the pump and signal propagate from low to high PMD fibre, the signal acquires most of its gain in the low PMD section. If the two propagate from high to low PMD fibre the pump is attenuated before it reaches the low PMD section resulting in less signal amplification. In the case of backward pumping the same analysis can be used to explain the slight difference in the gain in the two fibre arrangements. Similar results were obtained for PDG as shown in figure 4.5b and can be interpreted in the same way as with the on-off gain. The composite fibre displayed the same signal PDL when measured on either end as shown in figure 4.5b. The significance of these results lies in the fact that PDG can be drastically reduced in the design of the RFA by using fibres of varying PMD and making proper fibre arrangements. It has been shown theoretically that such an approach would achieve both a low PMD and PDG (Sergeyev *et al*, 2009).

4.3.4 Gain variation with wavelength

The Raman gain coefficient g_R in fibre depends on the pump-signal frequency shift Ω (section 3.1.3) and results in wavelength dependent Raman gain. It is therefore important to characterize the behaviour of the gain spectrum at different PMD coefficients. In the simulation the source wavelength was swept over the range between 1530 nm and 1565 nm in the forward pumping configuration while the fibre PMD coefficient was varied between $0.005 \text{ pskm}^{-1/2}$ and $0.1 \text{ pskm}^{-1/2}$. The length of the fibre was 25 km while the pump and signal powers were set at 200 mW and 1 mW respectively. In the experiment two SMF each of length 24.06 km and PMD coefficients $0.011 \text{ pskm}^{-1/2}$ and $0.113 \text{ pskm}^{-1/2}$ were used in the backward pumping configuration. The pump power was set at 22 dBm while the input signal was set at -10 dBm. The wavelength of a tunable laser source was varied between 1525 nm and 1565 nm and the gain determined for each wavelength. In the experiment wide bandwidth circulators were used instead of WDM couplers which have narrow bandwidth of $\pm 5 \text{ nm}$.

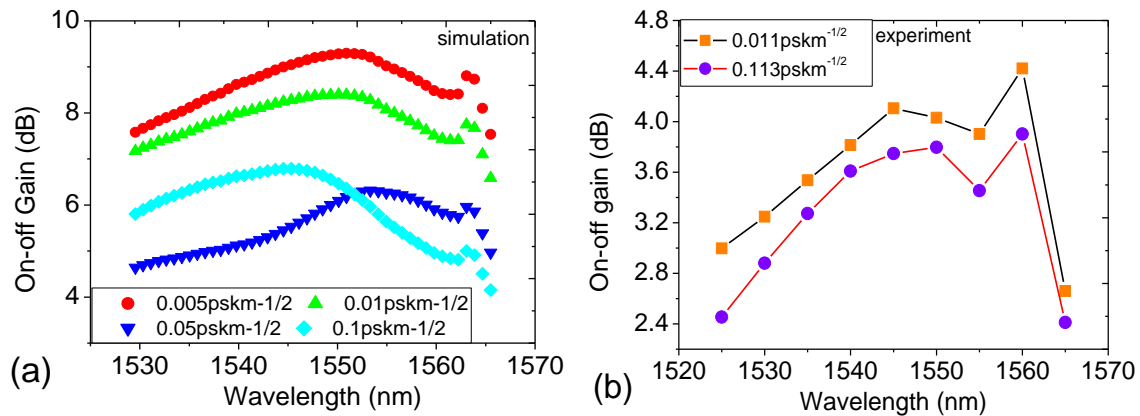


Figure 4.6 Variation of on-off gain with wavelength (a) simulations (b) experiment.

The results shown in figure 4.6 resemble the Raman gain spectrum for bulk silica (Stolen 2000; Bromage, 2004) where the gain increases with pump-signal detuning up to the peak wavelength before it starts decreasing. As can be seen in both simulations and experiment the gain is PMD dependent and decreases evenly with increasing fibre PMD for the entire amplification bandwidth. However simulation results in figure 4.6a show that for wavelengths below 1550 nm, the fibre with PMD coefficient of $0.1\text{pskm}^{-1/2}$ has a higher gain than that of PMD coefficient $0.05\text{pskm}^{-1/2}$. We can understand this behaviour by noting that the randomly distributed fibre birefringence is wavelength dependent (Rashleigh, 1982) which consequently influences the Raman gain. In the weak birefringence regime the pump and signal maintain their orientation over the amplification length and the signal gain is fairly high as in the case of fibres with PMD coefficient $<0.01\text{pskm}^{-1/2}$. In this regime the birefringence is also weakly dependent on wavelength. In the intermediate birefringence regime the pump-signal orientation cannot be sustained along the fibre. This results in gain fluctuation as can be seen with the fibre of $0.05\text{pskm}^{-1/2}$ PMD coefficient. We also have strong birefringence where the pump-signal SOP's rotation is maintained resulting in minimum gain fluctuations due to gain averaging. This strong birefringence is highly wavelength dependent. Alternatively, the results in figure 4.6a can be understood by considering the PMD bandwidths (section 2.3) of the four fibres used in the simulation. Simulated results displayed higher values of gain than was obtained by experiment. The difference largely depended on the Raman gain model used in the simulations and that no signal losses are created. Also noted is gain tilt with wavelength as the fibre PMD increases.

4.4 Influence of signal input states of polarization on Raman amplification gain in single mode fibres.

Theoretical analyses of Raman amplification in optical fibre suggest that the gain depends only on the pump-signal orientation (Lin and Agrawal 2003). It has been shown experimentally (Popov *et al*, 2004) that Raman gain also depends on the pump input SOP and that this gain dependence results in two pump SOPs which provide the maximum and minimum PDG. In this analysis we looked at the signal input states to evaluate their influence on Raman gain. The six degenerate SOPs that were used to illustrate the gain dependency are; Linear horizontal (LH), linear vertical (LV), linear+45 (L+45), linear-45 (L-45), right circular (RC) and left circular (LC) polarizations. A manual polarization controller (PC) was used to set the signal input SOPs which were monitored using a polarimeter, before coupling with the pump. The pump power was set at 22 dBm and the pump was scrambled at low speed to provide all input states of pump polarization. At the fibre output the amplified signal was filtered before the measurement using IQS 722xx high performance power meter.

4.4.1 Low PMD fibre

In this case, a WDM source operating at a wavelength of 1550 nm was used to provide a variable signal power while the pump power was set at 22 dBm. The fibre length was 24.06 km and PMD coefficient $0.011 \text{ pskm}^{-1/2}$.

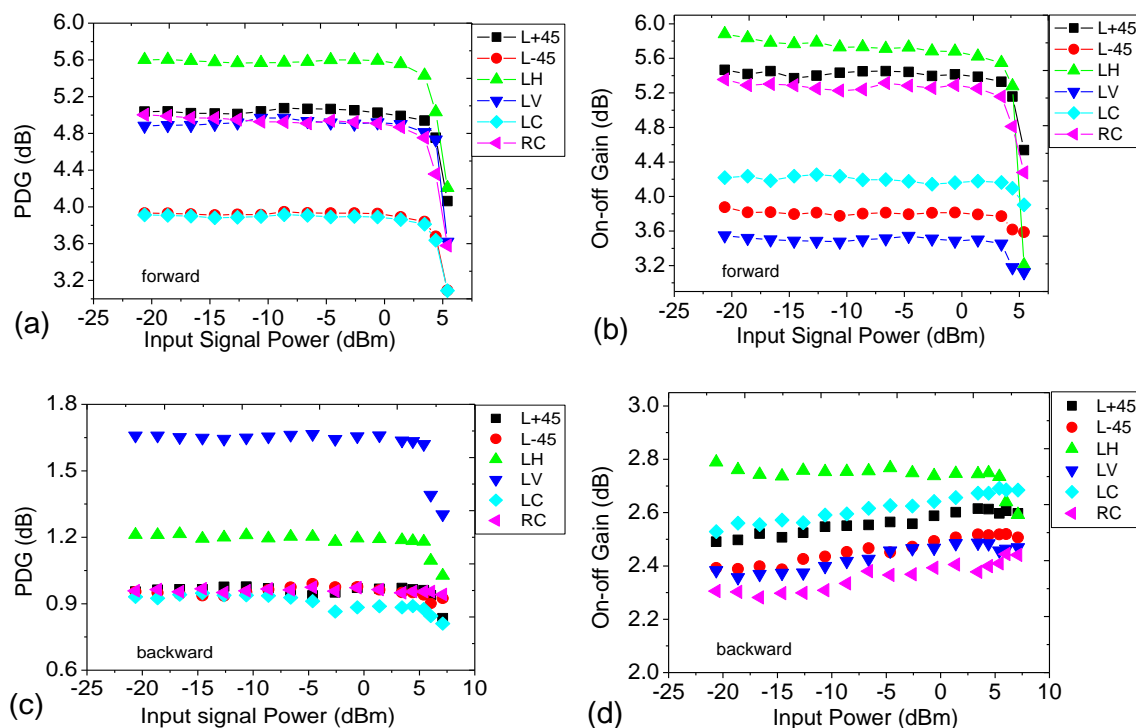


Figure 4.7: Dependence of Raman PDG and on-off gain on the input signal SOPs. (a) and (b) represent forward pumping, (c) and (d) represent backward pumping

As shown in figure 4.7 the Raman PDG and on-off gain highly depend on the input signal SOP. In the forward pumping case (fig 4.7 (a) and (b)) the PDG difference for LH-LC polarizations is > 1 dB while the on-off gain difference for LH-LV polarizations is >2 dB. The backward pumping (fig 4.7 c and d) also show a significant gain dependence on SOP of the signal at the input. There is a dependence of the amplifier level of saturation with the input signal SOP due to the same reason as given in section 4.3.2. It should be noted that the results in figure 4.7 cannot be used to predict the SOP that would provide the maximum or minimum gains. For example in the forward pumping (fig 4.7 (a) and (b)) the LC polarization provided the lowest PDG while the LV polarization provided the lowest on-off gain. The pumping configuration is also a contributing factor to the SOPs with maximum and minimum gains.

4.4.2 High PMD fibre

To investigate the influence of PMD on gain variation with the signal input SOPs, a fibre of similar length and PMD coefficient $0.113\text{pskm}^{-1/2}$ was used. By following the same procedure as used with the low PMD fibre, both the variation of the gain with signal input power and with the source wavelength were demonstrated. The small wavelength range of 10 nm involved was due to the narrow bandwidth of the WDM couplers.

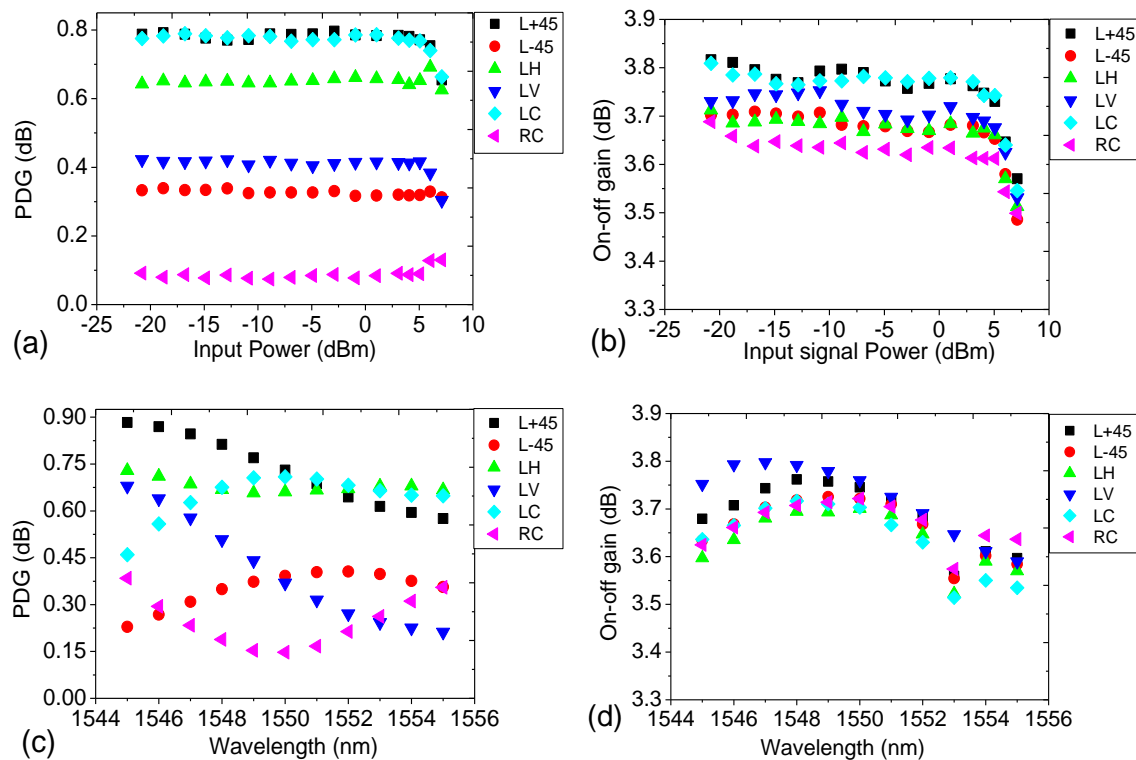


Figure 4.8: Dependence of Raman PDG and on-off gain with signal input SOPs for a high PMD fibre ($D_p=0.113\text{pskm}^{-1/2}$) in the forward pumping configuration.

The results in figure 4.8 show that when the fibre PMD is high the gain dependence on input SOP of the signal decreases. In this case, the difference between the maximum and the minimum PDG is less than 1 dB. However the PDG curves corresponding to the six signal SOPs at the input are well defined just as in the case of the low PMD fibre. The on-off gain curves in figure 4.8b show negligible dependence on the signal input SOPs. This is because the relatively high birefringence effectively rotates the pump and signal SOPs as both propagate in the fibre resulting in average gain. When the source wavelength is varied as in figure 4.8c the PDG variation with the signal input SOPs becomes wavelength dependent. The difference between the maximum and minimum PDG is still < 1 dB over the small bandwidth and narrows as the signal wavelength increases. Figure 4.8d show the variation of the on-off gain with the wavelength. Again in this case, the gain is clustered and show negligibly small dependence on the SOPs particularly for the wavelengths > 1550 nm. Apart from the fibre PMD contribution to the clustering of the gain, the decreasing Raman gain coefficient for the wavelengths between 1550 nm and 1560 nm is also a contributing factor. This is what was observed in the Raman gain spectrum for the two fibres in the backward pumping configuration (section 4.3.4).

4.4.3 Effect of fibre length on SOPs dependent gain

The dependence of the Raman gain on the length of the amplifying fibre prompts us to look into the length contribution to the SOPs with maximum or minimum gain. Two fibres of lengths 12.03 km and 24.06 km and having same PMD coefficients of $0.011 \text{ pskm}^{-1/2}$ were used. In each of the two setups the same pump power was applied in the forward pumping configuration while following the same procedure as outlined in section 4.4.

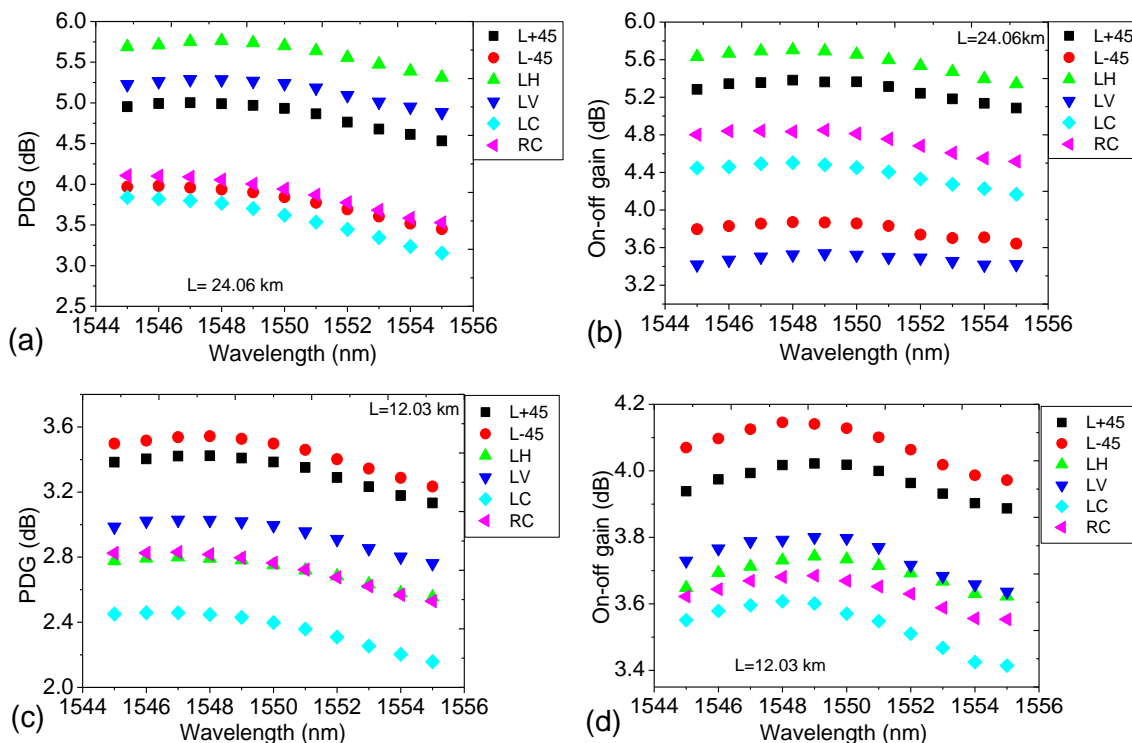


Figure 4.9: The length contribution to SOP dependent Raman gain. In (a) and (b) the fibre length is 24.06 km and in (c) and (d), the length is 12.03 km.

One thing is notable in figure 4.9 that for each of the SOPs, the gain variation is well streamlined over the small bandwidth of 1.25 THz. Comparing figure 4.9a and 4.9b it is clear that LH polarization is the only SOP that has corresponding maximum PDG and on-off gain. The other five input SOPs changed their positions randomly in the two curves. This behaviour is due to the fact that Raman on-off gain grows faster than PDG as the length of the fibre increases. It is therefore not easy to predict the SOP with corresponding maximum or minimum gain for this length of fibre. Figure 4.9c and 4.9d which is a case of short fibre length shows good correlation of the SOPs. That is the SOP displaying maximum or minimum PDG also contribute the maximum or minimum on-off gain. The reason for these well defined trajectories is attributed to PMD diffusion length of the fibre. For a low PMD fibre the diffusion length approaches the actual length of the fibre so that polarization mixing is highly inefficient. On the other hand a high PMD fibre has a small diffusion length and as such the mixing of the pump and signal SOPs is very efficient (Lin and Agrawal, 2003). We also note that the gain appear much more tilted for the 12.03 km fibre than for the longer 24.06 km fibre. This tilting is related to the difference in gain in the two fibres. Such gain tilt has been observed in EDFA (Hansen *et al*, 1993) and has been attributed to changes occurring at the amplifier input.

4.4.4 Gain variation with arbitrary SOPs

It is important to mention that the results in this section are not an independent study but serve as an extension to what has already been discussed. The aim here is to consolidate the idea of SOPs characterization of the gain by considering other signal SOPs and fibre PMD coefficients. In the simulation setup the signal power was set at 1 mW and the source wavelength at 1550 nm. The pump polarization at the input was changed by sweeping the polarization controller azimuth and ellipticity angles while keeping the input signal SOP fixed. The signal SOP at the input can be set to any of the six degenerate states but they all lead to similar results. In this case the signal SOP was set at LH polarization.

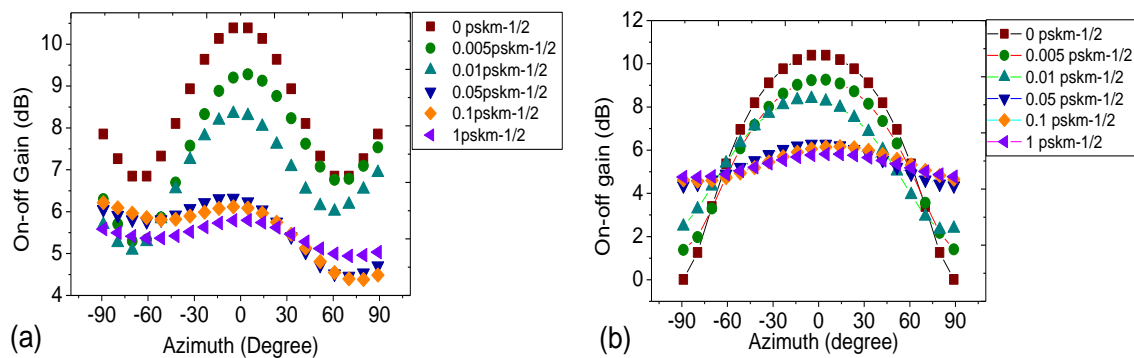


Figure 4.10: Simulations of (a) On-off gain variation with Azimuth angle of polarisation ellipse for various PMD fibre coefficients (azimuth and ellipticity both varied) (b) on-off gain variation with azimuth (constant ellipticity (0°)).

Figure 4.10 shows the simulation results obtained for on-off gain for fibres of varying PMD coefficient in the forward pumping configuration. It is evident that the weak birefringence is one of the reasons for the manifestation of the SOP dependent gain. At fibre PMD $> 0.05 \text{ pskm}^{-1/2}$ there is minimum gain variations as the input SOP of the pump is varied. At low fibre PMD the LH polarization displayed the maximum gain because the pump and signal are then aligned at the input resulting in the best coupling condition. As fibre PMD increases the initial coupling of the pump and signal is destroyed due to the rotation of their SOPs at different rates (Gordon and Kogelnik, 2000) resulting in low average gain. In figure 4.10a the pump azimuth and ellipticity was changed simultaneously between $(-90^\circ, -45^\circ)$ and $(90^\circ, 45^\circ)$ which correspond to LC and RC polarizations respectively. Thus, the LC pump polarization shows similar coupling for fibres of PMD above $> 0 \text{ pskm}^{-1/2}$. In figure 4.10b only linear states of the pump were launched and as can be seen, the gain is zero for a fibre of PMD coefficient $0 \text{ pskm}^{-1/2}$, if the pump and signal are orthogonally aligned at the input.

Therefore the small fibre PMD is necessary in rotating the initially orthogonal SOPs of the waves as they both propagate in the fibre thereby assisting the signal gain.

4.5 PMD effects and optical noise

The generation of noise during amplification is inevitable and is present in all optical amplifiers. In spite of its low noise characteristics (Rottwitt and Stentz, 2002), RFA noise can still reach unacceptable levels depending on the operating conditions. During the experiments we observed that the RFA would turn noisier depending on the environmental conditions. There are several sources of optical noise in RFA as mentioned in section 3.7. However the most important source of noise in RFA is amplified spontaneous emission (ASE) which is temperature dependent. In this work we limit our investigation to a system dominated by ASE generated noise. We investigate the fibre PMD contribution to the effects of ASE noise and the implication to the performance of amplified optical systems. The noise properties of RFA can be described by measuring the optical signal to noise ratio (OSNR) during amplification of the signal. In the simulation analysis (Fludger *et al*, 2000) using optical fibres of different properties it is shown that the OSNR of a distributed RFA improve as the pump power increase.

In the experiment we used the optical spectrum analyser (OSA) to measure the OSNR of a RFA as a function of the signal wavelength. The OSA was set to determine the OSNR over a reference bandwidth of 12.5 GHz. Two fibres each of length 24.06 km and PMD coefficients $0.011 \text{ pskm}^{-1/2}$ and $0.113 \text{ pskm}^{-1/2}$ were used in the measurements. The signal from a tunable laser source was set at -10 dBm while the pump power was set at 21 dBm in both the forward and backward pumping configurations. The signal was coupled with the pump using wide bandwidth filter-based WDM couplers.

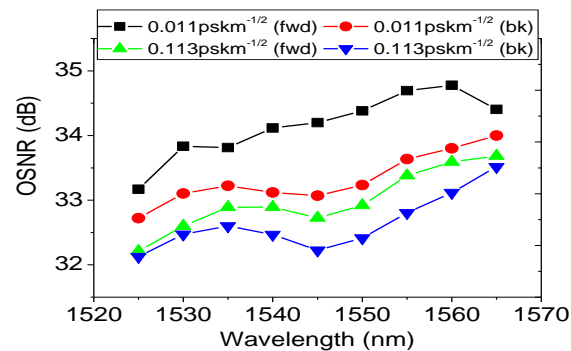


Figure 4.11: The variation of OSNR with wavelength for the two fibres in the forward (fwd) and backward (bk) pumped distributed RFA.

Figure 4.11 shows the OSNR as a function of the signal wavelength which was obtained using the two fibres. The OSNR increases moderately with pump-signal detuning in both fibres. This is caused by the fact that Raman gain efficiency (g_R/A_{eff}) increases with wavelength shift up to the peak frequency. One would expect OSNR to decrease after the peak wavelength but this is not the case. The reason for this behaviour is that the ASE generated noise is less for signal wavelengths that are farther from the pump wavelength than those that are near (Namiki *et al*, 2005). The fibre with low PMD coefficient has higher OSNR over the entire wavelength range in both pumping schemes. This is because the signal gain increases with decreasing fibre PMD coefficients and this translates into higher OSNR values. Higher values of OSNR were observed during forward pumping in each fibre which is an indication that backward pumping scheme is noisier.

4.5.1 Impact of ASE noise on system performance

The ASE noise of a distributed RFA accumulates along the fibre resulting in the degradation of the system OSNR at the output. In this case the system performance is mostly limited by the OSNR rather than the optical power received. Thus the receiver sensitivity is qualified by its ability to resist the influences of waveform distortion and optical noise (Essiambre *et al*, 2007). In this study we simulated the BER of a distributed Raman amplified link using the ASE noise loading technique (Hui, and O'Sullivan; 2009). The forward pumped simulation setup is shown in figure 4.12 and consists of a non-return to zero (NRZ) transmitter (TX) operating at 10 Gb/s at a carrier wavelength of 1550 nm and an ASE source. The choice of NRZ data format in this investigation is simply because it is used as a reference to other modulated data formats (Krummrich, 2007).

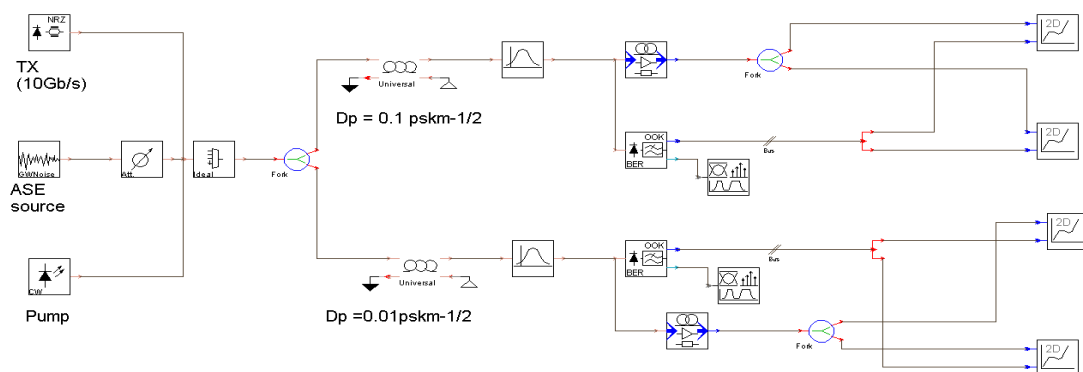


Figure 4.12: Simulated diagram of a distributed Raman amplified fibre link (see appendix V for an enlarged version)

Two SMFs each of length 100 km were used and their other specifications were set to be similar to those used in the experiment while the dispersion effect was assumed negligible. The pump power was set at 24 dBm to amplify a channel of 1 mW input power in the small signal gain region (no pump depletion). During the measurement the ASE source power was varied resulting in different values of OSNR at the receiver. The excess noise at the fibre output was filtered using a band pass filter at 40 GHz bandwidth (B_m). The receiver electrical filter bandwidth was set at 5 GHz to ensure that only the ASE generated noise co-polarized with the signal at the fibre output was used to determine the system BER. It should be noted that the receiver shot noise and thermal noise are assumed negligible compared with noise from the amplifier. Therefore only the ASE generated noise at the receiver is considered in the simulations.

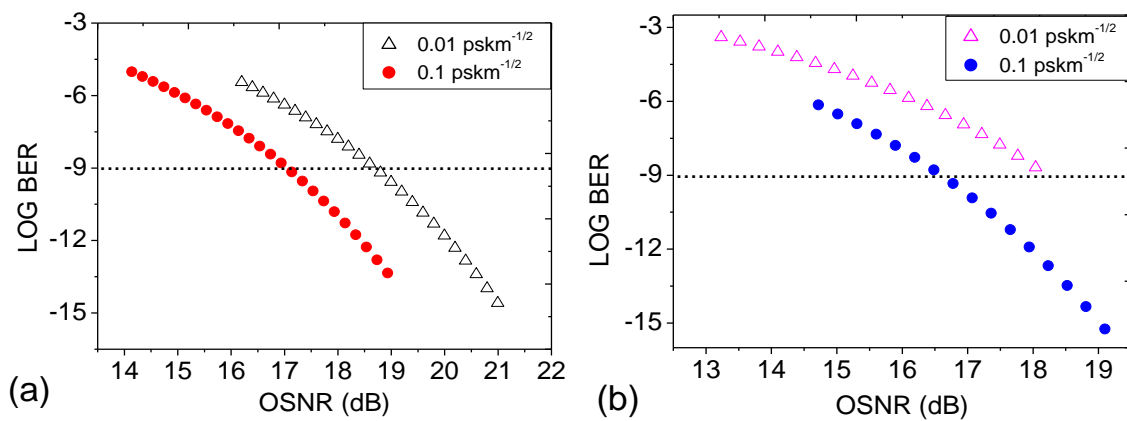


Figure 4.13: BER as a function of OSNR (a) forward pumping (b) back pumping configuration.

In figure 4.13 are the simulated results showing the variation of BER as a function of OSNR for the two fibres when the same range of ASE noise power is applied. In the forward pumping scheme (fig 4.13a), the 0.01 pskm^{-1/2} fibre has a better OSNR and therefore lower BER values while the fibre of 0.1 pskm^{-1/2} shows higher values. That is, the curve of the 0.01 pskm^{-1/2} fibre is shifted downward to lower BER values while that of the 0.1 pskm^{-1/2} fibre cannot attain the same low BER values, for the same range of loaded ASE noise. The difference in the BER performance of the two fibres is due to the fact that the lower PMD fibre provides a higher Raman gain to the signal. For the lower PMD the gain is higher because there is less scrambling of the SOPs, hence the SOP of the pump and the signal remain more coplanar. In the case of backward pumping (fig4.13b) the opposite happens where the lower PMD fibre shows higher BER values for the same range of ASE noise power. The minimum BER is above the acceptable 10^{-9} value. In this case the fibre with PMD

coefficient of $0.1 \text{ pskm}^{-1/2}$ has good ASE noise performance. This behaviour can be understood if we consider the fact that spontaneous noise generated near the input end of the fibre experiences less loss throughout the amplification length in the case of backward pumping, whereas the same noise experiences more losses in the case of forward pumping (Headley and Agrawal, 2005). At the same time signal losses occur throughout the full length of fibre in the case of backward pumping and most signal amplification occurs near the fibre output end where spontaneous noise is high compared with the signal (Jordanova, and Topchiev; 2008). Following this explanation and also the fact that the lower PMD fibre has higher Raman gain, its poor signal-ASE beat noise performance in the backward configuration can be understood. Its high Raman gain results in the spontaneous noise generated gaining more power compared to the same noise generated in the case of the high PMD fibre. We note here that Raman gain is limited by the input pump power P_{in} and fibre effective length (L_e) which is as a result of pump decay during propagation in the fibre (Lin and Agrawal, 2003). The long length of fibre used in the simulation may be another contributing factor to the nature of results observed in the case of backward pumping (Zyskind *et al* 2002)

4.5.2 Effects of ASE noise on the eye diagram

The same setup in figure 4.12 was used to investigate the effects of ASE generated noise on the eye pattern. The eye pattern was plotted by sending an alternating bit sequence of length 2^7-1 to the receiver when the ASE source spectral noise density was set at $5 \times 10^{-16} \text{ W/Hz}$.

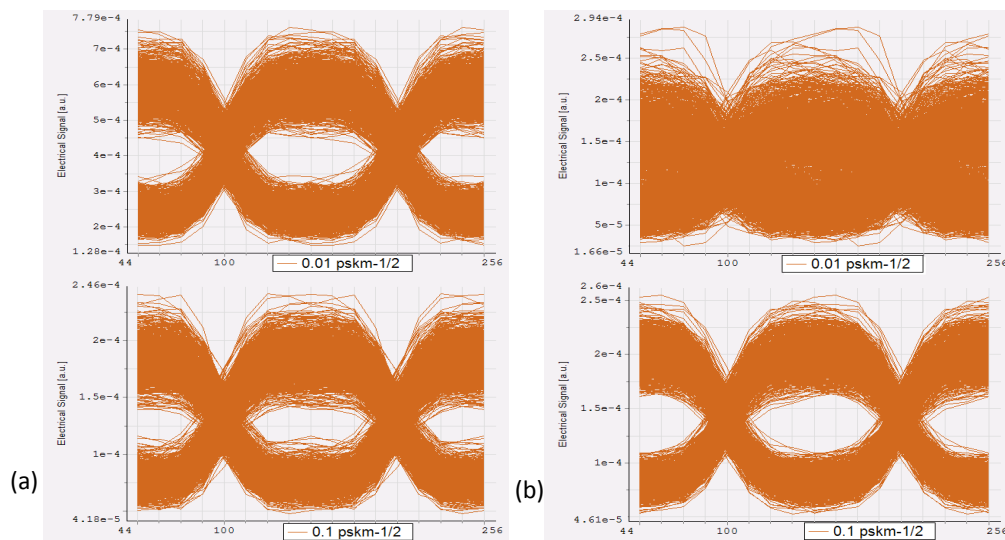


Figure 4.14 Eye diagrams of the two fibres in the (a) forward pumping and (b) backward pumping configuration.

Figure 4.14 is the simulated eye pattern after the NRZ modulated data was transmitted in the Raman amplified SMFs. In the forward pumping case (fig 4.14a) spontaneous noise effects on the eye diagram are almost the same for the two fibres. However, the eye opening of the fibre with higher PMD coefficient is slightly narrower and has less power than the eye of the low PMD fibre. This can be attributed to the lower signal gain of the high PMD fibre. In the case of backward pumping (fig 4.14b) the eye closure is complete for the low PMD fibre while the eye opening of the relatively high PMD fibre is moderate.

It is evident in both pumping schemes that ASE noise adds to the amplified signal and affects the eye by changing the power level of “ones” and “zeros” in a bit sequence. The difference observed in the “ones” and “zeros” is due to Raman gain of the channel which occurs when the laser light is on, and when the light is off no amplification takes place. Spontaneous noise effects observed on “zeros” is attributed to the fact that the externally modulated laser was simulated to provide a non-infinite signal extinction ratio (Pauer and Winzer; 2003). It is also worth noting that the eye closure depended on the spectral noise density and in this case only the worst case results were presented. Other results not presented showed that as the ASE spectral noise density decreases the eye opening increases, depending on the fibre PMD coefficient and the pumping scheme employed.

In summary Raman PDG and on-off gain in a transmission fibre depends on the fibre PMD, pumping scheme and frequency detuning of the channel. In low PMD fibres the gain depends upon the input SOPs of the signal, a factor that is attributed to coupling of pump and signal energies into the PSPs of the fibre. Spontaneous noise which is a by-product of amplification accumulates throughout the amplified transmission fibre and degrades the OSNR at the fibre output. The system OSNR depends on the fibre PMD and the pumping configuration. Forward pumping has superior ASE noise performance compared with backward pumping. The quality of signal at the receiver is consequently determined by Raman amplification and PMD effects. A low OSNR manifests itself as high BER and decreases the eye opening. A fibre with high PMD would perform better in the case of backward pumping. However, in a high bit rate system (>40 Gb/s) high PMD would cause inter-symbol interference thereby reducing the quality of the signal. In addition, PMD is complicated by random mode coupling in long fibres which makes the temporal response of the fibre to be undeterministic. This temporal response of fibre PMD is complicated further due to its sensitivity to environmental changes. The gain of RFA operating under changing environmental conditions will fluctuate

with time causing system instability. However in buried fibres of low PMD this temporal behaviour is minimum and consequently the detrimental effects of PMD are also reduced.

Chapter Five

Statistics of the Raman gain in single mode fibres

The characterization of Raman fibre amplifier (RFA) with respect to fibre polarization mode dispersion (PMD) discussed in chapter 4 shows that Raman on-off gain and polarization dependent gain (PDG) are closely related quantities. This implies that, even though each of these gain quantities has different implications in regard to the nature of the amplified signal, we can in many aspects obtain the behaviour of one by simply analysing the other. In this chapter we investigate the statistics of Raman gain using both high and low PMD fibres. We include results on the net gain, on-off gain and signal power fluctuations which were obtained for the three pumping schemes using polarization scanning techniques. Finally we demonstrate how the PMD coefficient of a fibre can be extracted by simply measuring the PDG and on-off gain of the signal.

5.1 Introduction

Previous analysis of Raman gain statistics as found in the literature show that gain fluctuation depends on the fibre PMD and the pump DOP. While using a complex experimental setup Ebrahimi *et al*, (2001) investigated the statistics of PDG in RFA using a 10 km DSF of $0.06 \text{ pskm}^{-1/2}$ PMD coefficient. Together with simulation results they found that the PDG decreases with PMD coefficient. The statistical properties of PDG were studied by Kee *et al*, (2002) using monte-carlo simulations and experiment. In their experiment, the Raman added gain or on-off gain was found to depend on DOP and the pumping configuration. In another study (Popov *et al*, 2002) it was found that the PDG is frequency shift dependent and decreases as the pump-signal frequency shift increases. In their study E. Son *et al* (2004 and 2005) developed an analytical model to describe the statistics of PDG in a Raman amplifier. Their model incorporated several design parameters and they found that the PDG of a RFA could be reduced by using a pump laser with low DOP, large frequency shift and a low-loss fibre of high PMD. Theoretical analysis of the Raman gain fluctuation induced by PMD was studied by Lin and Agrawal, (2002). They found that signal fluctuation becomes large for fibres of small PMD coefficient. In another theoretical analysis of the statistics of PDG, Lin and Agrawal, (Feb 2003) found that the average PDG is inversely proportional to the fibre

PMD coefficient. Similar results were obtained by Azami, (2004) while using a model based on the Jones matrix.

In our view the study of Raman gain statistics is still an important subject in the analysis of RFAs using modern optical fibres. Firstly, the results obtained in the previous studies are rather general and therefore not conclusive. For example it was shown analytically that gain fluctuations in the backward pumping is less by a factor of 30 at the wavelength shift of 13.2 THz (Lin and Agrawal, 2003). Elsewhere (Son *et al*, 2005) it was shown theoretically that backward pumping gain fluctuation is a third of the forward gain fluctuations. In this case no consideration was made on the contribution of different fibre PMD regime to gain fluctuations. In most of the experimental studies it has been assumed that gain fluctuations in the backward pumping are small. Again, we find that experimental work on this subject involves either monitoring the instantaneous gain changes with PMD (Ebrahimi *et al*, 2001, Son *et al* 2004) or scanning only the input SOPs of the signal (Popov *et al*, 2002; Mesquita *et al*, 2003). Monitoring gain fluctuations due to time changes in fibre PMD can be time consuming and may not be viable especially when low PMD fibres are involved. This is because such fibres have their PMD changing very slowly with time (Karlsson *et al*, 2000). At the same time, polarization scanning of the signal may largely influence the results since the Raman gain depends not only on pump-signal orientation but also the input SOP of pump and signal (Popov *et al*, 2004). In this work polarization scanning at the input of the RFA was implemented by scrambling both the pump and the signal. Other practical limitations encountered during the experimental work include the unavailability of a fibre of required length and PMD coefficient.

5.2 Statistics of net gain

Investigations of Raman net gain fluctuations were conducted by simulation using different fibre PMD coefficients. The simulation setup shown in Figure 5.1 consisted of a 1550 nm signal source, a 1450nm Raman pump operating at 200 mW, both of which were coupled into the fibre via a WDM coupler. The input signal was set at 1 mW before splitting it into two, to obtain the reference signal. The amplified signal was filtered and detected after 25km of amplification in a single mode fibre (SMF). Fibres of different PMD coefficients were used and signal net gain determined statistically with the pump polarized and when the pump was depolarized. The process was repeated for backward pumping configuration.

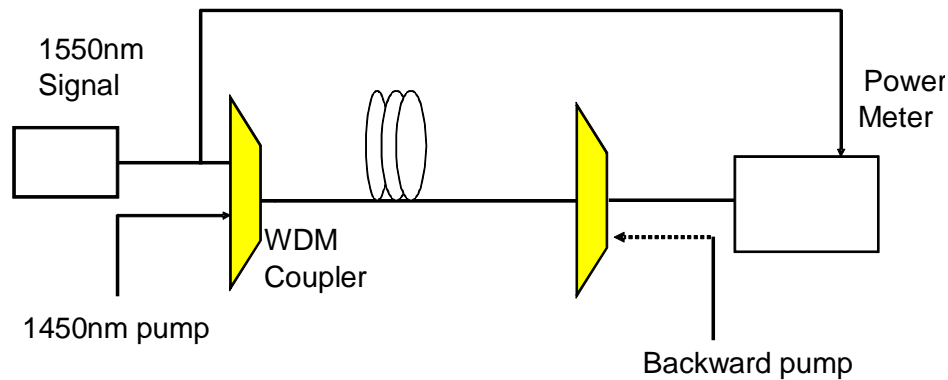


Figure 5.1: Schematic diagram of a Raman fibre amplifier used in the simulation.

Figure 5.2 shows the histograms bearing information on net gain fluctuation with respect to fibre PMD, pumping schemes and pump depolarization. According to figure 5.2a, which is the case of the forward polarized pump, the net gain fluctuation is negligible when the fibre PMD coefficient is very small and increases as PMD increases up to some value before decreasing again. In the case of the backward polarized pump (fig 5.2c), the opposite happens where the net gain is seen to spread more as the fibre PMD coefficient becomes small. This behaviour is rather strange though in agreement with the analytical model by Lin and Agrawal (Feb 2003). The implication is that a forward polarized pump would be more efficient, having negligible gain fluctuation at relatively higher PMD ($<0.01 \text{ pskm}^{-1/2}$). On the other hand a backward polarized RFA would require a fibre of much lower PMD coefficient ($<0.001 \text{ pskm}^{-1/2}$) to achieve negligible signal power fluctuations. As seen in both figure 5.2a and 5.2c a signal can experience net loss when polarized pumping is employed. When the pump is depolarized, gain fluctuations decrease as shown in figure 5.2b and 5.2d. The depolarized pump minimizes power fluctuations for all PMD coefficients but considerably reduces the signal gain, with low PMD fibre having the lowest gain. It is noticeable that the backward depolarized pump performed better than the forward depolarized pump in terms of the mean gain achievable for all four fibre PMD coefficients tested. It should be noted that there is no net loss in the case of depolarized pumping although the average net gain is very small. Thus the net loss is attributed to polarization effects on the pump and the signal during amplification.

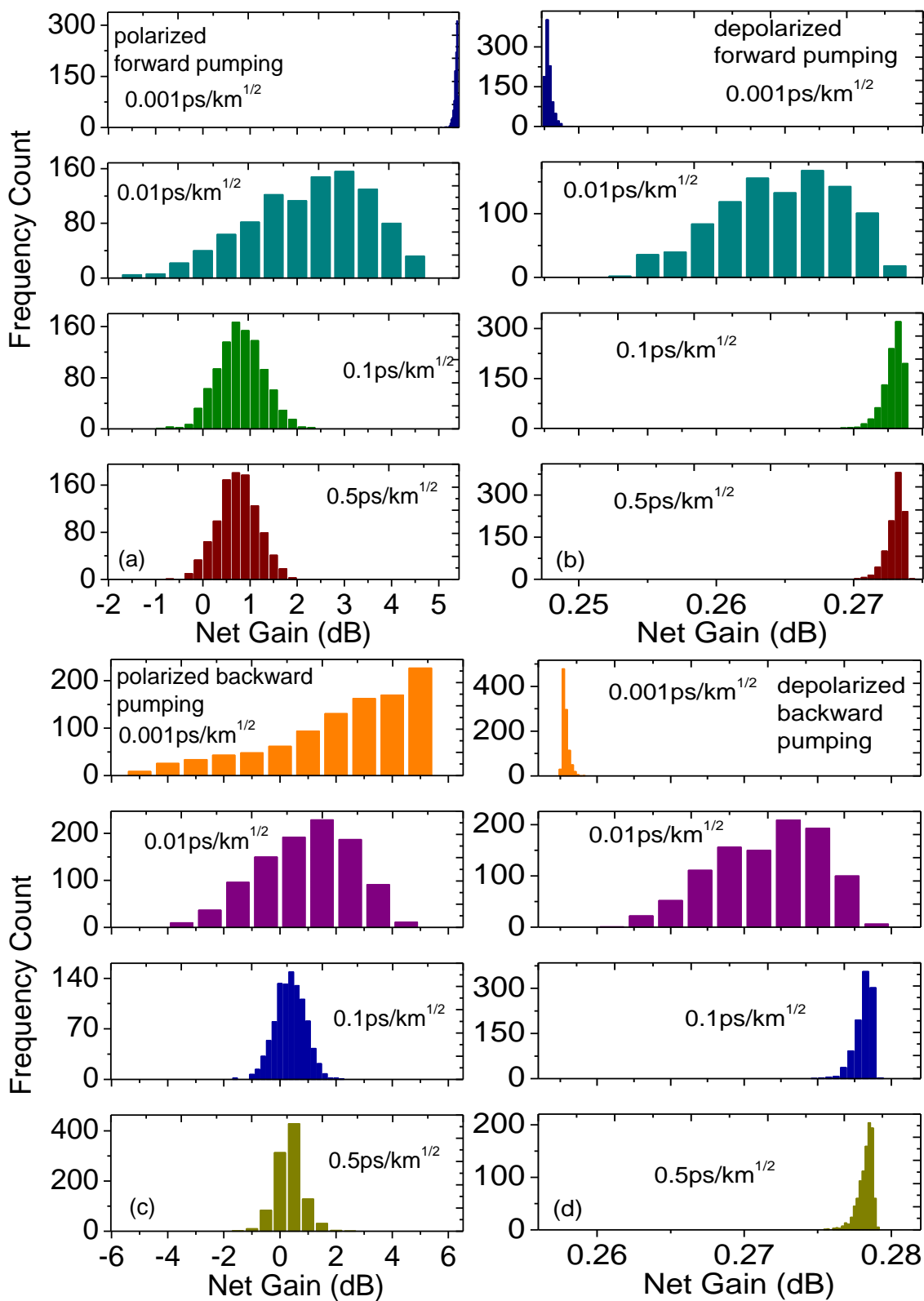


Figure 5.2: The net gain distributions of four SMFs of different PMD coefficients in (a), (b) forward and (c), (d) backward pumping with polarized and depolarized pump.

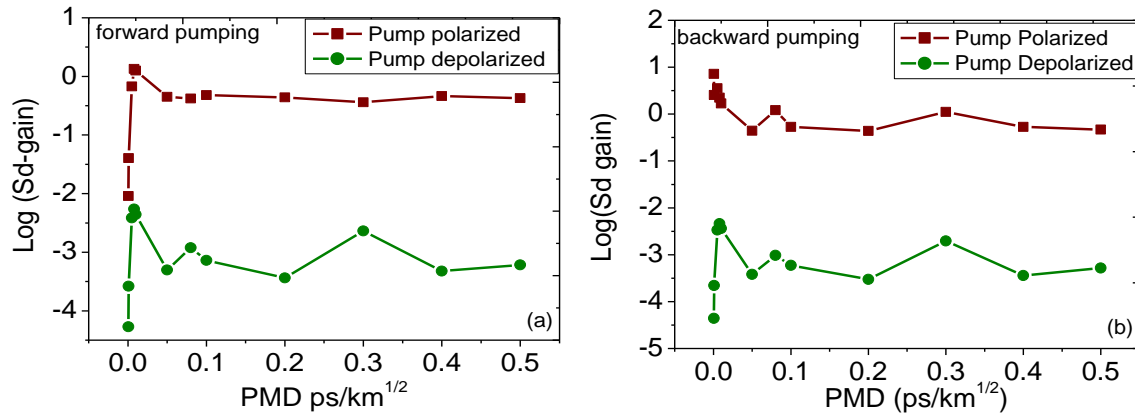


Figure 5.3: Standard deviation of net gain as a function of fibre PMD coefficient in the (a) forward pumping and (b) backward pumping configuration.

Figure 5.3 shows the analysis of the standard deviations of the net gain when the fibre PMD coefficient is varied within the range 0-0.5 pskm^{-1/2}. In figure 5.3a both the polarized and the depolarized pump show similar trends as the fibre PMD is changed but the gain deviations of the polarized pump are higher and therefore shifted upward. In this case the gain fluctuation is maximum in the vicinity of a PMD coefficient of 0.008 pskm^{-1/2} and decreases rapidly as the PMD coefficient drops further. For PMDs above 0.1 pskm^{-1/2}, there is negligible change in gain fluctuation. In the polarized case of figure 5.3b, there is no convergence of the gain fluctuations as the PMD decrease to very small values. In the theoretical model by Lin and Agrawal (2003), it is stated that in the backward pumping configuration, the convergences of the gain fluctuations occur at much lower PMD values than in the case of forward pumping. Interpreting these results in terms of PMD effects would then mean that the effects are much stronger in the backward pumping and therefore a fibre of much lower PMD value is required to maintain the pump signal orientation during amplification. In our case the lowest value of PMD used was 5×10^{-4} pskm^{-1/2} which is practically very small. Again it is evident that there is similarity in the gain fluctuations in both pumping schemes when the pump is depolarized.

5.3 Experimental setup

Figure 5.4 depicts the experimental setup that was used in the analysis of Raman gain statistics and will be referred to for the rest of this chapter. The pump power was 22 dBm and the signal source was either varied over a range of values or set at a fixed value of -10 dBm. The signal was obtained from a WDM or a tunable source and a tunable filter was used to remove stray pump and noise power from the amplified signal.

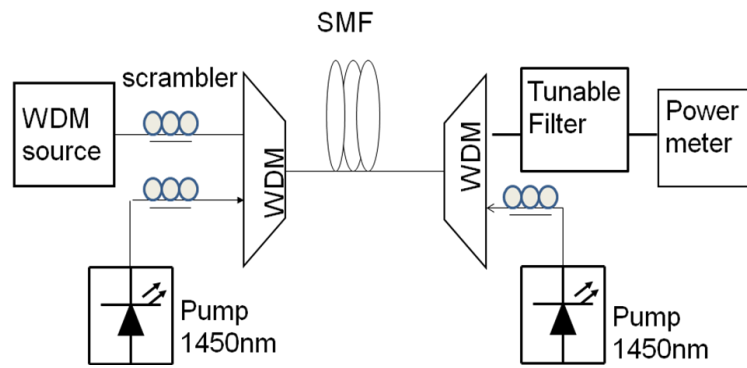


Figure 5.4: Schematic diagram of a distributed Raman fibre amplifier used in the experiments.

5.4 Effects of polarization scrambling technique

Most researchers who have previously investigated the statistics of Raman gain in fibres used the technique of polarization scanning of the input signal. This has advantage in that only a low optical power polarization scrambler is required. Here it is demonstrated that the magnitude of PDG as well as on-off gain can be affected by the polarization scrambling method at the input. In the forward pumping scheme, the PDG and average on-off gain were determined firstly when scrambling the SOPs of the signal alone, secondly the pump and finally when both the pump and signal were scrambled. Three fibres of different PMD coefficients were tested.

Experimental results in Figure 5.5 clearly show that the Raman PDG and the on-off gain depend upon the criteria of polarization scrambling at the input of the RFA before the pump and signal are coupled into the fibre. Figure 5.5a and 5.5b show the two gain quantities when a 24.06 km SSMF of PMD coefficient $0.011 \text{ pskm}^{-1/2}$ was employed in the measurements at a signal wavelength of 1550 nm. The average on-off gain was at its highest when the pump SOP at the input was fixed and the signal scrambled. It can be seen that scrambling the pump and signal simultaneously provided the highest PDG values. Similar results were observed in figure 5.5c and 5.5d when a NZDSF of length 24.7 km and $0.025 \text{ pskm}^{-1/2}$, PMD coefficient was used. The high gain characteristic of the NZDSF is expected and is due to the level of doping which is higher than that of the SSMF (Kang, 2002). This is the reason why it has a higher gain than the fibre of lower PMD coefficient. The high average on-off gain observed with these two low PMD fibres when only the signal was scrambled is attributed to the fact that the Raman gain is pump polarization dependent. Therefore, when the pump SOP at the input is fixed the gain distribution becomes skewed upon scrambling of the signal and as such the average gain shifts to a higher value.

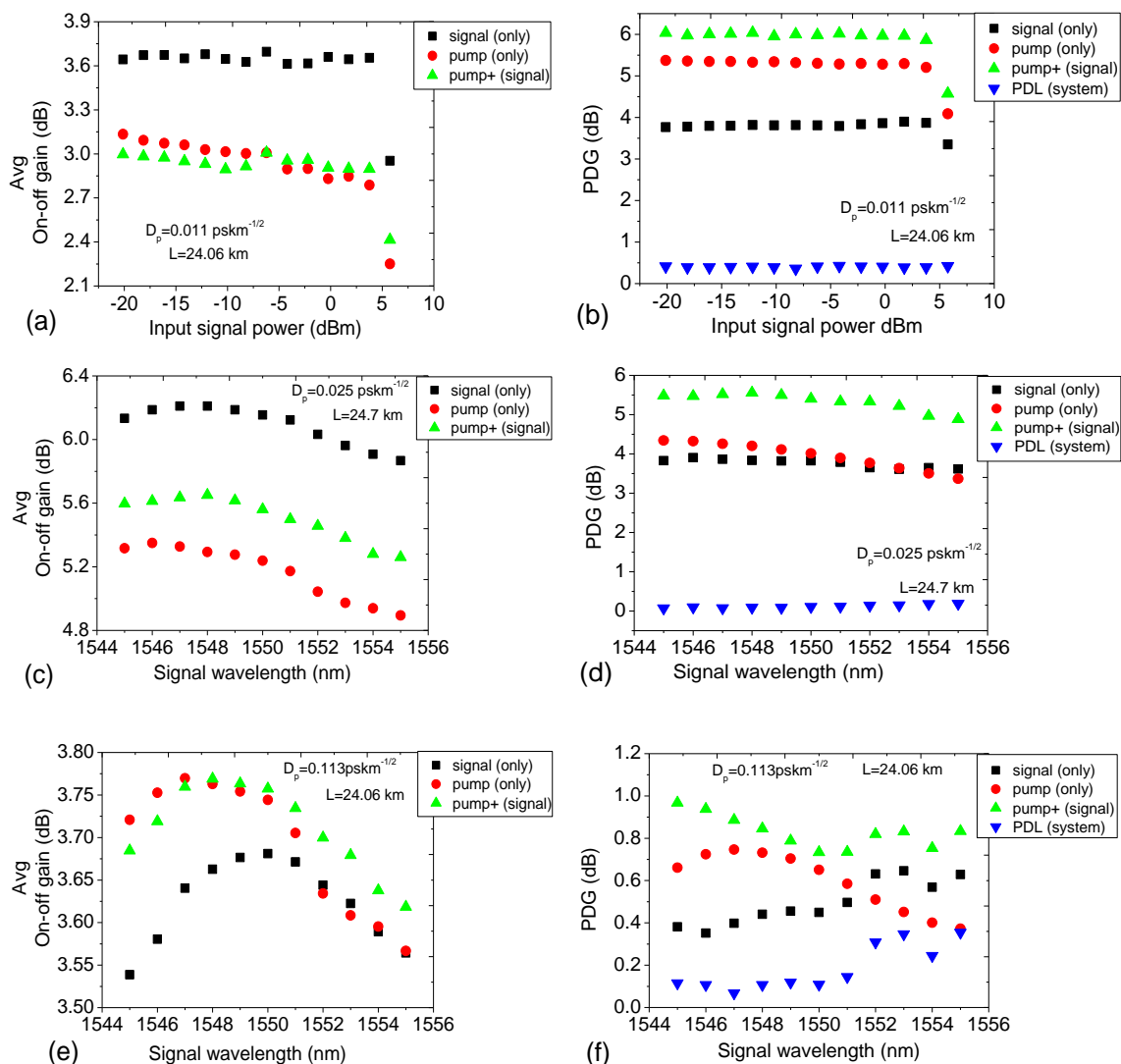


Figure 5.5: Variation of average on-off gain and PDG with respect to polarization scrambling at the input.

When a high PMD fibre is involved the gain quantities become less dependent on polarization scrambling at the input as seen in figure 5.5e and 5.5f. This is because high PMD rotates the SOPs of both the pump and signal as explained earlier, resulting in polarization mixing so that after a short distance of propagation the fields of the waves completely lose memory of the input SOPs (Wai and Menyuk, 1996). This results in gain averaging and we would expect even less gain variation with polarization scrambling as the fibre PMD increases above $0.1 \text{ pskm}^{-1/2}$. We also note that there is a wavelength dependence of the gain quantities which is clearly seen for the high PMD fibre. The curve for system PDL is included to indicate its magnitude during the measurements. In this case the system PDL is low enough and does not show any effects on the gain quantities.

5.5 Raman on-off gain distribution

In this case we demonstrate the on-off gain distributions of both high and low PMD fibres. Specifically we investigated SSMFs of lengths 6.07 km, 12.03 km and 24.06 km. The long fibre of length 24.06 km was obtained by splicing two, 12.03 km fibres of similar PMD coefficients. The reason why we used these different lengths is to evaluate how the length of the fibre affects the gain distribution. It is important to note that the 6.07 km and the 12.03 km fibres used in this experiment were cabled in two spools which were fabricated by different companies. It is therefore possible that the two spools have different Raman gain coefficients. The WDM source wavelength was set at 1550 nm and a 100 GHz spacing WDM demultiplex was used to filter the signal before the measurements. In the measurement both the pump and signal input polarizations were scanned using the EXFO 5100B polarization scramblers before coupling into the fibre and at the output the signal power was determined using EXFO IQS 1700 power meter. The pump power of 22 dBm was applied in each of the three pumping schemes to obtain the gain distributions.

5.5.1 Short fibre length

In this case two fibres of PMD coefficients $0.025 \text{ pskm}^{-1/2}$ and $0.38 \text{ pskm}^{-1/2}$ in a cabled spool of 6.07 km were used in the experiment. This length is similar to that used in the design of the discrete RFA. In each of the fibres three gain distributions corresponding to the three pumping schemes were obtained and evaluated for normality.

Figure 5.6 shows the histograms and the corresponding probability plots of the 6.07 km spool of two fibres that differ only in their PMD parameter. The distributions were plotted by applying the same size bins. The solid lines are a Gaussian fit for the distributions while $\langle G_{\text{dB}} \rangle$ is the average gain and S_{dB} is the gain standard deviation. In this case the two fibres have similar average gains in the forward and the bidirectional pumping. However the gain fluctuations are still high for the low PMD fibre. Similarly the gains and standard deviations of the gains of the two fibres are comparable in the case of backward pumping. In figure 5.6b the linear fit indicates that the points form a nearly linear pattern when the backward and the bidirectional pumping are applied. Therefore the Raman on-off gain distributions of these two schemes appear to be a normal distribution. However the forward pumping scheme shows minor deviations from the linearity with a tail on both ends. In figure 5.6d the data from each of the pumping schemes shows only mild deviations from the linear fit but the distributions cannot conclusively be interpreted as normal. For this short fibre it is evident that the distributions are less sensitive to the pumping scheme employed.

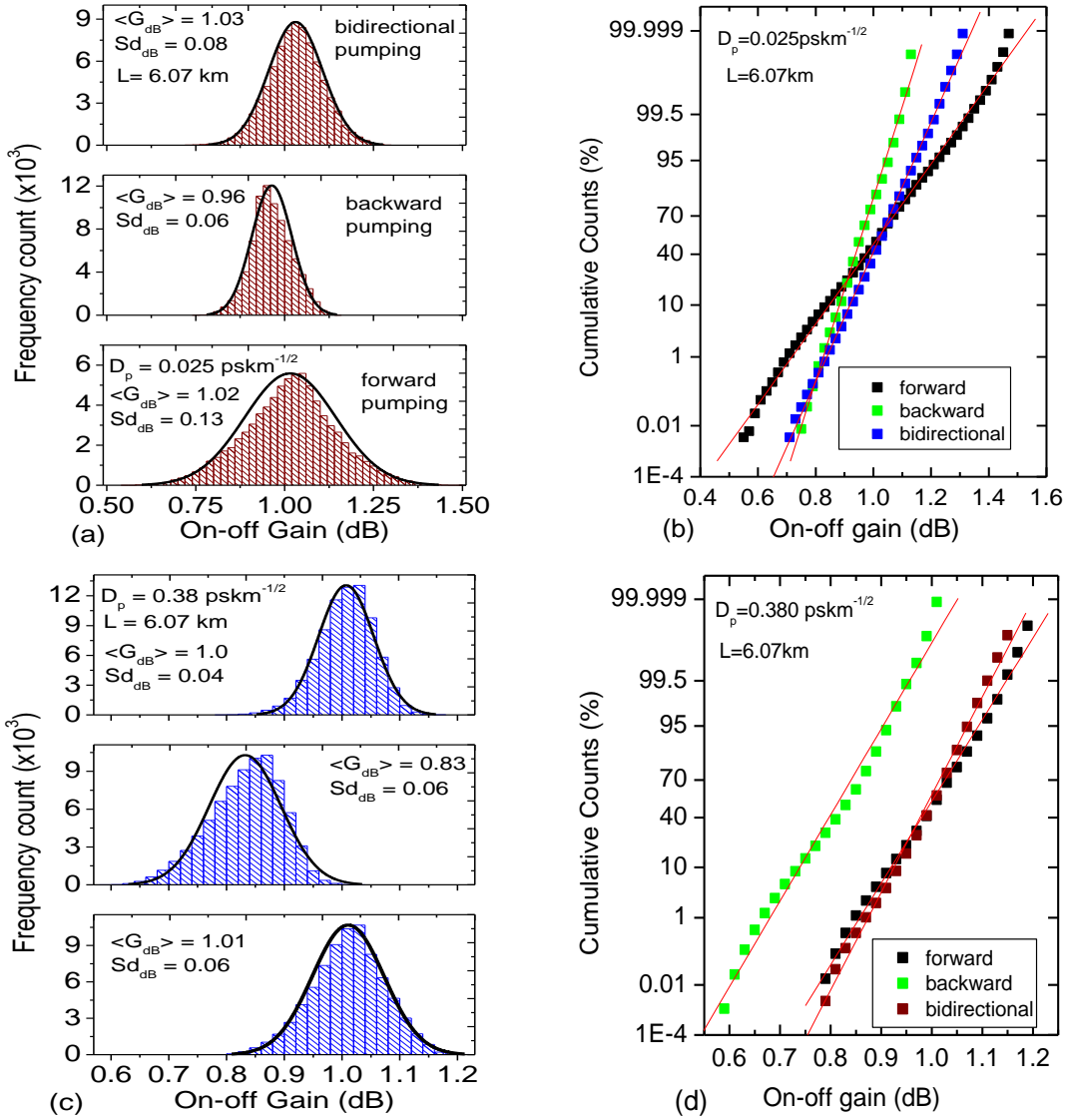


Figure 5.6: Gain distributions and probability plots of two fibres of the same length and different PMD coefficients. In (a) and (b), $D_p = 0.025 \text{ pskm}^{-1/2}$ while in (c) and (d), $D_p = 0.380 \text{ pskm}^{-1/2}$.

In the last chapter (section 4.3.1) we showed that Raman gain in fibre increases exponentially with fibre length up to a maximum before it begins to drop. Here the pump remains strong throughout the fibre length and therefore signal losses are small leading to comparable gain averages. However the PMD contribution to the gain fluctuation is clearly seen for the low PMD fibre in the forward pumping configuration.

5.5.2 Standard length fibre

In this case two fibres each of length 12.03 km and respective PMD coefficients $0.011 \text{ pskm}^{-1/2}$ and $0.113 \text{ pskm}^{-1/2}$ were used in the measurements. These fibres were classified as of standard length because their length is similar to the one mostly preferred in experiments as well as numerical analysis.

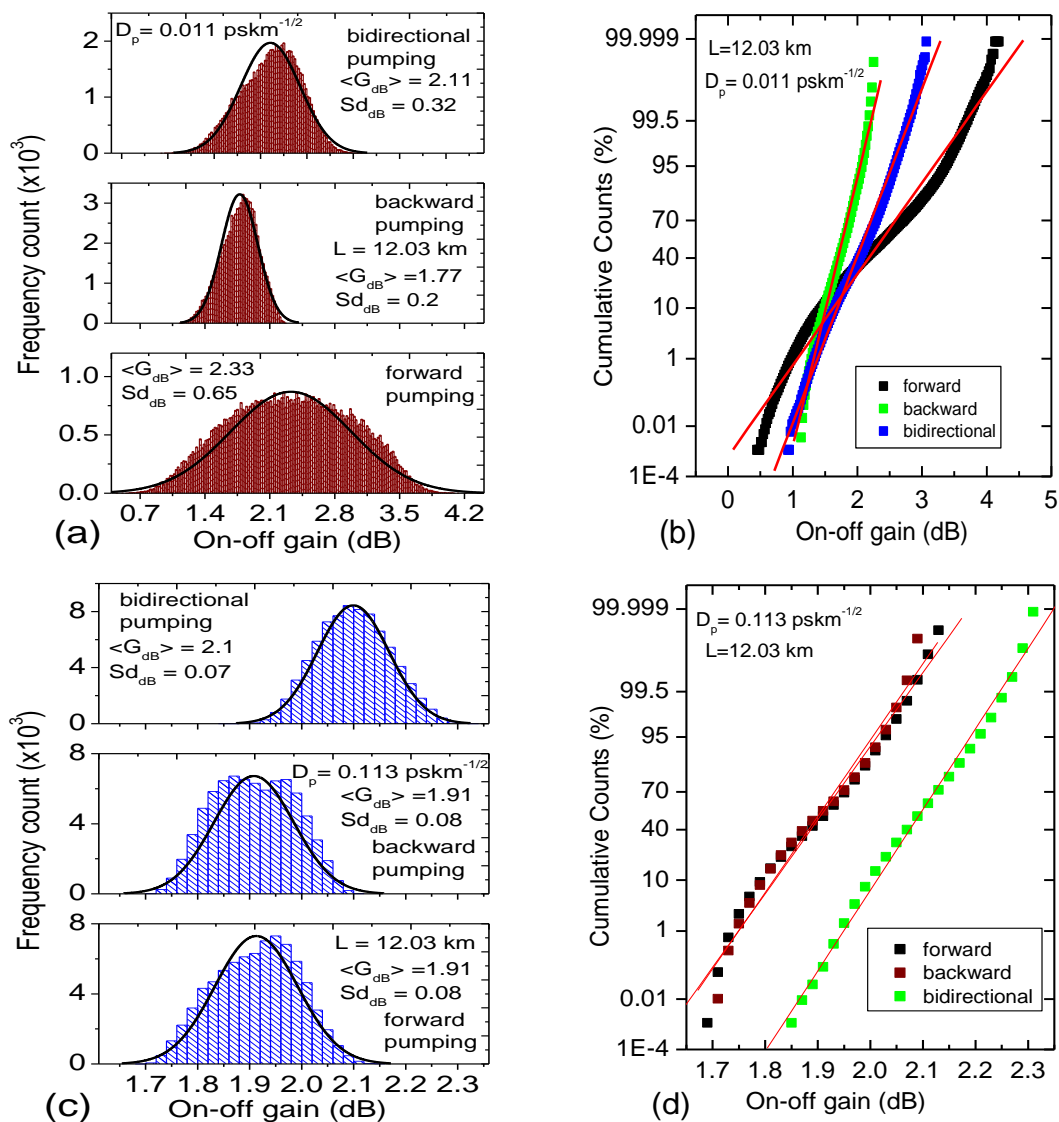


Figure 5.7: Histograms and probability plots of two fibres of length 12.03 km. In (a) and (b), $D_p=0.011 \text{ pskm}^{-1/2}$ while in (c) and (d), $D_p=0.113 \text{ pskm}^{-1/2}$.

Figure 5.7 shows the on-off gain distributions and probability plots which were obtained for the two fibres of length 12.03 km. These fibres had similar characteristics and differed only in their PMD coefficients. As can be seen in figure 5.7a and 5.7c, the gain fluctuations depend mostly on the fibre PMD parameter while the pumping schemes employed determine the location of the mean of the distribution. The low PMD fibre show considerable gain fluctuations in the forward pumping while gain fluctuation is greatly reduced in the backward pumping where the average gain is shifted to a lower value. For the high PMD fibre there is negligible difference in the average gains and also the standard deviations in the forward and backward schemes. The gain averages of the bidirectional pumping compare well in both fibres. The probability plot in figure 5.7b shows a strongly linear pattern in the case of the

backward and the bidirectional pumping with minor deviations from the line fit to the data points. The forward pumping case shows a non-linear behaviour with the first and the last few points showing a complete departure from the reference fitted line. In this case the gain distribution is not a normal distribution. In figure 5.7d the bidirectional pumping shows strong linearity with only minor deviations. However the backward and the forward pumping curve shows departure from the fitted line particularly the lower tail and a mild S-like pattern at the middle. This indicates that these distributions are not a normal distribution.

5.5.3 Long length fibre

In this case the length of each of the two fibres was doubled to 24.06 km.

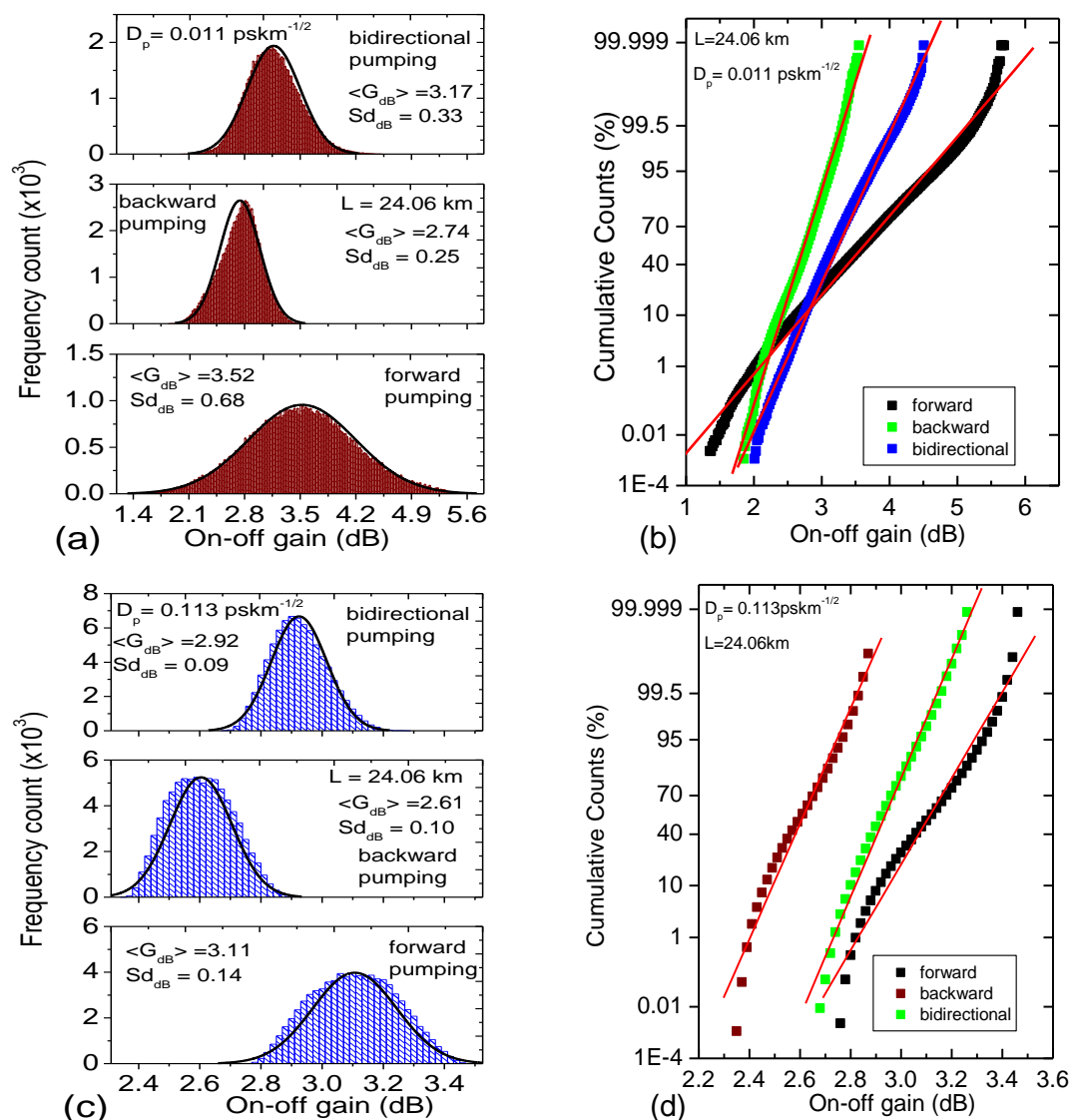


Figure 5.8 Gain distributions and their corresponding probability plots of the two 24.06 km fibre.

The results in figure 5.8 can be compared with those in figure 5.7 because the fibres used in both cases only differ in their lengths. Figure 5.8a shows that increasing the length of the fibre from 12.03 km to 24.06km in the low PMD regime has little effect on the gain deviations for the three pumping directions. However, the gain averages have higher values because some gain occurred in the added fibre. Similar effects were observed in the high PMD fibre when its length was doubled. The probability plots of both fibres show some remarkable results. In figure 5.8b which is the plot for the low PMD fibre, increasing the length of the fibre improves the linearity of the data at the centre when forward pumping is employed. However the tail of the forward distribution is not affected when compared with figure 5.7b. The backward and the bidirectional pumping still show a reasonably linear pattern in the middle of the data. In figure 5.8d, increasing the fibre length separated the probability curves for the forward and the backward pumping with the latter shifting to lower gain values. A mild S pattern in the middle of the data is clearly displayed by this fibre which indicates that the gain distributions are out of the normal.

According to Lin and Agrawal (Aug 2003), the PDG_{dB} display different distributions depending on the fibre effective length L_{eff} and the PMD diffusion length L_d . When $L_{eff} \gg L_d$, the PDG distribution is Maxwellian and if $L_{eff} \ll L_d$, the distribution is Gaussian. Since the PDG gain and the on-off gain are linearly related, it would imply that both gains have similar distributions if the test fibre meets the above criteria. Thus for a low PMD fibre where $L_{eff} \ll L_d$ the on-off gain should approximate the normal distribution. While this criterion could not be perfectly met in this analysis, it is evident that the gain distributions of the low PMD fibres used are inclined toward a normal distribution and those of the high PMD fibres tend to fall away from a normal distribution with some dependence on the pumping scheme. However, the distributions of the fibre of PMD coefficient $0.38 \text{ pskm}^{-1/2}$ are exceptional and imply that a close to normal distribution is achievable for fibres of high PMD parameter. This behaviour is attributed to the fact that for short length fibre the Raman gain is small but dominant over fibre losses and almost linear (section 4.3.1) and does not vary much with fibre PMD. This is not the case with the 12.03 km and 24.06 km fibres where even though the gain is high, the fibre losses are also more and gain is highly PMD dependent. A similar explanation about the net gain efficiency of short fibres is given by Namiki *et al.*, (2005).

5.6 Dependence of PDG and signal gain fluctuation on fibre PMD

It is of interest to observe how the root mean square (RMS) value of PDG and the on-off gain vary with the PMD parameter. In this case several fibres in the cabled spool of length 12.03

km were evaluated to obtain these two quantities. Measurements were obtained at a signal wavelength of 1550 nm.

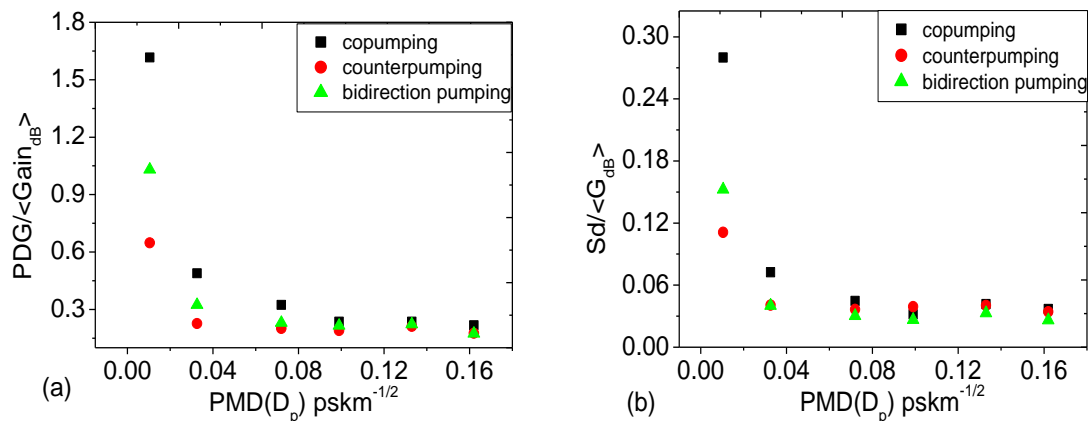


Figure 5.9: Normalized (a) PDG and (b) on-off gain standard deviation as a function of fibre PMD coefficient.

Figure 5.9 present the variation of the PDG and on-off gain standard deviation in the three pumping configurations. Normalization of both quantities with respect to average on-off gain eliminates their dependence on pump power. (Lin and Agrawal, Feb 2003). Results in Figure 5.9 show that PDG and signal gain fluctuations depend on the pumping scheme and increase rapidly for co-pumped configuration at low PMD ($< 0.03 \text{ pskm}^{-1/2}$). However, as the PMD increases both the gain fluctuations and the PDG values of the three pumping schemes decrease to the same level as predicted by Lin and Agrawal, (Feb 2003). One interesting feature in figure 5.9 is that the two quantities vary in the same way though they are of different magnitudes. This implies that we can predict the effects of PDG if we know the on-off gain distribution of the Raman fibre amplifier. The system PDL in each of the measurements was $< 0.2 \text{ dB}$ and was observed to have no influence on the results.

5.6.1 Field measurements for high PMD fibre

Measurements were performed on deployed cable at Sidwell Telkom SA exchange in Port Elizabeth. This cable connects two stations and was looped during the measurements to make a total length of 28.8 km. The fibres constituting this cable had their PMD coefficient in the range $0.4\text{-}2 \text{ pskm}^{-1/2}$. The same setup used in the laboratory measurements (section 5.3), was employed in the field measurements.

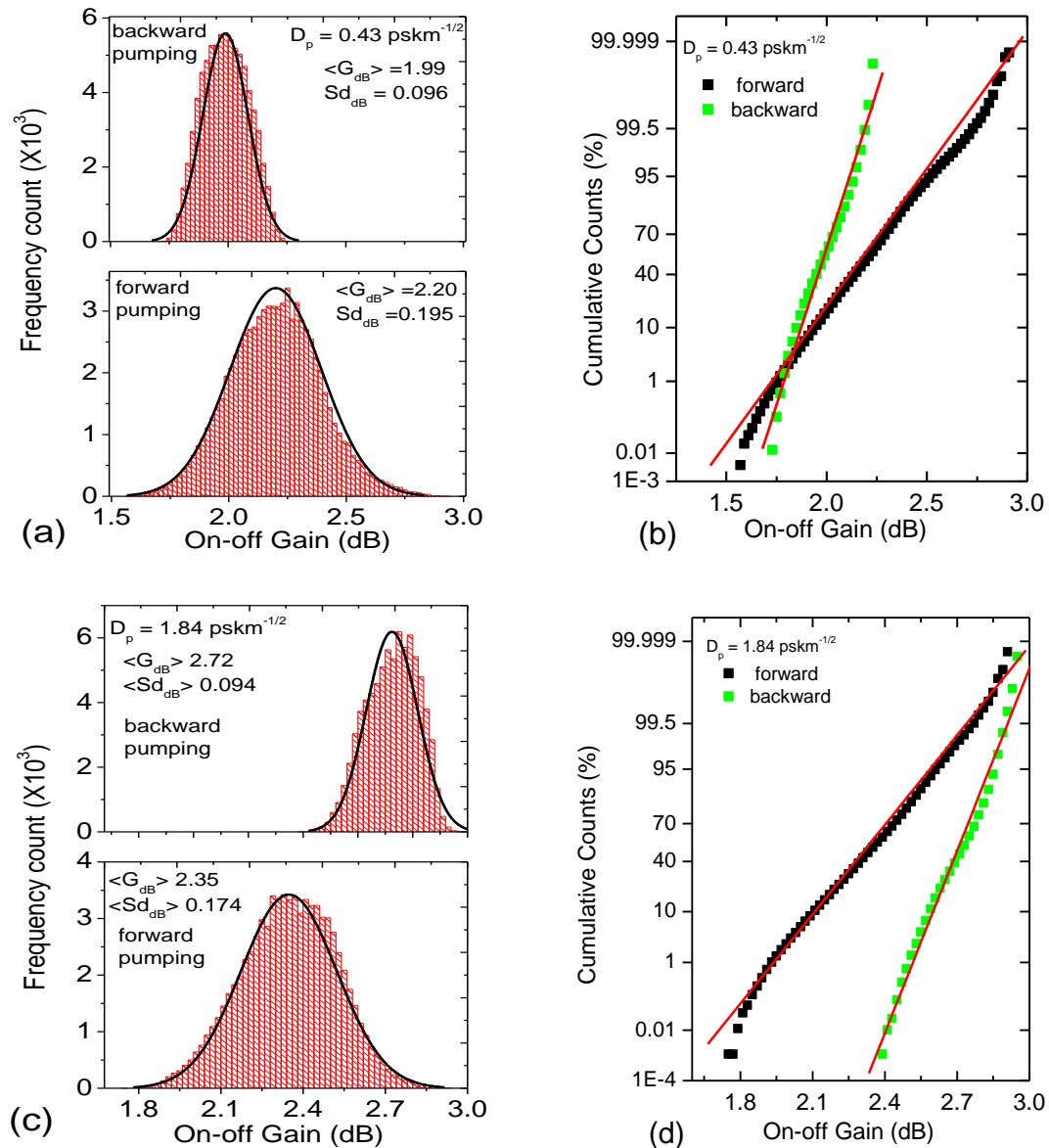


Figure 5.10 Distributions and probability plots of two deployed high PMD fibres. In (a) and (b) $D_p=0.43 \text{ pskm}^{-1/2}$ and in (c) and (d), $D_p=1.84 \text{ pskm}^{-1/2}$.

The on-off gain distributions of deployed fibres were unusual and gave inconsistent gain averages. In figure 5.10 the $1.84 \text{ pskm}^{-1/2}$ fibre shows slightly higher gain averages than the fibre of $0.43 \text{ pskm}^{-1/2}$ PMD coefficient. This is rather unusual and could be attributed to non uniformity of the birefringence (section 4.3.3). It is likely that these fibres have high birefringence sections as earlier measurements on similar fibres showed (Visser *et al*, 2003). These high birefringence sections would cause the fibre to have a high PMD coefficient without a corresponding reduced gain. We performed the test (section 4.3.3) for concatenated fibres and found the field fibres to have similar results to those obtained in the laboratory. This was an indication that the two looped fibres were of different PMD coefficients.

However, the gain fluctuations of these two fibres are consistent because of their high PMD which results in the asymptotic nature of the RMS value of the gain (section 5.6). In figure 5.10b the forward pumping shows a strong linear pattern in the middle with a small deviation from linear fit near the upper end and a tail on the lower end. At the same time backward pumping shows tail-less ends and a mild S-pattern at the centre. In figure 5.10d the forward pumping again shows strong linearity with minor deviations and a long tail at the lower end while the backward pumping displays a mild S pattern at the middle with a tail at the upper end. There is a clear indication that the distributions for both fibres are tightly bunched round their mean values which is mainly because of their high PMD. Thus in the high PMD regime, the rapid rotations of pump and signal SOPs culminate to efficient gain averaging which tends to incline the gain distribution to a normal.

A similar approach as in section 5.6 was performed on the deployed fibres to establish the variation of PDG and RMS value of gain as a function of PMD.

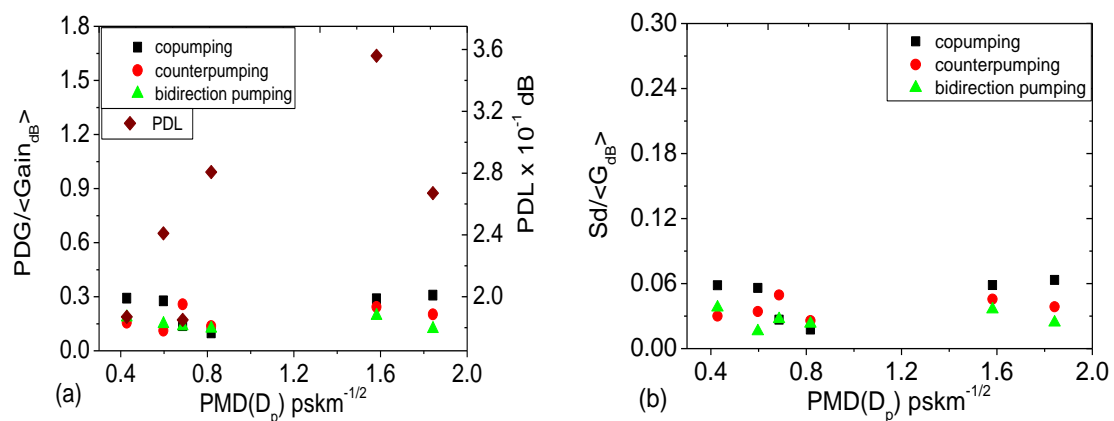


Figure 5.11: Normalized (a) PDG and (b) gain standard deviation of deployed fibres as a function of PMD.

As is evident in figure 5.11, both PDG and gain fluctuation hardly change as PMD of the fibre increases. This is a confirmation of the asymptotic nature of both quantities as the PMD increases to higher values. In the three pumping schemes the measured values of PDG were below 1 dB and the calculated gain standard deviations below 0.25 dB for all the fibres tested. The measured PDL of each fibre also included in figure 5.11a showed no effect on the PDG values. One thing worth mentioning here is that these buried cables were noisy depending on the time when the measurements were taken. Again the values of measured gain quantities would change within a span of a few hours. For example the data obtained before midday was quite different from that obtain in the afternoon. This indicated that their

PMD values changed depending on external conditions (De Angelis *et al*, 1992 and Cameron *et al*, 1998). Finally we note that, despite the fact that high PMD virtually eliminates the gain fluctuations it also reduces the Raman gain and introduces signal distortions at high data transmission bit-rates.

5.7 Signal power distribution

Amplified signal power distribution is another aspect in understanding the effects of PMD during Raman amplification. The data for signal power distributions is the same which was used to obtain the on-off gain distributions and therefore no independent measurements were required. In this case the power distributions of the six fibres discussed in section 5.5 were analysed.

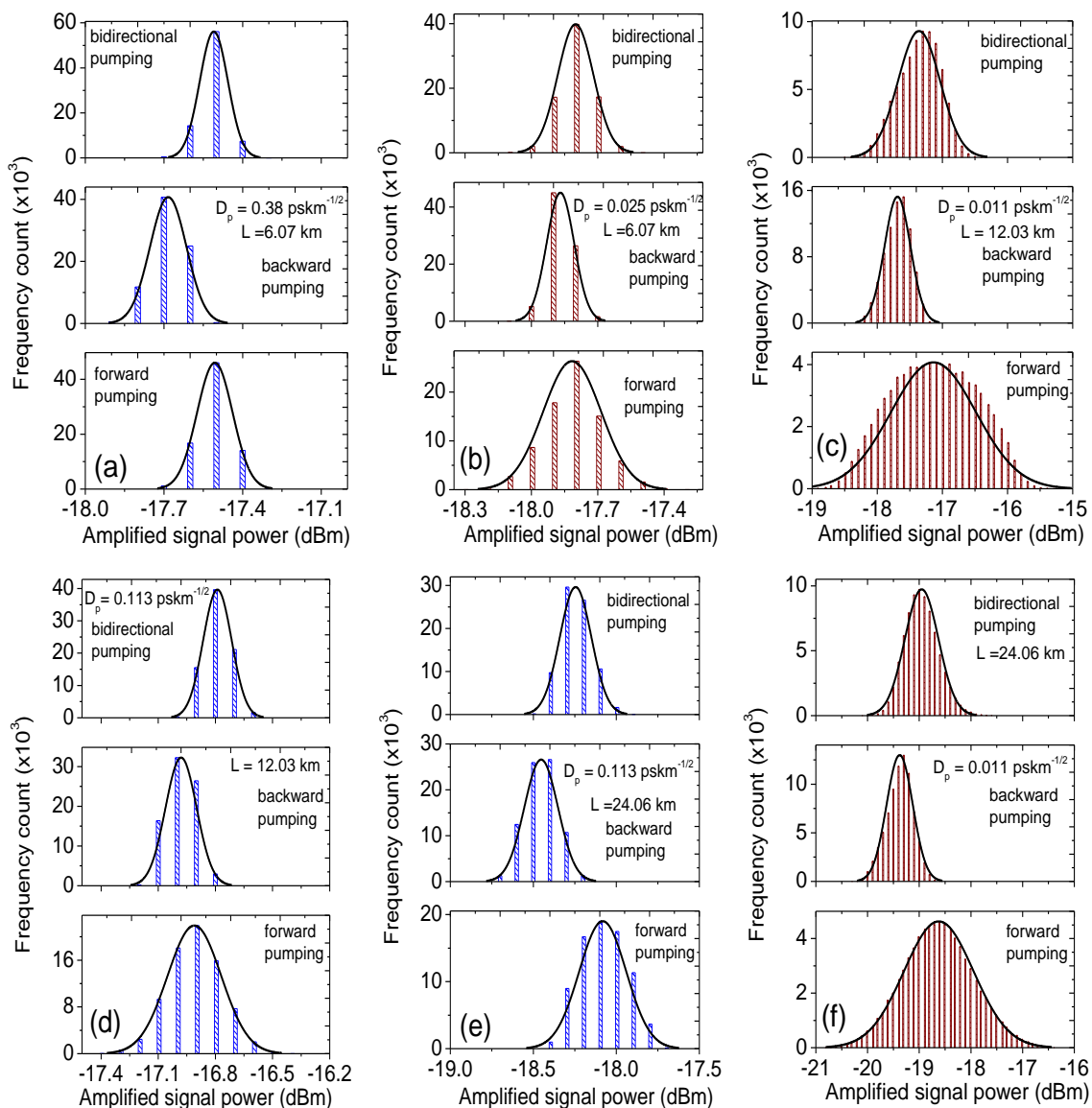


Figure 5.12: Distribution of signal power of six fibres of varying length and PMD.

Figure 5.12 shows the histograms of signal power in the dBm scale which were plotted with bins of equal size. The solid line indicates a normal distribution fit to the profile. One advantage of using the dBm scale is to get rid of the decimals associated with the signal power because it is in microwatts (μW) range on the linear scale. The main difference between these distributions and those of the gain (section 5.5) is the discreteness of the bins which may be a result of using logarithmic data. The signal power fluctuation is dependent on the fibre PMD as well as the pumping technique as can be seen in all the six distributions. According to figure 5.12a and 5.12b, the three pumping schemes shows that the signal power at the peaks of the distributions is lower for the fibre of PMD coefficient $0.025 \text{ pskm}^{-1/2}$. Since these two fibres have the same length, it implies that the higher PMD enhances power averaging of the output signal. At the same time the low PMD fibre allows the amplified signal power to take a wide range of values because its PMD diffusion length is comparable to the actual length of the fibre and therefore the output power depends on the input conditions. That is, the output signal depends on the input SOPs of the pump and signal. In figure 5.12c which is a case of low PMD fibre, the power distribution is broadened for the forward pumping compared with the superimposed Gaussian fit. However the signal power is well bunched around the peak in the backward and bidirectional pumping. When the length of this fibre is doubled in figure 5.12f there is a strong confinement of the power distribution to the superimposed normal fit. The distributions shift to lower power values simply because of signal losses in the added fibre. A similar analysis of figure 5.12d and 5.12e, which is the case of a high PMD fibre, reveals that there is less confinement of the distribution profiles to the Gaussian fit. In this case, doubling the length of the fibre resulted in negligible broadening of the profiles but increased the frequency count of the side bins relative to the central peak. This is the reason for the loss of confinement as is clearly evident in all the pumping schemes. The results in figure 5.12 are in agreement with the theoretical analysis by Lin and Agrawal (2003) where normalized signal power (net gain G_{dB}) was predicted to have a normal distribution for fibres of PMD coefficients $0.002 \text{ pskm}^{-1/2}$ and $0.1 \text{ pskm}^{-1/2}$. Their choice of these coefficients was mainly to ensure that the low PMD coefficient does not misalign the pump-signal SOPs during amplification and the high PMD coefficient eliminates the dependence of the amplified signal on the input SOP. In real fibres this condition may not be realizable but as is evident in figure 5.12 the amplified signal power distributions are close to the normal distribution and therefore confirms the theoretical findings. According to statistical analysis of random variables the logarithm of a variable produces a normal distribution if the variable is lognormal distributed (Papoulis, 1991). Consequently, the log of

the normal distribution provides a good model for amplified signal power in the PMD regime, $D_P < 0.01 \text{ pskm}^{-1/2}$ and $D_P > 0.1 \text{ pskm}^{-1/2}$.

5.8 Raman gain and PMD characterization of fibre

In this section we take advantage of the vector theory of RFAs (Lin and Agrawal, 2002 and Aug 2003) to demonstrate a simple technique of extracting the fibre PMD coefficient from the measurement of PDG and on-off gain. Measurements of PMD in optical fibres have been a subject of extensive research over the past three decades (Kogelink *et al*, 2002 and Hernday, 1998). At high bit rates ($>10\text{Gb/s}$) and long span transmission, which is the state of art in a modern fibre network, the PMD effect causes signal impairments that would lead to system failure. The old fibre exhibited high PMD and only allowed low bit rate-distance transmissions. Modern fibre fabrication technology has greatly improved the quality of the fibre thereby enabling the production of low PMD fibre (Kogelink *et al*, 2002). There is a need to accurately assess the intrinsic PMD of the modern single-mode fibres for telecommunication applications. In a long haul transmission network the small residue birefringence still present in modern fibres accumulates and can cause pulse distortions and signal fading resulting in system penalties (Poole *et al*, 1991 and Chowdhury, 1999]. PMD characterization of a fibre during and after cabling and also after installation remains an important step toward improving the quality of an optical link. PMD effects have instigated the development of many measurement techniques, most of which can be easily classified as either time domain or frequency domain methods (Kogelink *et al*, 2002 and Hernday, 1998). The uncertainty of the measurement associated with these techniques increases with decreasing PMD values (Williams, 2004). Time domain methods are limited to laser source coherence times and environmental perturbations while frequency scanning methods require a wide bandwidth source for sufficient accuracy of measurement. The random nature of fibre birefringence and its evolution with time causes PMD to be statistical in nature. This further complicates the measurements especially in unstable environmental conditions (McCurdy, 2004). Recently, Raman amplification has been demonstrated as a new technique for making PMD measurements (Heras *et al*, 2006; Sergeyev *et al*, 2008). In their analysis Heras *et al* (2006) extracted the fibre PMD coefficient by measuring the RFA signal gain distribution along the fibre using a P-OTDR. Sergeyev *et al* (2008) using their model Sergeyev *et al*, (2006) characterized fibre birefringence by analyzing maximum and minimum PDG of the RFA.

5.8.1 Relation between PDG and on-off gain

In this case we take the advantage of the analytical model presented by Lin and Agrawal, (Aug 2003) to show that by relating PDG and on-off gain for the forward pumping configuration we can extract the PMD coefficient of the fibre. Substituting the decibel form of equation 3.8 in 3.9 we obtain the relation:

$$\langle \Delta \rangle_{\text{dB}} = \frac{8 \langle G \rangle}{\sqrt{\pi} D_p \Omega_R} \left(\frac{1 - \alpha_p L_{\text{eff}}/2}{L_{\text{eff}}} \right)^{1/2} \quad 5.1$$

and

$$\langle G \rangle_{\text{dB}} = a g_R P_{\text{in}} L_{\text{eff}}/2 \quad 5.2$$

where $\langle \Delta \rangle$ and $\langle G \rangle$ is the average PDG and the average on-off gain respectively, $\Omega_R = \omega_p - \omega_s$ is the Raman shift where ω_p and ω_s is the respective pump and signal frequency, L_{eff} is the Raman effective length of the fibre, α_p is the pump attenuation coefficient, D_p is the PMD coefficient, $a = 10/\ln 10 \approx 4.343$, g_R is the Raman gain efficiency and P_{in} is the input pump power. Again, numerical simulation and theoretical analysis (Ebrahimi *et al* 2001; Lin and Agrawal Feb 2003) have shown that the normalized PDG is related to the fibre PMD coefficient by the relation:

$$\frac{\langle \Delta \rangle}{\langle G \rangle} = \frac{k}{D_p} \quad 5.3$$

where k is a constant of proportionality which, according to equation (5.1) is given by;

$$k = \frac{8}{\sqrt{\pi} \Omega_R} \left(\frac{1 - \alpha_p L_{\text{eff}}/2}{L_{\text{eff}}} \right)^{1/2} \quad 5.4$$

It is interesting to note that k has the same units as D_p ($\text{pskm}^{-1/2}$) and for a known length of the fibre we only need to measure PDG and the corresponding signal on-off gain to determine D_p .

5.8.2 Determination of fibre PMD parameter

In the experiment the same setup as the one used to evaluate Raman gain statistics (section 5.5) was employed. Four standard single mode fibres (SSMF) in a cabled spool of length 12.03 km were used in the measurements. The fifth fibre of length 24.7 km (TrueWave) which is a non-zero dispersion shifted fibre (NZDSF) was also tested. For comparison, the Jones matrix eigenanalysis (JME) measurements were performed on each of the fibres and their PMD coefficients calculated. The JME technique yielded the PMD coefficients of the five fibres to be in the range between $0.01 \text{ pskm}^{-1/2}$ and $0.1 \text{ pskm}^{-1/2}$. A -10 dBm signal from a tunable laser source and the forward Raman pump were scrambled continuously at low speed to provide a full Poincaré sphere coverage of their SOPs before coupling them into the fibre.

The average PDG and on-off gain of each fibre was then determined using two approaches. First, with the tunable laser source set at 1550 nm the pump power was varied between 135 mW and 330 mW in steps of 5-10 mW and both gains measured for each pump power using the IQS-1700 power meter. The amplified signal was filtered before measurements using a 100 GHz wavelength division multiplexer (DWM). In the second setup, the pump power was set at 200 mW and the source wavelength was changed between 1520 nm and 1565 nm at intervals of 5 nm. Residue pump power and the amplified spontaneous emission (ASE) noise generated were filtered using a digital tunable filter before the measurements of signal gains at each wavelength. The system polarization dependent loss (PDL) and the signal to noise ratio (SNR) were determined for each fibre and at different wavelengths of the signal. The attenuation coefficients of SSMF and NZDSF at pump wavelength were found to be 0.269 dB/km and 0.251 dB/km respectively.

A major advantage with this approach is that determination of gain is insensitive to SOP fluctuations which can occur as a result of fibre movement and vibrations during measurements. Secondly, the effects of signal losses due to fibre attenuation, imperfect connectors and other system losses cancel out in the measurement of PDG and signal on-off gain and therefore need not to be known. It is noted here that applying this technique and the conversion procedure outlined in Lin and Agrawal, (Aug 2003), in the case of backward pumping does not yield the correct PMD coefficients. When the same fibres were tested in the backward pumping configuration the resultant PMD coefficients were very small and did not match the values obtained using JME or forward pumping. This implies that a different approach is required for backward pumping analysis (Galtarossa *et al*, 2006). Figure 5.13 shows the variation of Raman PDG with signal on-off gain as pump power increases. The solid line superimposed on the curves is the linear fit of the data distribution which is in agreement with the theoretical analysis (Lin and Agrawal, Feb 2003). The y-intercept of the solid lines graphs indicates the residue PDL of the measuring system. The PMD coefficients indicated in figure 5.13 were obtained by applying equation (5.1) and using the slopes of the linear fits. Alternatively one can use equation (5.1) and pairs of PDG and on-off gain values obtained at each pump power to calculate the average fibre PMD. The PMD coefficients of the five fibres as determined by the JME technique were $0.033 \text{ pskm}^{-1/2}$, $0.073 \text{ pskm}^{-1/2}$, $0.12 \text{ pskm}^{-1/2}$, $0.025 \text{ pskm}^{-1/2}$ and $0.011 \text{ pskm}^{-1/2}$ respectively. The values obtained using this technique therefore validates equation (5.1) in determining the PMD coefficient of a fibre in the low regime. The system PDL values of the five fibres were 0.140 dB, 0.186 dB, 0.149 dB, 0.168 dB and 0.187 dB respectively. It should be noted that a signal wavelength of 1520 nm

was used in the case of the fibre of PMD coefficient $0.12 \text{ pskm}^{-1/2}$ because the system PDL was lowest at this wavelength. This means that at low PDL ($< 0.15 \text{ dB}$) this technique would still determine PMD coefficients above $0.1 \text{ pskm}^{-1/2}$ with good accuracy.

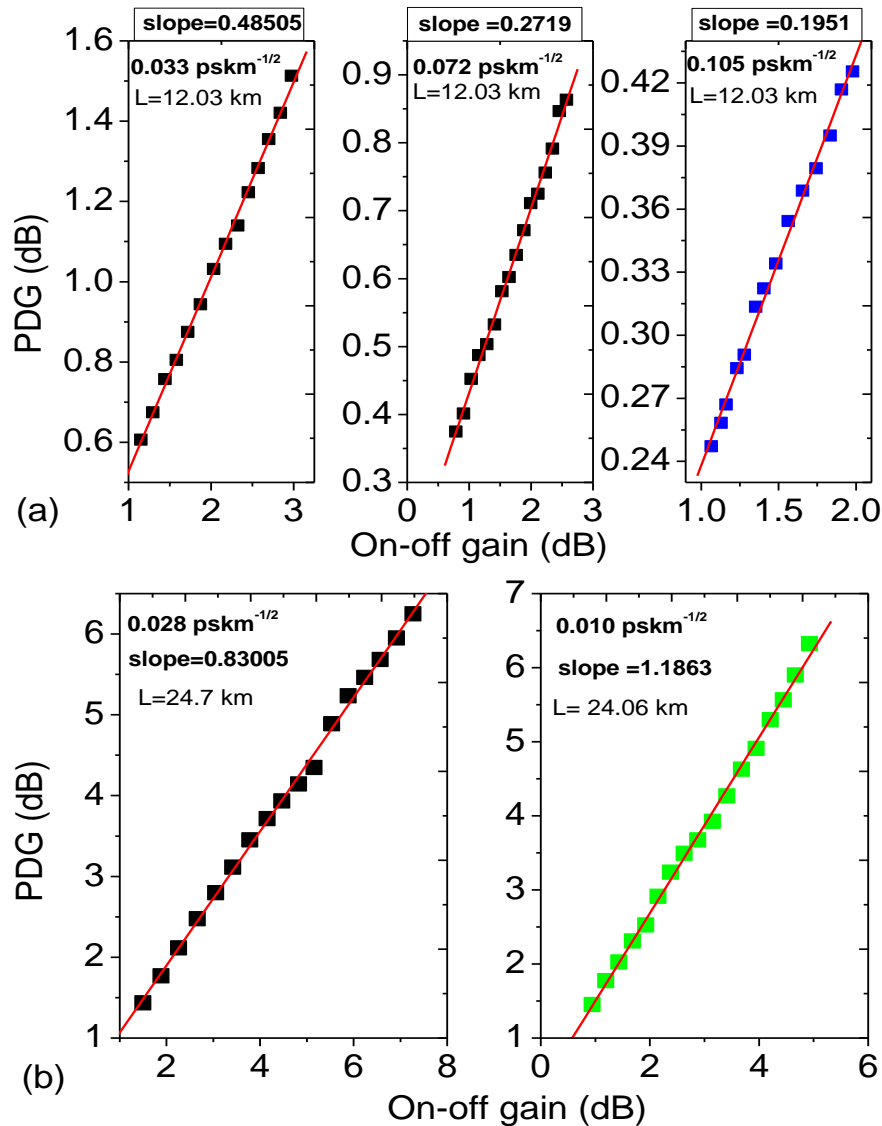


Figure 5.13: Raman PDG as a function of average on-off gain of five low PMD fibres. Their respectively lengths and the corresponding PMD coefficients are indicated.

Figure 5.14 compares the values of DGD obtained from Raman gains with JME signatures of two fibres in the wavelength range between 1520-1565 nm. The DGD values were obtained by calculation (section 2.2.2) and the PMD coefficients of the fibres at different signal wavelengths were extracted from the gain measurements. Figure 5.14a shows a fairly consistent trend for the DGD values obtained using the Raman gain as the wavelength is increased. In figure 5.14b the DGD values show a more evident deviation as the signal

wavelength increases. This behaviour was caused by several factors that could not be controlled during the measurements. These factors included the system PDL and the signal to noise ratio (SNR) which was found to change with wavelength. Again, the DGD of the fibre in figure 5.14b was found to vary within a short time span (in the course of the measurements) as shown by the embedded seven JME trials. The two fibres also show differences in their DGD trends because the SSMF is cabled while the NZDSF is not. The DGD of a cabled fibre will be least affected by external perturbations such as changes in room temperature. (van Antwerpen *et al*, 2003; Li *et al*, 2000).

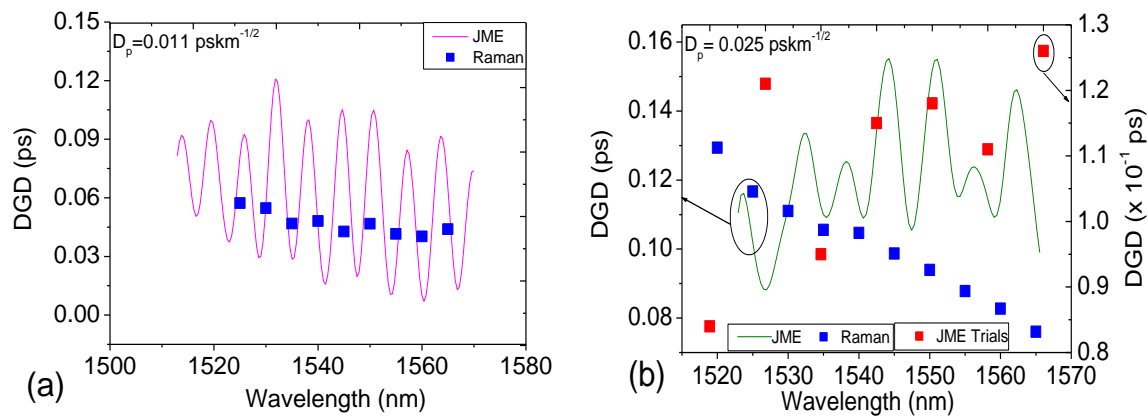


Figure 5.14: DGD as a function of pump-signal detuning of (a) SSMF of length 24.06 km (b) NZDSF of length 24.7 km. Embedded is the DGD signature of the fibres as measured by JME. Included are seven DGD values obtain by JME for the NZDSF at different times during the measurements.

5.8.3 Effects of PDL and SNR

Characterization of fibre PMD using Raman gain analysis basically involves the measurement of amplified signal power. The accuracy of the measurements may be affected depending on the noise in the RFA and the PDL of the experimental setup. Other factors that may introduce errors in the measurement include unclean fibre connectors and splice losses. A lot of care was taken in the measurements to reduce errors emanating from the later to the minimum.

Figure 5.15a and 5.15b show that the maximum PDL of the measurement system for the signal wavelength between 1520-1565 nm was ≤ 1 dB. It is evident that within this range of wavelengths the PMD coefficient decreased as the system PDL increased. Figure 5.15c and 5.15d indicate that the calculated PMD coefficients at different pump-signal detuning follow closely the pattern of the system SNR in the two fibres. It is clear that at low system PDL

(<1 dB), the SNR degradation will be the main contributor to errors in the determination of fibre PMD coefficient.

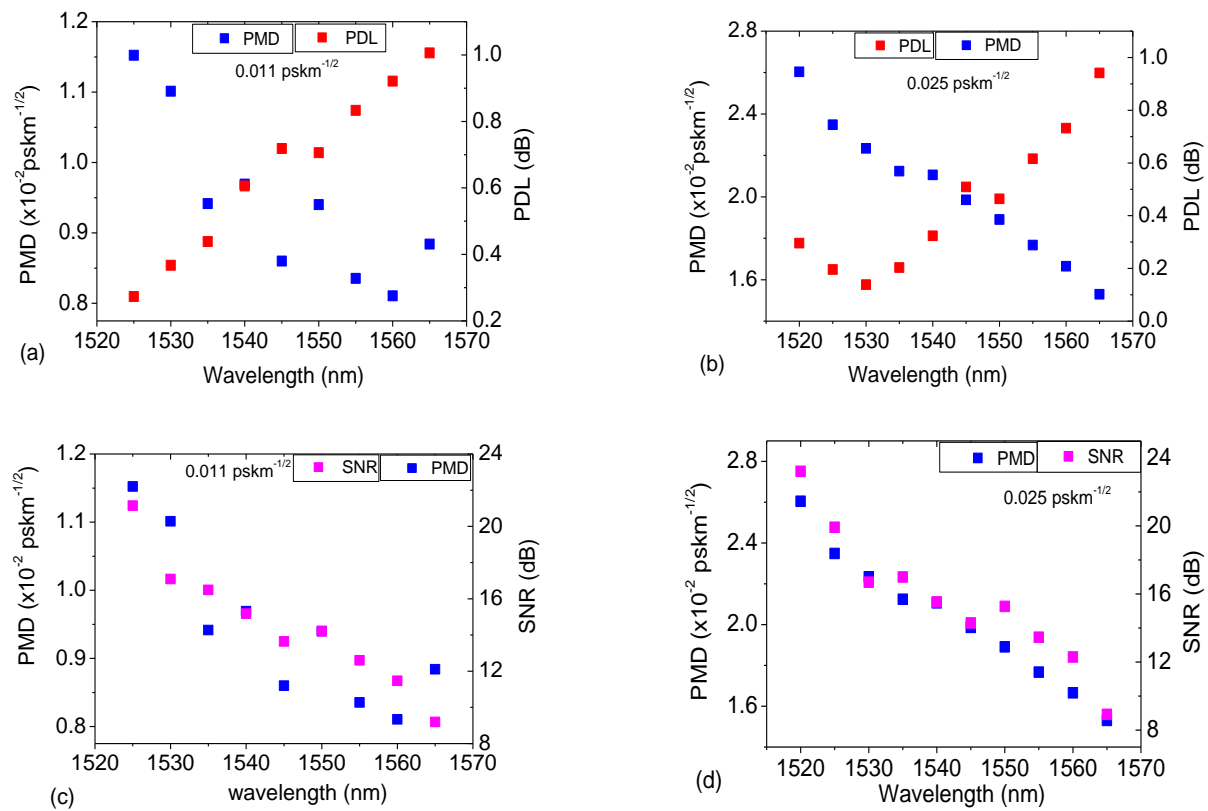


Figure 5.15: PMD coefficient variation due to PDL and the SNR at different pump-signal detuning. The fibre used in (a), (c) is a SSMF and (b), (d) is a NZDSF.

The presence of ASE which is a by-product of the amplification process generates signal-spontaneous beat noise and is a major source of SNR degradation. Improved filtering can be achieved if a narrow wavelength filter is used or a wavelength division multiplexer WDM tuned to the signal frequency. As seen in figure 5.15c and 5.15d the SNR above 20 dB is sufficient for accurate measurements using this technique. The system PDL will also contribute to errors in the values of the calculated PMD coefficient. In the absence of system noise, PDL interaction with Raman PDG will manifest as a lower than expected value of PMD coefficient. It was observed that PDG sensitivity to system PDL depends on the fibre PMD coefficient. At low PDG (high PMD) the system PDL should be kept below 0.1 dB to maintain high measurement accuracy. Low system PDL can be achieved by using WDM couplers and a tunable filter with small PDL values. In our setup the filter was found to have a PDL as high as 0.65 dB at some signal wavelengths.

5.9 Forward and backward pumped Raman PDG

It is important to closely investigate how Raman PDG relates in forward and backward pumping for fibres of different PMD coefficients and lengths. Though PDG depends on pump-signal detuning, evaluating its magnitude at the peak of the Raman spectrum would give us a good understanding of its relation in the two pumping schemes. Using the same setup as in section 5.5 the Raman PDG values of several fibres were obtained while varying the pump power between 130-330 mW.

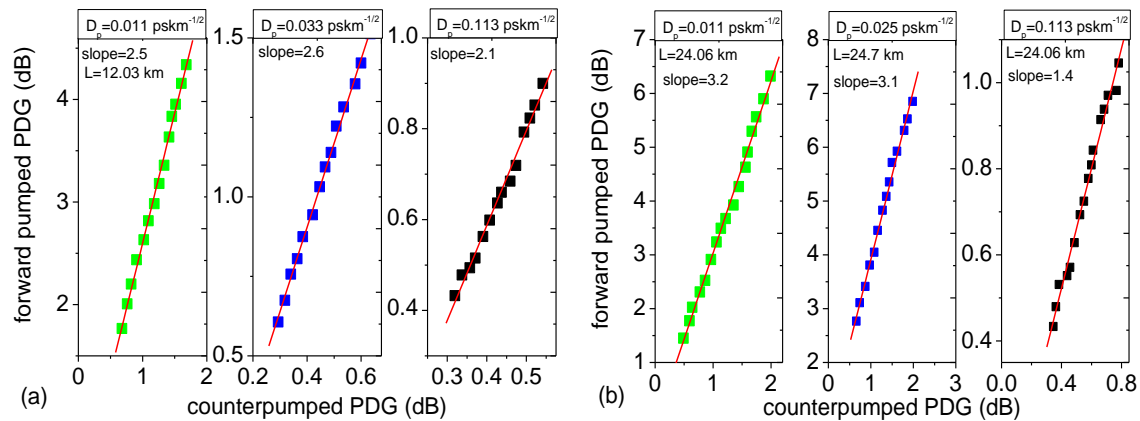


Figure 5.16: Relation between backward and forward pumped Raman PDG. In (a) each fibre has a length of 12.03km and in (b).the lengths L are indicated. The pump detuning is 100 nm.

As can be seen in figure 5.16 there is a good correlation between the PDG (dB) of backward pumped and forward pumped signal. However this correlation depends on the length and the PDM coefficient of the fibre as the slopes indicate. In figure 5.16a where the fibre length is 12.03km there is no remarkable change in the slope as the fibre PMD coefficient is increased from 0.011-0.113 $\text{pskm}^{-1/2}$. This implies that within this range of fibre PMD the back pumping changes the effects of the Raman amplification process in a similar way if the length (L) of the fibre is comparable to the effective length L_{eff} . The attenuation increases linearly with length and when the length of the fibre is small the pump remains strong all along the fibre even to the output. In this case, the PDG in the forward pumped configuration increased by a factor of 2-3 when compared to the backward pumping configuration. Figure 5.16b shows that the effect of backward pumping on the amplification process depends largely on the fibre PMD. The results show a reduction in the slope by a factor of two when the fibre PMD coefficient is increased by a factor of ten. In this case the fibre is long compared to its effective length and most of the pump power gets attenuated. Previous report by Son *et al* (2005) concluded that backward pumping reduces PDG by a factor of three. Our

results contradict this earlier report which did not account for the length of the fibre. However there is some agreement for the fibre with low PMD. We find here that in order to determine how the PDG in the backward pumping configuration relates to PDG in the forward pumping configuration it is important to properly account for the length and PMD of the fibre. It is also important to ensure that the pump remains un-depleted by keeping the input signal power moderately low.

In summary, the gain statistics of a RFA can be described using the three gain quantities which are: PDG, on-off gain and net gain. Statistical distributions of the three gains depend on the PMD parameter of the fibre and the DOP of the pump. The length of the fibre also influences the statistics of the gains. Polarization scanning techniques can be used to characterize the gains in low and high PMD fibres. However, low PMD fibres require the scanning of both pump and signal SOPs at the input. This is because uneven coverage of input SOPs on the Poincaré sphere may result in skewed distributions of the gains. This behaviour is caused by the fact that the gains depend on the pump input SOP. At high PMD this dependence is nullified due to enhanced polarization mixing. The gain statistics are also dependent on the pumping schemes where forward pumping has the highest gain fluctuation for both low and high PMD fibre. Raman PDG and on-off gain are well related and their averages can be used to extract the PMD coefficient of a fibre. Finally it was found that the PDG in the forward and backward pumping are proportional. The ratio of this proportionality decreases as the fibre PMD increases.

Chapter Six

Effects of polarization dependent loss on Raman gain

Raman polarization dependent gain (PDG) and polarization dependent loss (PDL) are two polarization effects which are different in terms of their generation mechanism. However, in their measurement and determination these effects bear similarities since they both affect the optical intensity of a signal. In this chapter we investigate the behaviour of Raman on-off gain and PDG in the presence of PDL.

6.0 Introduction

In practical fibre optic communication systems there exist numerous inline optical components whose polarization dependent loss (PDL) is non negligible. Furthermore, every RFA is configured into the optical system by the use of optical components such as WDM couplers, isolators, filters and gratings, all of which exhibit PDL (Burgmeijer *et al*, 1990). Studies have shown that adapting a more dynamic configuration would greatly improve the performance of a RFA. In most cases this involves introducing extra optical component(s) (Zheng *et al*, 2002; Li *et al* 2006). It has been confirmed by Kimsas *et al* (2004) that inserting an isolator in between two gain media consisting of dispersion shifted fibre (DCF) would greatly improve the noise characteristics of the Raman amplifier. When considered alone, PDL is known to induce OSNR fluctuations in a system (Mecozzi and Shtaif, 2004; M. Yu *et al* 2002). Previous studies that dwelt on the impact of PDG and PDL in long-haul amplified systems showed that the combined effect of PDL and PDG has adverse effects on the system performance (Lichtman, 1993, Bruyere and Audouin, 1994, Lichtman, 1995). Chowdhury, and Bhagavatula (2001) simulated the impact of PDL on the gain ripple of an EDFA and found that PDL distorts the flatness of the gain spectrum. Other analysis on parametric amplifiers (Yaman *et al*, 2006) showed that none orthogonality of two pumps caused by PMD and PDL is detrimental to the performance of a dual-pump parametric amplifier. They stated that the effect of the PDG is equivalent to that of polarization independent gain followed by a PDL component. The fundamental issues regarding the interaction of Raman PDG and PDL are greatly significant and have not been fully understood. As a result PDG/PDL effects have been assumed to be the same because of similarities in characteristics

(Haunstein and Kallert, 2001; Yan *et al*, 2002; Dong *et al*, 2006). In their experimental work, Yan *et al* (2003) argued that the presence of PDG in a system with non-negligible PDL is necessary in order to suppress PDL effects. This may be true for an EDFA which has low PDG, but the case for a RFA requires further investigation. In their investigation on statistical properties of PDG in a RFA, Lee *et al* (2002) stated that PDL effects result in nominal gain variations when the pump degree of polarization (DOP) is small. In this work, we investigate by simulations and experiment the effects of PDL in a distributed RFA. Our focus here is mainly on the behaviour of Raman PDG as well as the statistics of on-off gain in the presence of PDL and the role of PMD in the interaction.

6.1 Measurement setup

In the experimental setup of the distributed RFA, a PDL emulator of known value was introduced. Measurements were taken each time with the PDL connected at different locations (1-4) as shown in figure 6.1.

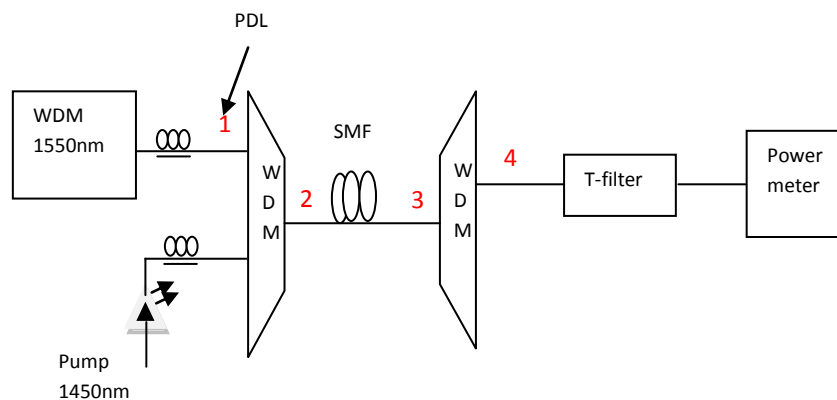


Figure 6.1: Schematic diagram for evaluating PDL effects on Raman Gain. (T-filter refers to a tunable filter and WDM-narrow band WDM coupler).

The WDM source wavelength was set at 1550 nm and its power changed each time while observing the signal gains. The pump and signal were scrambled separately at low speed before coupling the two into the fibre. The reason for polarization scrambling is to provide all possible SOPs at the input thus activating the emulator PDL and also generating PDG.

Figure 6.2 shows the PDG variation in the forward pumped RFA in the presence of the PDL emulator. The fibre used was that of PMD coefficient $0.011 \text{ pskm}^{-1/2}$ and length 24.06 km. This fibre provided enough PDG which would otherwise be small if a high PMD fibre was used.

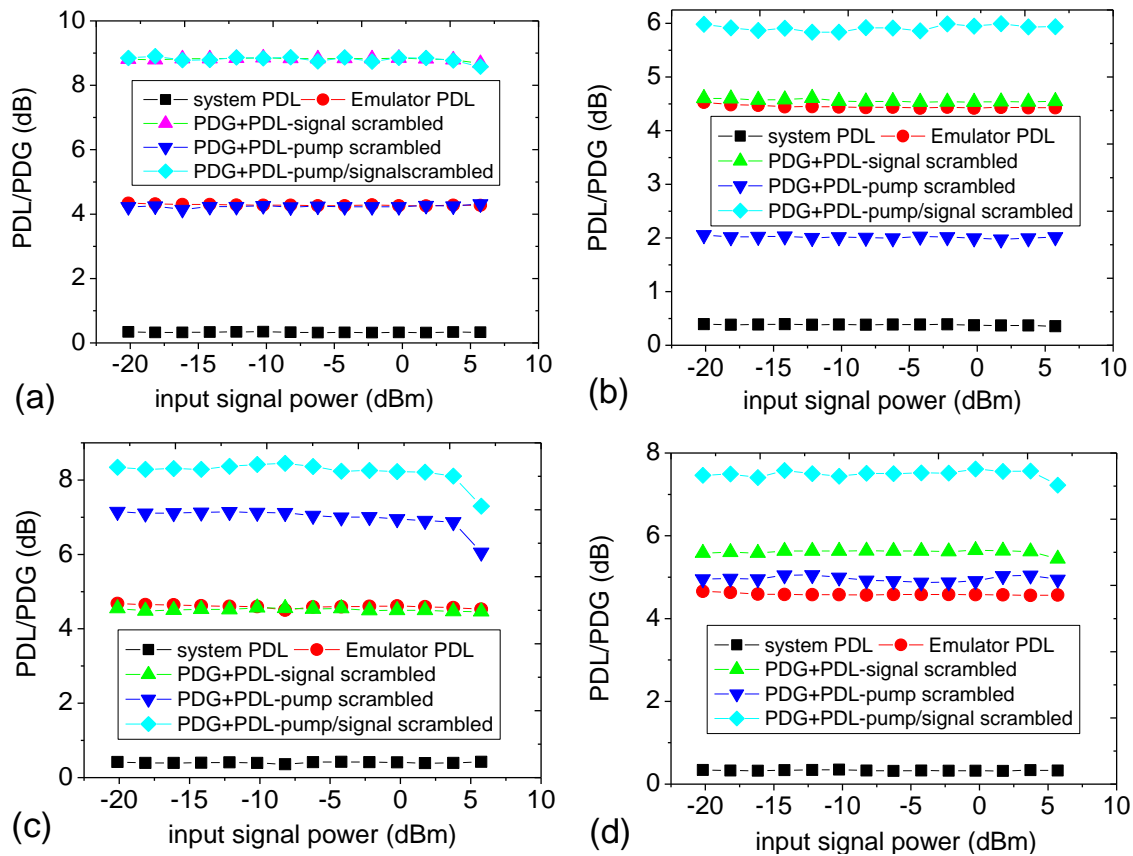


Figure 6.2: Raman PDG variation with input signal power in the presence of a PDL emulator placed at the following positions: (a) one (1), (b) two (2) (c) three (3) and (d) four (4). (Refer to figure 6.1).

Polarization scanning was achieved first by scrambling the signal alone, then the pump, and finally both the pump and signal. Incorporated in the figure are the system PDL and also the total PDL with the emulator connected at different positions. The total value of the PDL with the emulator connected ranged between 4.3-4.8 dB which is higher with respect to telecom optical components. However, such a large PDL value is significant and enabled us to emphasise the interaction of PDG and PDL. Figure 6.2a shows the PDG-PDL behaviour when the emulator is connected at position one. In this case, only the signal experiences loss due to PDL while the pump is not affected. As can be seen, the resulting PDG due to the scrambling of the pump has the same value as the measured PDL of the emulator. Also, scrambling the signal alone gave similar results as when both the pump and signal input polarizations were scanned. The implication is that when the PDL is high the PDG becomes independent of pump input polarization, similar to the case of high PMD fibre. In figure 6.2b the PDL emulator was connected at position two immediately after the input WDM coupler so that both the pump and signal experience attenuation due to PDL. In this case, the sum of PDG and PDL generated by scanning the signal input SOP is similar to the emulator PDL

value. The PDG value obtained with the pump scrambled is less because of pump losses at the PDL emulator. We also note that the sum of PDG and PDL measured while scanning both the pump and signal input SOPs is less than that obtained in figure 6.2a for the same reason. Results in figure 6.2c were obtained by connecting the emulator at position three which is immediately before the output WDM coupler. The results show that the sum of PDG and PDL measured while scanning the signal input SOP is similar to the global PDL. This corresponds to a situation where the signal PDG is completely eliminated after it passes through the PDL emulator. In the same figure, scanning the pump or both the pump and signal result in the weighted sum of PDG and PDL. There is also the evidence of amplifier saturation as the input signal power increased, signifying large PDG contributions to the weighted sum. Similarly, in figure 6.2d the contribution of the scanned pump to the weighted sum of PDG and PDL is very small compared to that due to pump-signal scrambling. The results in figure 6.2 imply that the weighted sum of PDG and PDL cannot be less than the emulator PDL. That is to say in a practical system the PDL associated with the optical components used to configure RFA always add to the Raman PDG. We can understand this behaviour if we consider the transmission properties of a component with PDL when subjected to an optical field and the nature of PDG in a Raman amplifier. An optical element exhibiting PDL has two mutually orthogonal axes which correspond to axes of maximum and minimum power transmission. On the other hand, PDG emerges as a result of changing orientation of the pump and signal SOPs which is caused by time variation of PMD in the fibre. The overall effect of PDL and PDG is to increase power fluctuation at the output so that a maximum-minimum power meter will measure the weighted average of the two.

6.2 Statistics of RFA gain in the presence of PDL

In this case we investigate the effects of PDL on Raman on-off gain statistics using the fibre of length 24.06 km and PMD coefficient $0.011 \text{ pskm}^{-1/2}$. The gain statistics become important in understanding simulation model(s) which would best represent the interaction between PDG and PDL. The same PDL emulator used in section 6.1 was involved and the source wavelength was set at 1550 nm. Using the same setup as depicted in figure 6.1, the gain was determined while scanning the input SOPs of the pump and signal simultaneously.

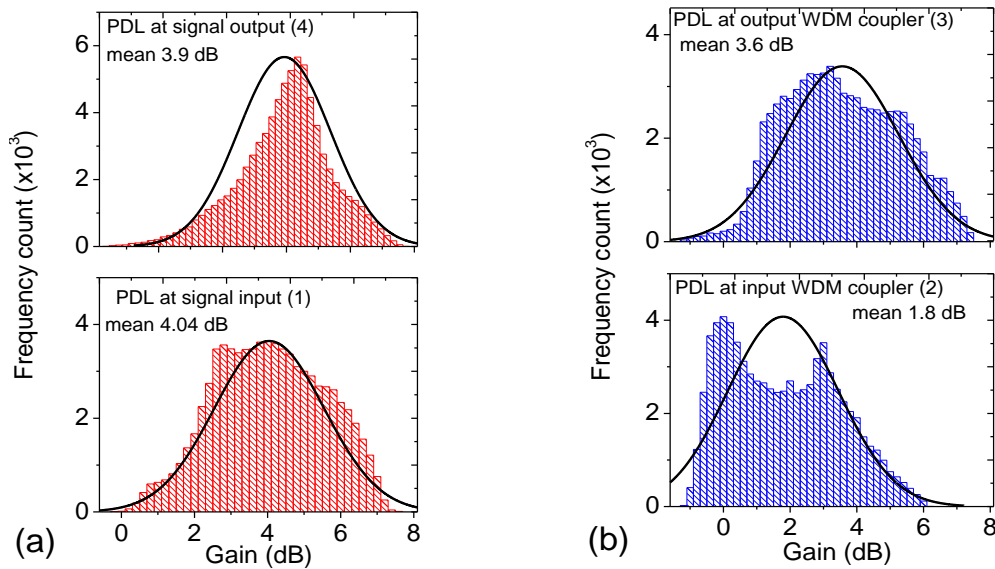


Figure 6.3: Raman on-off gain distribution in the presence of PDL. Fibre PMD, $D_p=0.011 \text{ pskm}^{-1/2}$.

Figure 6.3 represents the distribution profiles which were obtained with the PDL emulator connected at positions 1-4. The overlaid Gaussian fit reveals the deviations of the gain distributions that were caused by the PDL of the emulator. The negative gain (which is actually a loss) was due to high power attenuation of the loss axis of the PDL emulator. It is clear from the figure that the gain distributions depend on the position where the PDL is placed. Figure 6.3a is a comparison of the profiles obtained when the signal loss was followed by gain (position 1) and when the signal gain was followed by loss (position 4). In these two cases, the PDL emulator affects the signal power while the pump power remains unclipped during SOPs scrambling. As can be seen, the gain profiles are different even though the means of the distributions are almost equal. In particular, we find that a power loss occurring after signal amplification would depopulate the centre of the distribution as well as enhance the tails. Figure 6.3b shows a similar comparison where the emulator is connected after the input coupler (position 2) and before the output coupler (position 3). This second situation represents a case where the pump and signal paths plus the input and output WDM couplers have high PDL. With the PDL emulator at position 2 the profile shifts to a low mean value and appears to be bimodal. This behaviour is due to attenuation of the pump by the PDL which results in varying pump power. Thus the pump SOPs that are least attenuated result in gain that is distributed about the right peak while the left peak is associated with signal gain when the pump power is most attenuated. This effect is enhanced in the low PMD fibre which causes the pump and signal SOP to remain in the same orientation over a long distance because of poor polarization mixing. A relatively high PMD (appendix I) would

ensure efficient SOP mixing resulting in reduced PDG. It was observed that the on-off gain decreases more when the pump encounters high PDL. In practice, both the fibre birefringence and the principal axes of the optical component vary with time because of environmental changes (Kogelnik *et al*, 2002). It is therefore not possible to minimize PDL effects by alignment of the signal and pump with the axes of maximum transmission. Instead, optical components with very low PDL have been fabricated using modern technology (Eldada, 2001) and offer the best solution. It has been mentioned that the effect of PDG is equivalent to polarization independent gain followed by PDL (Yaman *et al*, 2006). However, we have seen that PDL more often than not always enhances PDG effects.

6.3 Simulation of PDL/PDG interaction in the presence of PMD

In an effort to gain a better understanding of PDL effects during Raman amplification, simulations were performed using commercially available software VPI 8.6. The issue here was to investigate the behaviour of Raman PDG and on-off gain at increasing values of PDL.

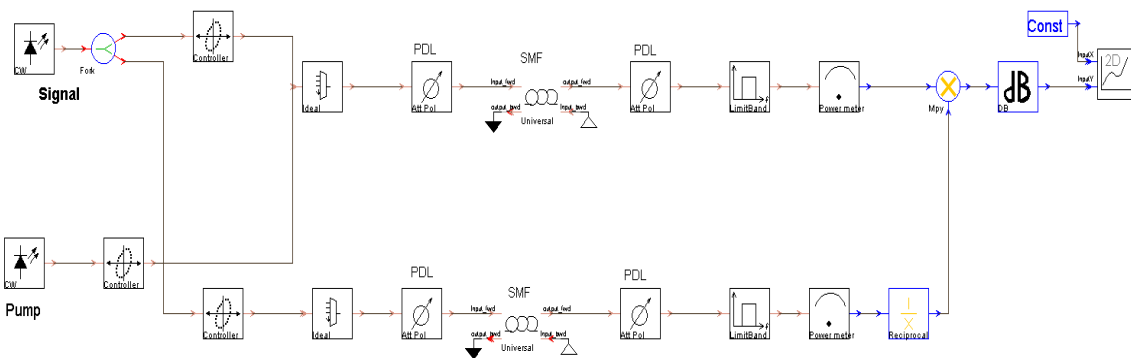


Figure 6.4: Simulation schematic used for measuring the effects of PDL in a distributed RFA. (See an enlarged version in appendix VI)

Two fibres of PMD coefficient $0.01 \text{ pskm}^{-1/2}$ and $0.1 \text{ pskm}^{-1/2}$ and length 25 km were used in the simulations. The component PDL was simultaneously introduced near the input WDM coupler and at the output of the fibre as shown in figure 6.4. The PDL module was set with the least attenuated axis corresponding to the horizontal (x-axis) while the most attenuated axis was the vertical (y-axis). The wavelengths of the pump and signal were set at 1450 nm and 1550 nm respectively, and their optical powers were correspondingly set at 22 dBm and -10 dBm. The input SOPs of the pump and signal were set using polarization controllers so that both were either orthogonal or parallel to the PDL axis (x-axis) at the input.

Figure 6.5 shows the contribution of fibre PMD to the effects of PDL on RFA gain. Again, larger values of PDL than typically found in an optical fibre link were used in order to

emphasise the influence of PDL on Raman gain. Figure 6.5a represents the PDG/PDL obtained with the pump on (left scale) and the PDL measured at the output of the two fibres without the pump (right scale).

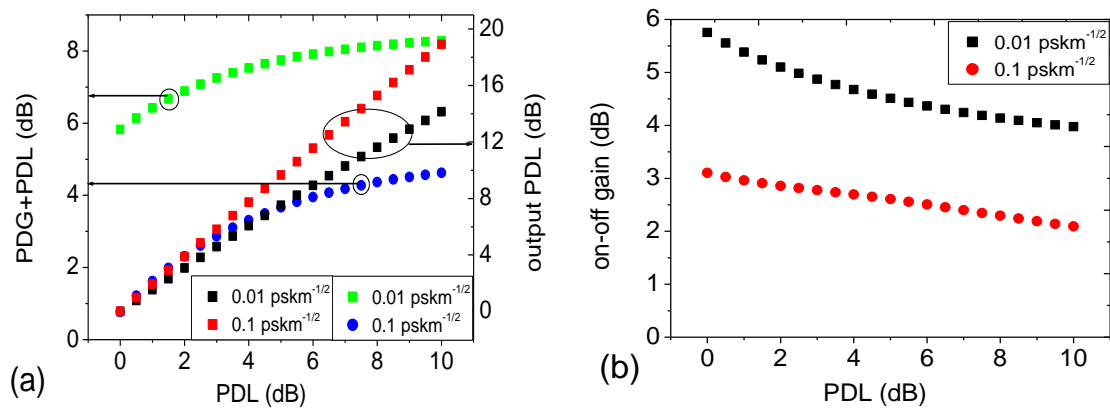


Figure 6.5: Variation of (a) PDG and (b) on-off gain for a RFA, as PDL at the input and output WDM couplers increase.

This is the worst case scenario where the pump and signal input SOPs are linearly polarized. The results clearly show that when the pump is on, the PDL adds to PDG in a weighted manner and the resultant value is asymptotic when the PDL become predominantly high. This behaviour is attributed to the interaction of PMD with PDG/PDL. It is known that PMD will rotate the SOPs of light in the fibre during propagation. As a result the orientation of light with the PDL component changes with time, which leads to a varying PDL. At the same time PMD will rotate the SOPs of the two waves (pump and signal) resulting in PDG. Since PDG and PDL are known to be stochastic in nature their interaction through PMD is also stochastic. Conversely, in the absence of the pump, the PDL at the output increases almost linearly as the applied PDL increases. The results show a significant difference between the values of output PDL (pump off) obtained for the two fibres with the high PMD fibre having the higher values. This difference is a manifestation of PMD polarization scrambling in optical fibres. A high PMD fibre is more efficient in polarization scrambling so that the output SOP is independent of the input SOP. On the other hand, a low PMD fibre will barely influence the orientation of the signal SOP as it propagates and consequently enhances alignment with the principal axes of the PDL elements, thus reducing PDL effects. That is to say, it requires a much longer fibre for polarization scrambling to be complete when the fibre PMD is low. Results in figure 6.5b indicate that the on-off gain decreases as the PDL increases and approaches some asymptotic value when the PDL is high. This is in agreement with the fact that the pump loses power every time it traverses a PDL component which

results in less power available for signal amplification. It is important to note that a PDL element changes the SOP of light traversing it, so that in an event where the PDL is increasing, the SOP after each PDL will be different (Huttner *et al*, 2000; Damask, 2005). The decrease in the on-off gain with increasing PDL cannot be linear because the pump and signal SOPs are changing due to the increase in PDL.

6.3.1 Wavelength dependence of RFA gain in the presence of PDL

One of the most important characteristics of the RFA is that of broadband amplification which has found practical application in dense WDM transmission. The contribution of optical components with PDL to the nature of the RFA broadband gain is an important aspect in understanding the factors that influence the amplifier efficiency. The setup in figure 6.4 was used to investigate the effects of PDL on the signal gain while sweeping the source wavelength between 1525-1570 nm. Two fibres, each of length 25km and respective PMD coefficients of $0.01 \text{ pskm}^{-1/2}$ and $0.1 \text{ pskm}^{-1/2}$ were used in the simulations. To ensure small-signal amplification, the input signal power was set at -10 dBm and the pump power at 22 dBm .

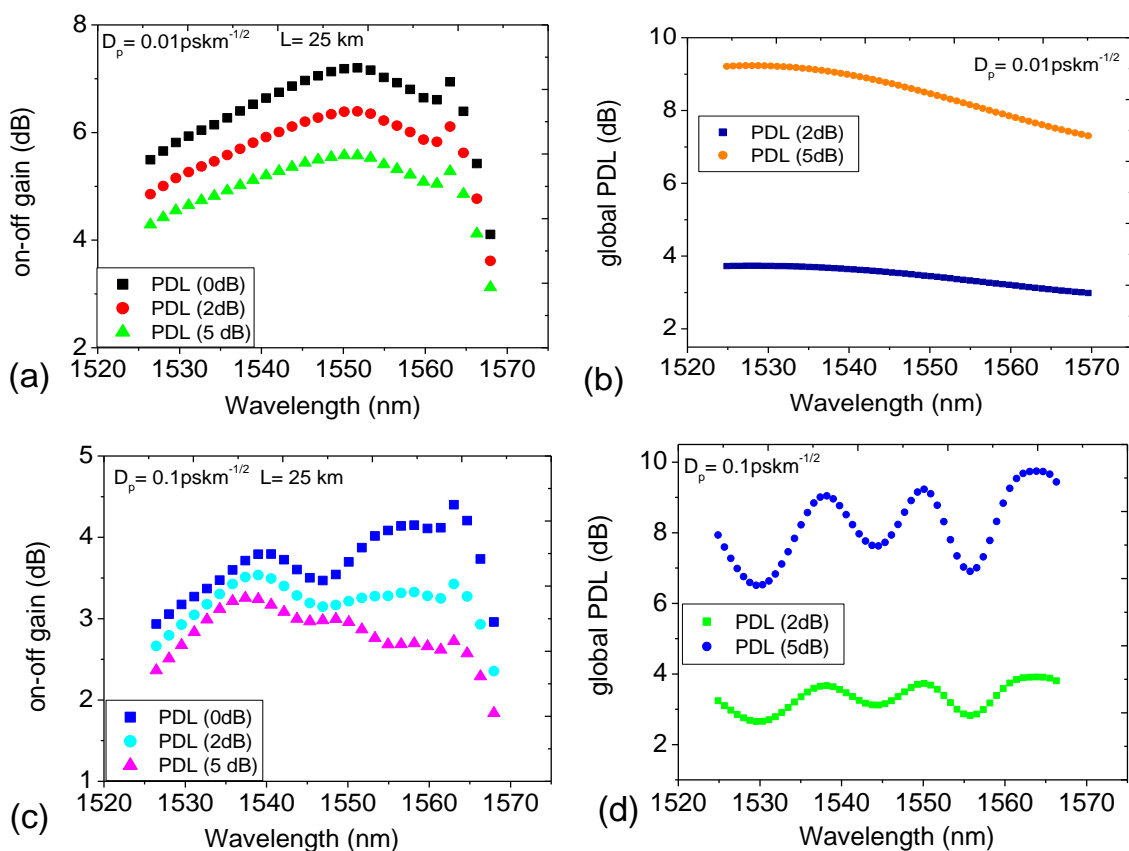


Figure 6.6: (a) and (b) represent Raman on-off gain variation with wavelength of two fibres in the presence of PDL, while (c) and (d) are the global PDL variations with wavelength in the absence of the pump.

Figure 6.6a and 6.6b shows the effects of PDL on Raman on-off gain, evaluated by setting the PDL modules at 0 dB, 2 dB and 5 dB. These curves were obtained with the input SOPs of the pump and signal right circularly (RC) polarized. Similar gain curves were obtained for the other five degenerate SOPs. As can be seen there is a general decrease in the gain across the signal spectrum as the PDL increases. In figure 6.6a, there is a gradual tilt in the slope of the gain curve as the PDL increases. This is attributed to the weak dependence of PDL on the signal frequency when the fibre PMD is small. Also observed is a systematic decrease in gain as the PDL increases which is again related to the low PMD of the fibre. As explained in the last section, the weak birefringence associated with this fibre allows the light waves to maintain their alignment over long distances of propagation, in the absence of external perturbations. As a result, the input SOP of the signal into the PDL elements will maintain the same orientation during the wavelength sweep. This explanation is firmly supported in figure 6.6b, which shows the global PDL of the concatenation in the absence of the pump. Results in figure 6.6b imply that in a concatenation consisting of fibre and PDL components, the output SOP of the signal will be less dependent on signal frequency if the fibre PMD is very small. Alternatively, this behaviour can be explained by considering the PMD vector bandwidth which is known to depend inversely on the DGD of the fibre (Poole *et al*, 1991; Betti *et al*, 1991; Bruyère, 1996 and Aso, 1998). Figure 6.6c reveals the role of the fibre PMD in the interaction between PDG and PDL. Apart from gain clipping, the presence of PDL introduces gain tilting which can be clearly seen in the signal wavelengths that are further away from the pump. In this case the fibre birefringence is strong enough to rotate the SOPs of the pump and signal as both propagate in the fibre. In the frequency domain this implies that for a fixed input SOP of the signal, the output SOP changes as the source frequency is scanned (Poole and Wagner, 1986). This causes the relative orientation between the PDL axis of the elements at the RFA input and the ones at the output to change continuously with frequency sweep which leads to frequency dependent PDL. (Amari *et al*, 1998). Figure 6.6d illustrates the behaviour of global PDL in the absence of the pump and confirms our explanation reasonably well. The results show that the global PDL fluctuates with frequency when a high PMD fibre is involved in the concatenation. We also observe that the fluctuation of global PDL increases as the local PDL increases.

In summary it is clear that the interaction of Raman PDG and optical component PDL will result in even more signal fluctuations than when only one of the two is involved. The nature of gain fluctuation depends on the value of the PDL and its location in the system. The overall effect of PDL is to reduce Raman gain and this can even result in signal loss.

Simulation results have shown that in a RFA the interaction of PDG and PDL is mediated by PMD in the fibre. High PMD enhances this interaction and results in wavelength dependent tilting of the signal gain. Simulations also revealed that both PDG and PDL effects tend to dominate each other depending on their relative magnitudes. This simply means that in an event where the PDL is small the PDG effects will dominate, and vice versa. Finally, it is important to note that optical components used in the RFA configuration and optical communication systems have moderate PDL, and the effects observed in this study will obviously be less severe. However, this study provides an excellent experimental framework that can be used to support and give insight into the development of accurate theoretical and numerical models incorporating PDG, PDL and PMD.

Chapter Seven

Polarization pulling during Raman amplification in fibres

The need to control the polarization of light in optical communication and photonic applications has recently been a subject of great interest. It is a fact that one of the most useful passive devices in the study of polarization in optical fibres is the fibre-based polarization controller (PC) which is manually operated. Many different solutions to polarization control have been emerging which are mostly to alleviate its effects. In this chapter we investigate polarization pulling occurring in RFA.

7.0 Introduction

The random nature of the SOP of light in fibre has been a challenge in every development stage of an optical communication system (Garnier *et al* 2002). Although a direct detection receiver is insensitive to polarization changes, some new applications demand proper control of the input SOP. Among other things, there is the need to implement more efficient signal processing techniques such as coherent detection (Walker and Walker 1990; Ip *et al*, 2008), as well as the application of advanced data formats such as polarization division multiplexing (PolDMX) of channels (Hill *et al*, 1992; Noé *et al*, 2001). The success and realization of these applications demand predictable polarization of light with long term stability. The principal behind PMD compensation in high bit rate (> 10 Gb/s) systems is based on active tracking of the polarization of channels (Heismann *et al*, 1998; Sunnerud *et al*, 2002). Many optical amplifiers and optical devices are polarization sensitive and their full potential can only be achieved if we find some means of stabilizing the polarization. Solutions seeking to address the control of the polarization of light have been reported by several groups. Heebner *et al* (2000) demonstrated the design of a non linear photorefractive crystal which converts unpolarized light into linearly polarized light with unit efficiency. In a different approach Pitois (2004), demonstrated the control of light polarization in isotropic fibres by the nonlinear process of four-wave mixing of two counter propagating beams. More recently, Pitois (2008), designed a polarization attractor for telecommunication applications using highly nonlinear fibre (HNLF). Around the same time Martinelli *et al* (2006), theoretically and experimentally developed an active electro-optic feedback technique for polarization

control. Polarization attraction induced by stimulated Brillouin scattering (SBS) has also been demonstrated in fibre where the input SOP of the signal was found to match the SOP of a counter-propagating pump at the output (Thevenaz *et al*, 2008). Brillouin gain in fibre is polarization dependent such that maximum gain occurs when the signal is aligned with the pump and zero gain when they are orthogonal. It has been found that PDG due to SBS and the weak random birefringence in modern fibre is the cause of polarization pulling (van Deventer and Boot, 1994).

Polarization attraction occurring during stimulated Raman scattering (SRS) in fibre was recently demonstrated by Martinelli (2009). In their experiment a pump and a signal were co-propagated in a 2.1 km dispersion shifted (DS) fibre of PMD coefficient $0.075 \text{ pskm}^{-1/2}$. It was found that a scrambled signal was attracted to the pump SOP at the output. The level of attraction increased as the pump power increased. Further numerical and experimental analyses were carried out by Ferrario *et al* (2010) with the aim of establishing the optimum conditions that would provide effective polarization pulling for application in optical communication. In their work they evaluated the contribution of pump power, fibre length and PMD in determining the effectiveness of polarization pulling. It was found that pulling increased as the PMD of the fibre decreased and that it also depended on fibre length. Their analysis involved pump powers above 500 mW and fibre lengths below 20 km. Numerical simulations reported by Ursini *et al* (2011) showed that Raman polarization pulling in fibre is limited by pump depletion at high pump power due to increasing nonlinear polarization rotation (NPR). All these reports show various aspects of Raman polarization pulling while assuming nonlinear effects such as XPM and SPM to be negligible. Besides, there is a need to investigate polarization pulling at lower pump power and longer fibre lengths than the ones that have been recently reported. Our aim here is to consolidate the various aspects of polarization pulling with the view of gaining deep insight into the subject as well as to compare our results with the previous findings. Using simulations and experiments we explore the subject of polarization attraction in single mode fibres during Raman amplification.

Similar to the case of SBS, polarization attraction due to SRS in fibre is caused by the strong PDG and the small fibre birefringence in the modern fibres. PMD in fibre causes signal polarization randomization and is therefore a limiting factor in polarization pulling. There is also the aspect of NPR which is caused by power dependent nonlinear birefringence. Its effects on signal SOPs emerge as soon as the linear birefringence is too small. Some

manifestations of NPR are the nonlinear SPM and XPM which result in polarization scattering. The theory of polarization pulling is derived from the vector theory of stimulated Raman scattering (Lin and Agrawal, Aug 2003). The dynamic equations governing the pump and the signal SOPs during Raman amplification were included in chapter 3 of this thesis for quick reference.

7.1 Measurement setup

Figure 7.1 shows the experimental setup that was used in the measurement of polarization pulling effects of the pump on the signal. The source wavelength was set at 1550 nm and the signal power at -10 dBm while the pump could provide a maximum power of 25 dBm.

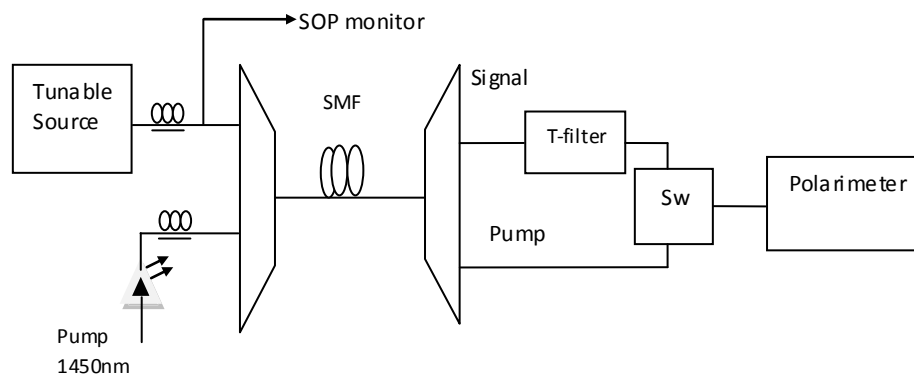


Figure 7.1: Schematic diagram for the measurement of polarization attraction. (Sw-refers to optical switch and T-filter refers to tunable filter).

The SMF in a cable of length 24.06 km was used in the measurement. At the output the signal was filtered of excess noise and connected to the polarization analyzer via an optical switch. Similar connections were performed on the pump without filtering. We noted that the excess pump power at the output was still high and needed to be attenuated before connection to the polarimeter. This made it unnecessary to filter the pump because the noise magnitude and the signal leaking into the pump output port is negligibly small to affect the measurements.

7.1.1 Effects of scrambled pump on signal pulling

In previous experiments the input signal was scrambled to provide all possible SOPs at the input while the input SOP of the pump is fixed. In our case the pump was scrambled instead and the input signal was set in turn to each of the six degenerate SOPs. The purpose here is to address the fundamental issues that result in polarization pulling in low PMD fibres. The pump power was set at either 200 mW or 360 mW and the signal output SOP was determined.

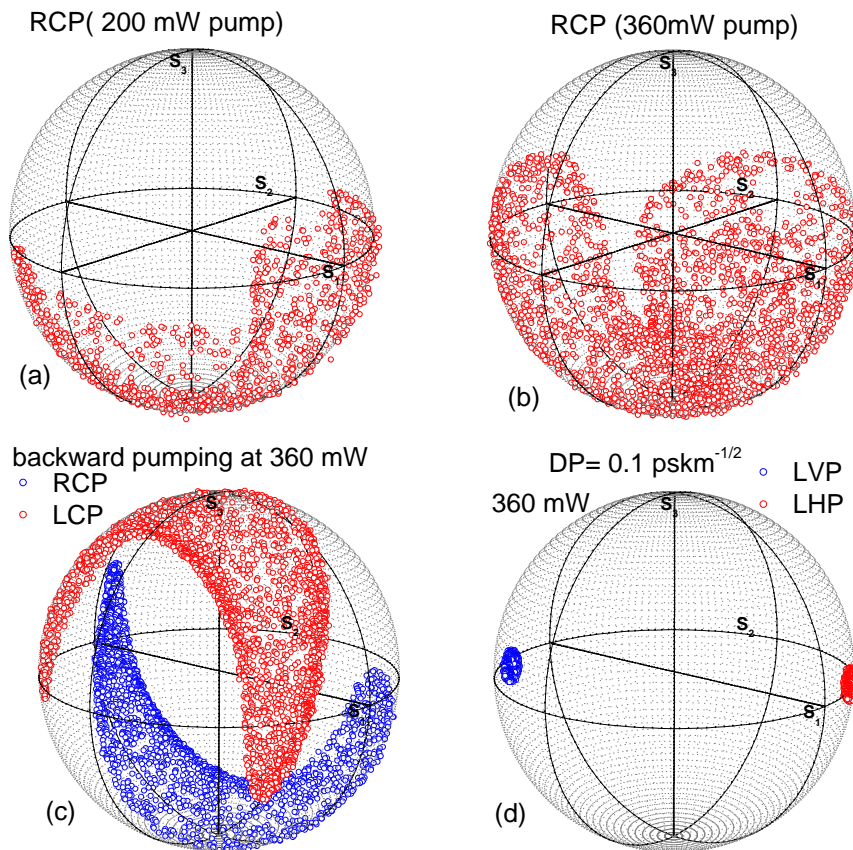


Figure 7.2: Poincaré sphere representation of the output signal SOPs when the pump is scrambled. (a), (b) and (c) represent the fibre of PMD coefficient $0.011 \text{ pskm}^{-1/2}$, (d) $0.113 \text{ pskm}^{-1/2}$. RCP refer to right circular polarization, LCP -left circular polarization, LHP- linear horizontal polarization and LVP- linear vertical polarization; of the signal at the input of the fibre

Figure 7.2 illustrates the effect of the scrambled pump on the signal when the input SOP of the signal is fixed. The signal output SOP executed a controlled motion on the sphere tracing the patterns shown. The positioning of the patterns on the Poincaré sphere depended on the input SOP of the signal which is a characteristic of random birefringence in the fibre. It is also observed that there is similarity in the patterns of each pair of orthogonal input SOPs on the Poincaré sphere and therefore one can be mapped onto the other by a rotation while observing the handedness of polarization. However the simple Jones and Mueller matrix formalism cannot be used to analyse the relation between input and output signal SOPs in this case, because one input SOP maps into many output SOPs. It was observed that the shapes of the patterns were determined mainly by the strength of the linear birefringence when the pump power is low. When the pump power was increased to 25 dBm which was the highest power available, the patterns increased in size but their shapes remained the same as is evident in figure 7.2a and 7.2b. In an event where the pump power is sufficiently high,

polarization pulling will be complete and the signal SOPs would fill the whole sphere. Similar results were obtained for backward pumping but the pulling pattern occupied a smaller area, as shown in figure 7.2c. In this case the PDG is small which translates into less SOP pulling. The role of linear birefringence in defining the location of the pattern is clearly evident. Results in figure 7.2d were obtained for the fibre of PMD coefficient $0.113 \text{ ps km}^{-1/2}$ and show very small signal SOP excursion. The implication here is that the modal birefringence is strong enough to keep the signal SOP away from the pump. It was observed in all cases that orthogonally incident SOPs resulted in output SOP patterns that are symmetric about the diameter of the Poincaré sphere. It is noted here that polarization pulling is always present even at low pump power but cannot be observed when the input signal is scrambled and the pump SOP fixed. When the pump power is high a scrambled signal will converge to the pump SOP at the fibre output; this has already been confirmed (Pitois *et al.*, 2008).

7.2 Pump-signal orientation on the Poincaré sphere

In this case we investigate experimentally the effect of increasing the pump power on the relative angle between the pump and the signal as determined on the Poincaré sphere. The output SOPs of the pump and signal were initially set at known states on the Poincaré sphere. This was accomplished by setting the corresponding input SOPs using the manual PC. The pump power was then varied over the range between 50 mW and 350 mW while measuring the SOPs of both the pump and signal.

Figure 7.3 shows the change in the relative angle between the SOPs of the pump and signal at the output of the RFA, with increasing pump power. Several combinations of the six degenerate SOPs were evaluated, of which only a few of these cases are illustrated. It should be noted that orthogonal SOPs in Jones space are 180° apart in Stokes space. Thus, two points on the surface of the Poincaré sphere that are oriented at 90° to each other are 45° in Jones space. (Goldstein and Collett, 2003). The projection angle of two SOPs is therefore equal to half the relative angle between them on the Poincaré sphere. Results in figure 7.3a were obtained for the fibre of length 12.03 km and demonstrate polarization pulling when the output SOPs of the pump and the signal are initially orthogonally polarized (180°) and when both are at 90° in Stokes space. Similar results were obtained for the fibre of length 24.06 km as illustrated in figure 7.3b. The later results show that increasing the length of the fibre enhances the pulling. Figure 7.3c represents the behaviour in the 12.03 km fibre when the output SOPs of the pump and the signal are initially parallel in Stokes space.

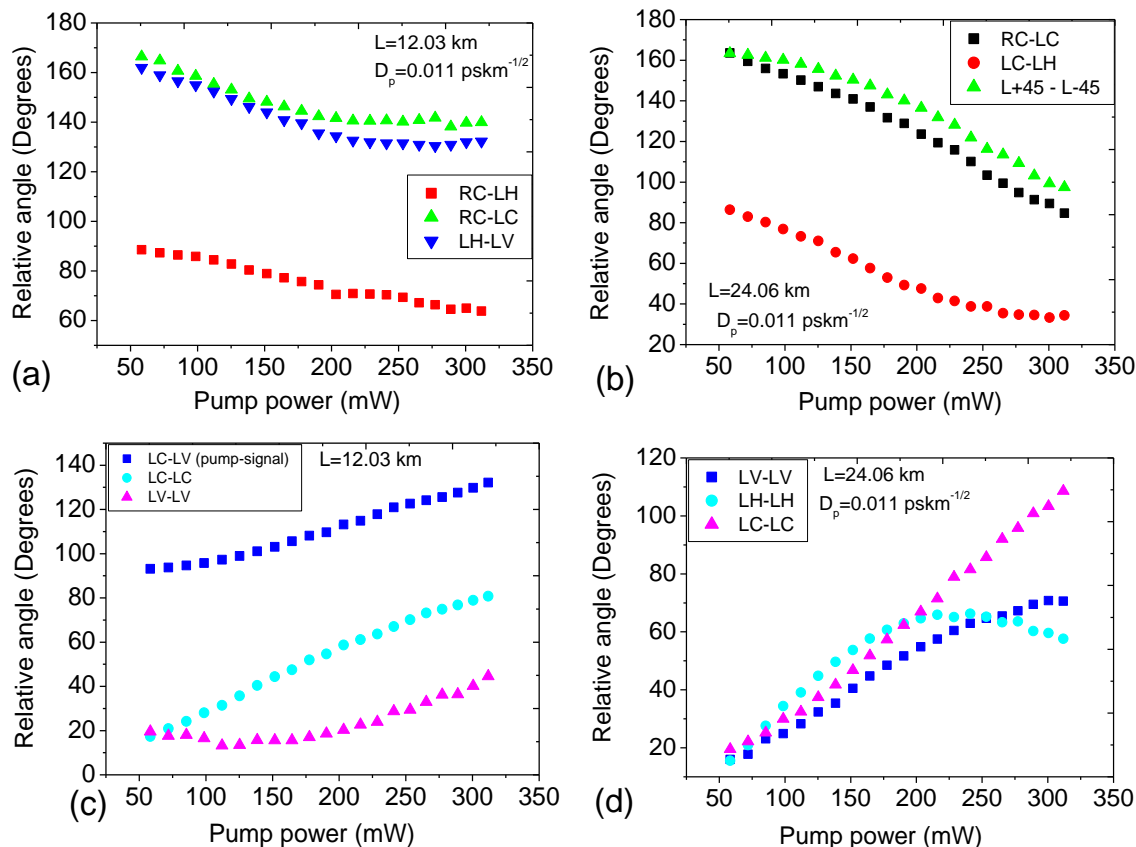


Figure 7.3: Relative angle between the pump and signal as a function of pump power for a fibre of PMD coefficient $0.011 \text{ pskm}^{-1/2}$. The length of the fibre in (a), (b) is 12.03 km and in (c), (d) is 24.06 km.

This is a clear manifestation of polarization scattering due to the small linear birefringence. The power dependent nonlinear birefringence is known to interact with linear birefringence but the effect is negligible in this case. Figure 7.3d shows similar results when the length of the fibre is doubled. As can be seen, doubling the length of fibre enhances SOP scattering. However, if the pump power is sufficiently high equilibrium can be reached where the signal SOP becomes attracted again to the pump. This is clearly demonstrated in figure 7.3d for the case when the pump and the signal are initially horizontally polarized (LH-LH). The nature of the results in figure 7.3 can be understood from a theoretical model given by Martinelli *et al* (2009). That is, polarization attraction is dictated by the mutual orientation of the pump and signal to the local birefringence vector. In this case, the nonlinear birefringence is negligibly small compared to the linear birefringence. When the pump and signal are copolarized the scattering effect of the linear birefringence is maximum because the pump power is still very small to maintain pulling. If the two are orthogonally polarized then the resultant birefringence acts in the favour of polarization pulling. Alternatively, we can

explain the same results using equation 3.2 in chapter three. The second term in the equation represents the SRS process and is responsible for polarization pulling which manifests when linear birefringence is very weak. The third term causes the signal SOP to rotate as dictated by the interaction between the linear and nonlinear birefringence. This rotation keeps away the SOPs of the signal from the pump as long as the weak linear birefringence dominates the power dependent birefringence (Agrawal, 2007 chapter 6).

A clear visualization of Raman polarization attraction can be obtained by representing both the SOPs of the pump and signal on the Poincaré sphere. Figure 7.4 shows the behaviour of these SOPs in the case of the 24.06 km fibre when pump power is increased. It should be noted that the pair of SOPs used in figure 7.4 are the same used to obtain figure 7.3b and 7.3d.

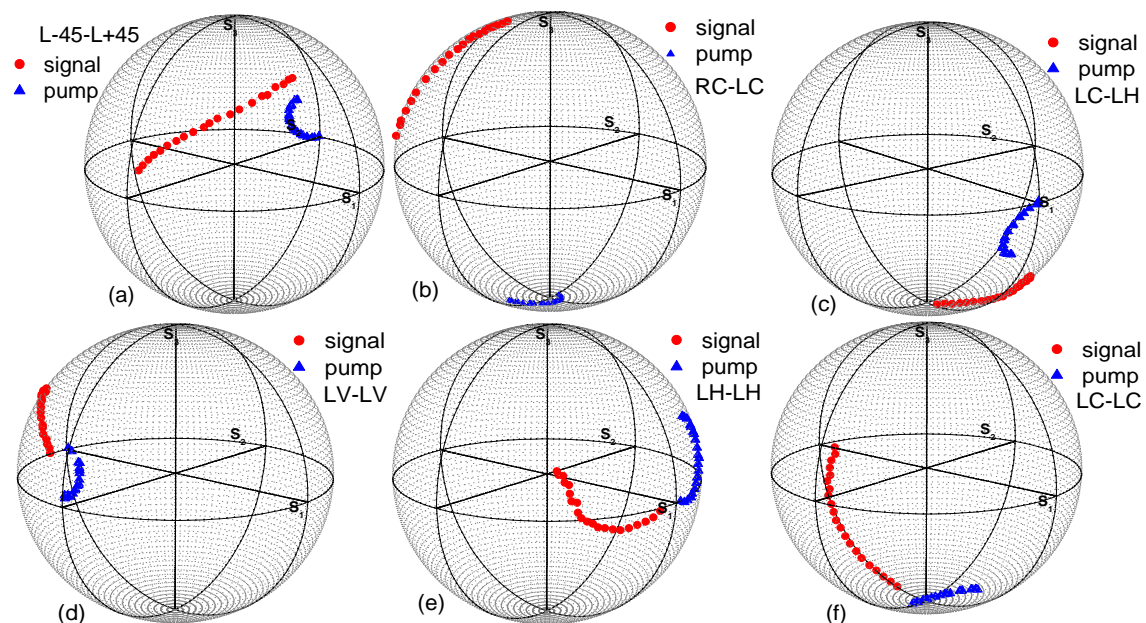


Figure 7.4: Pump and signal SOP trajectories on a Poincaré sphere as pump power is increased. The SOPs indicated mark the beginning of a trajectory.

In figure 7.4 the signal SOPs are seen moving toward the pump and also away from the pump (depending on the initial SOPs setting on the Poincaré sphere). In particular, figure 7.4 a, b and c illustrates polarization pulling when the initial SOPs of pump and signal are orthogonally polarized. Note that the signal SOPs are displaced from their initially set positions on the Poincaré sphere because they would shift the location after switching on the pump. The pump SOP is also seen to execute almost a circular trajectory as pump power increases. The behaviour is related to SPM and is due to self polarization evolution. Figure 7.4d, e and f shows the behaviour of the SOPs of pump and signal when both are initially

parallel. In these cases both SOPs are seen moving away from each other but along their respective circular tracks. This phenomenon reveals that polarization scattering observed earlier in figure 7.3c and d is actually due to the SOPs of the pump and signal assuming opposite directions (handedness) along their paths when pump power is increased. If the pump power continues to increase the signal SOP would trace out a complete circle so that it finally aligns with the pump. The phenomenon of polarization evolution has been observed during XPM (Collings and Boivin 2000) and has been discussed in details by Agrawal, (2007). However there is a clear difference when Raman amplification is taken into account and also the spacing between the pump and signal. It was observed that the DOP of the signal remained high as the pump power increased while the pump DOP decreased slightly depending on the input SOP. This decrease in the pump DOP was attributed to the phenomenon of self-polarization evolution which is clearly seen in figure 7.4. Such depolarization of signals due to the nonlinear Kerr effects has been reported and is known to be polarization dependent (Bononi and Vannucci, 2003).

7.3 Effects of fibre length and PMD on polarization pulling

Several factors come into play when polarization pulling and amplification occur simultaneously. A good understanding of the parameters influencing polarization pulling and their interplay is the key to effective polarization control. It has already been seen in section 7.2 that the length of the fibre influences polarization pulling. Consequently this section is devoted to evaluating the aspect of fibre length and fibre PMD in polarization pulling. In this investigation simulations were performed using commercially available *VPI 8.6 software* which is capable of configuring any optical device and system. In the forward RFA configuration, a $1\mu\text{W}$ signal at source wavelength of 1550 nm was amplified using fibres of different lengths and PMD coefficients. The pump power was varied between 50 mW and 3 W for each fibre arrangement while evaluating the SOPs of the pump and signal at the output.

Figure 7.5 illustrates the nature of Raman polarization pulling when different lengths of the fibre and PMD coefficients are involved. This case represents the relative angle between the SOPs of the pump and signal as observed on the Poincaré sphere when both are orthogonally polarized at the input. Similar results were observed for initially copolarized pump and signal except that the later subtend a lower initial relative angle. Figure 7.5a shows that for a fibre of known PMD coefficient, polarization attraction depends on the length of the fibre as well as the pump power. The minimum relative angle of attraction is seen to decrease as the length of

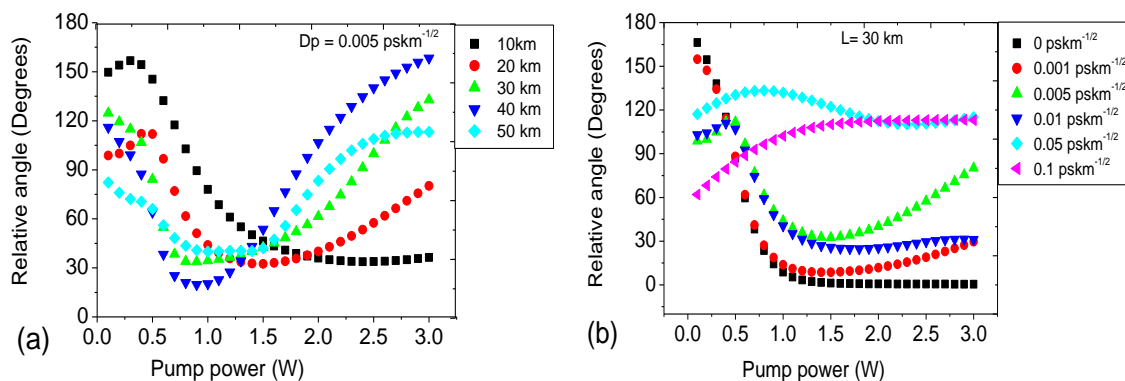


Figure 7.5: Relative angles between the pump and the signal in Stokes space for: (a) fibres of different length but the same PMD coefficient, (b) fibres of varying PMD coefficient but the same length, as a function of pump power.

the fibre is increased. At the same time, the pump power required to observe maximum polarization attraction decreases as the length of the fibre increases. However, the results suggest that there is a maximum length of the fibre above which the minimum relative angle of attraction begin to increase irrespective of the increasing pump power. It is also observed that polarization attraction decreases when the pump power is increased above the value at minimum relative angle of attraction for each fibre. This behaviour is attributed to pump depletion which causes the pump to transfer most of its energy to the signal thus reducing its polarization characteristics. It should be noted that Raman PDG, which is the main contributor to polarization attraction, increases with fibre length and therefore each fibre will saturate at a different pump power. At the same time there is pump attenuation which is proportional to the length of the fibre. These two attributes lead to the nature of the curves observed in figure 7.5a for pump powers above the value for minimum angle of attraction. In a practical scenario where the fibre length can be $> 100 \text{ km}$, the onset of chromatic dispersion is inevitable (Menyuk 1999). This may limit polarization attraction for such long lengths of fibre, but for shorter lengths as used in this investigation such effects are negligible. The results in figure 7.5b were obtained using an arbitrary but reasonable length of the fibre of 30 km. As can be seen, polarization attraction depends on the fibre PMD and decreases as the fibre PMD coefficient increases. At $0 \text{ pskm}^{-1/2}$ PMD coefficient, polarization attraction becomes complete as soon as the pump power is sufficiently high to maintain the attraction. The implication here is that linear birefringence is actually the major cause of pump-signal SOPs misalignment in RFA and a perfect amplifier would result if PMD in fibre can be eliminated. This result implies that effective polarization attraction can only occur when fibre PMD is below $0.01 \text{ pskm}^{-1/2}$. Modern fibres have PMD coefficients ranging between

0.1-0.01 pskm^{-1/2} but with improving fabrication techniques values as low as 0.005 pskm^{-1/2} have been reported (Galtarossa *et al*, 2005).

7.3.1 Dependence of pulling on signal wavelength

The broadband nature of the RFA gain spectrum is another important aspect in understanding polarization pulling. The fact that RFA gain and fibre birefringence are wavelength dependent, intuitively leads to the idea of wavelength dependent polarization pulling. In this section we investigate by simulations and experiment the polarization pulling effect at different wavelengths. A fibre of length 25 km was used in the simulation while in the experiment a 24.06 km fibre was employed. In the simulation the PMD coefficient was set at 0.01 pskm^{-1/2} while the PMD coefficient of the 24.06 km fibre was 0.011 pskm^{-1/2}. Using forward pumping at a wavelength of 1450 nm, the Stokes angles between the pump and signal were determined at increasing pump power.

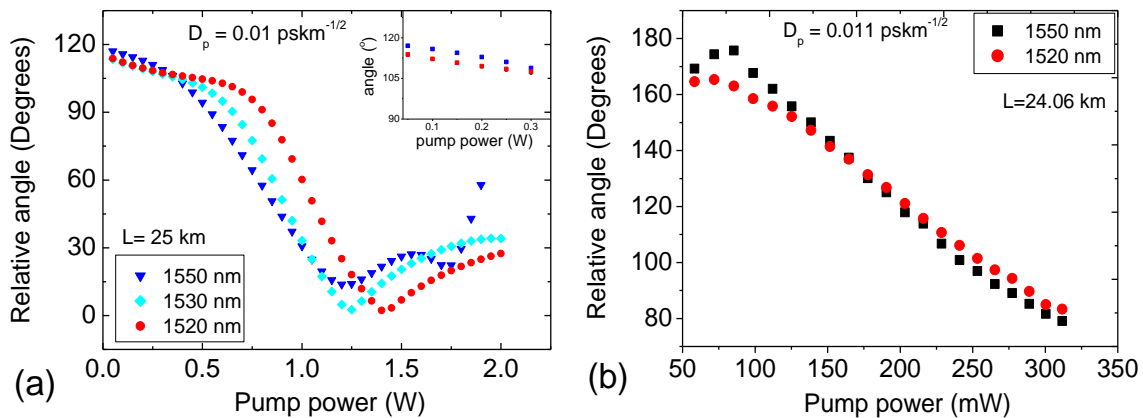


Figure 7.6: The relative angle of pump and signal Stokes vectors as a function of pump power at different signal wavelengths: (a) simulations, (b) experiment.

Figure 7.6 illustrates the dependence of relative pulling angle on the signal wavelength for orthogonally polarized pump and signal. Simulation results in figure 7.6a clearly show that in the linear region of RFA, the greater the frequency shift the lower is the pump power required for achieving the same pulling angle. This however is true only for wavelengths that are below the Raman peak frequency shift of 13.2 THz. As can be seen, the difference in relative angles for these three wavelengths is more evident for pump powers between 0.5-1 W. At the minimum achievable relative angle, each wavelength shows a different pump power with the lowest wavelength of 1520 nm having the highest power. This implies that more power is needed to align the signal SOPs with the pump when the frequency shift is small. At the same time, wavelengths near the peak of the gain spectrum display a much higher minimum pulling angle, as can be seen with the 1550 nm wavelength. This is because the high gain

causes the signal power to increase at the expense of the pump power, resulting in the reduction of the pulling effect. Consequently, pump power beyond the minimum pulling angle results in polarization scattering, as is evident in all the wavelengths. This SOP scattering phenomenon is a manifestation of a depleted pump and is a major drawback for polarization pulling using long fibres. Further simulations using fibres of the same length of 25 km but lower PMD parameters resulted in similar results. It was observed that the wavelength dependence polarization pulling increased as PMD decreased. Experimental results in figure 7.6b were obtained following the same procedure as in section 7.2 for the two signal wavelengths. These results show variation at low pump power and were obtained using a Raman pump of maximum power of 360 mW. As can be seen the results compare well with the simulations in fig 7.6a (inset), over the small power range. The highlighted simulation results correspond to the range of pump power used in the experiment. Less pulling effect was observed in the simulation over this power range because the SOPs of the pump and signal were set orthogonal at the amplifier input to demonstrate the worst case scenario.

7.4 Limitations of Raman polarization pulling in fibre

It has been observed that the small PMD in modern transmission fibres is one of the factors that facilitate polarization attraction in a RFA. When such fibres are used for Raman amplification, the pump and the signal SOPs remain aligned over long distances because of the weak birefringence associated with these fibres. This alignment enables the signal to acquire more gain from the pump as both propagate in the fibre. If the length of the fibre is long as is usually the case with distributed RFA, the signal power can become very high. Simulation results have shown that high pump power does not guarantee effective pulling in the case of long lengths of fibre. In order to address the challenges underlying polarization attraction in the presence of Raman amplification, it is important to evaluate the pump and the signal power variations in relation to fibre PMD and length. While fibre parameters such as length can be fixed, other parameters such as PMD are subject to fabrication technology which may not deliver as low fibre PMD as may be required for pulling. On the other hand, the amount of experimental demonstrations which can be used to verify theoretical results is often limited by the availability of fibre and a pump which can deliver the appropriate optical power. For this reason it is important to resort to numerical simulations which can accurately predict the pulling behaviour in a RFA. In this section the power variations of RFA with pulling has been investigated.

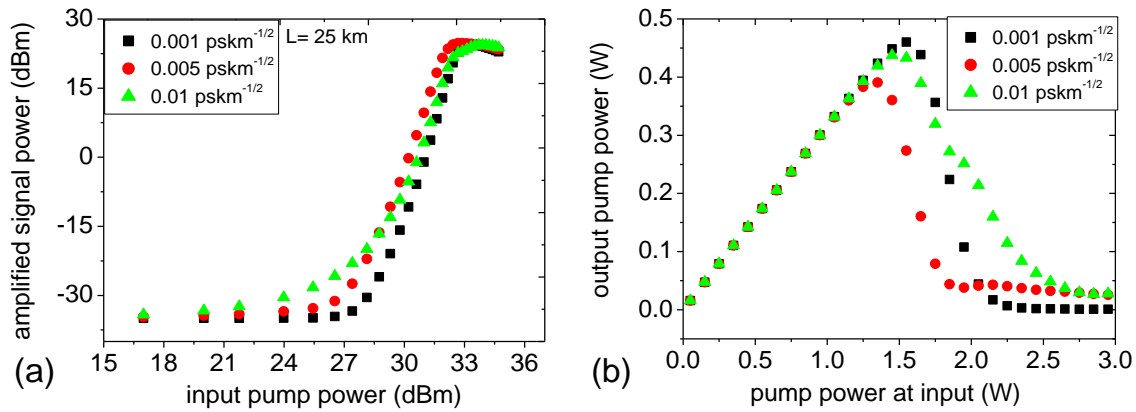


Figure 7.7: Power variations in (a) the signal, (b) the output pump as a function of input pump power.

Simulation results in figure 7.7 were obtained for three PMD coefficients using a fibre of length 25 km, when the pump and the signal were orthogonally polarized at the input. The signal wavelength was set at 1550 nm while that of the pump was set at 1450 nm. As can be seen in figure 7.7a the amplified signal power remains moderately low when the pump power is < 1 W. This is because the pump power is enough to compensate for signal attenuation during propagation in the fibre thus maintaining the signal power at the same level. Low amplified signal power is quite acceptable because other nonlinear effects are greatly reduced (Islam, 2002). Low signal power also guarantees that the amplifier operates in the linear region. However, the power of the signal cannot be too low because of the noise which is generated in the process of amplification (Bromage, 2004). When the power of the pump is > 1 W it is seen that the signal power increases sharply to values that are above 0 dBm. This is because the pump is strong enough to overcome signal losses and also boost the power level of the signal. High signal power excites Kerr nonlinear effects and also results in pump depletion. Figure 7.7b shows what happens to the pump in the course of amplifying the signal. It is clear that there is a linear relationship between the input and output pump power as long as the signal is not strong enough to cause pump depletion. The pump completely transfers its power to the signal as soon as pump depletion sets in. When the amplified signal power becomes very large or equivalent to the pump power at the output, both waves begin to modify the SOPs of each other through XPM (Bononi and Vannucci, 2003). At the same time, Raman PDG decreases so that the polarization pulling effect is completely lost. It is noted that the PMD coefficient of the fibre influences the depletion of the pump. In this case the PMD coefficient of 0.005 pskm^{-1/2} seems to cause early pump depletion. We can ascertain why this is so if we consider the fact that, the fibre birefringence rotates the SOPs of optical waves during transmission. Since the two waves were orthogonally launched, the associated

birefringence corresponding to the $0.001 \text{ pskm}^{-1/2}$ is too weak compared to the birefringence corresponding to $0.005 \text{ pskm}^{-1/2}$, such that it will take longer transmission distance for the later to turn the signal SOPs so that it start gaining from the pump. As a result, the lower PMD would require a longer fibre to achieve the same amplification. On the other hand, the birefringence associated with a fibre having PMD coefficient of $0.01 \text{ pskm}^{-1/2}$ is strong enough to cause considerable signal SOP rotations which in turn result in average signal gain. In summary, polarization attraction during Raman amplification is enabled by the small fibre PMD present in modern fibres. The extent to which a signal is attracted to the pump depends on the pump power. When a small signal co-propagates in the fibre with a high energy pump of appropriate wavelength, the signal becomes amplified through SRS. The SRS phenomenon is polarization dependent such that the gain is maximum when the pump and the signal are co-polarized and minimum when both are orthogonally polarized. The high energy pump also excites the power dependent refractive index in the silica fibre which results in a nonlinear birefringence. This power dependent birefringence begins to manifest as soon as the linear birefringence becomes very low. Polarization attraction in a RFA is based on Raman PDG and also the interaction of the linear and nonlinear birefringence. Pulling effect can be enhanced if the interaction of the two birefringence results in less birefringent fibre. High PDG which improves the pulling effect can be achieved by increasing the pump power and the length of the fibre. However, the pulling effect can be lost in an event where the power of the signal become very high, eventually leading to amplifier saturation. Thus effective polarization pulling would require stringent optimization of the fibre length, PMD and pump power. Polarization pulling at lower frequency shifts can be advantageous because lower pulling angles can be obtained but at the expense of more pump power.

Chapter Eight

Discussions and concluding remarks

Polarization effects in optical fibre and optical components have been a subject of great interest and concern to the fibre community. In this thesis, the effects of PMD and PDL in distributed RFA designed using modern optical fibres ($D_p \leq 0.1 \text{ pskm}^{-1/2}$) were investigated. The phenomenon of polarization pulling in the RFA which is quite significant has also been addressed. Unlike the fibre attenuation and dispersion mechanisms which are inherent to the glass material and are manageable to a great extent, polarization effects can be quite elusive. In particular, PMD effects have been recurring as optical transmission moves to higher bit rates. In an effort toward further improvement of fibre capacity and performance of optical devices, these effects have continued to be a centre of focus in the fibre industry. Modern fabrication technology has greatly reduced the intrinsic birefringence of the fibre to very small values. However, there is still interest in PMD which now centres on the small residue birefringence still present in optical fibres. In addition, transmission at high power has become inevitable due to the same reason as increasing fibre capacity. As a result there has emerged a power dependent birefringence which is now known to interact with the small linear birefringence leading to complex polarization behaviour in fibre. On the other hand, optical components form a large part of all optical systems and passive optical networks. These components have inherent PDL which is non negligible and which is known to interact with PMD, resulting in more severe effects than when only one of them is involved.

In chapter 4, simulations and experimental results on the characterization of the RFA with respect to PMD revealed remarkable differences in the gain when low and high PMD fibres were used as medium for Raman amplification. In the low PMD regime ($\sim 0.01 \text{ pskm}^{-1/2}$), Raman PDG and on-off gain increase exponentially as pump power increases and has a strong dependence on the pumping scheme employed. Backward pumping reduces PDG drastically and results in a similar on-off gain to forward pumping. Theoretical analyses show that the two pumping schemes have the same gain. However, the experimental results show a higher gain in the forward pumping which is attributed to different pump losses at the splices and connectors for both directions and also the dependence of the Raman gain coefficient on pump polarization. In applications where gain fluctuations can be a drawback, it would be

highly beneficial to apply moderate pump power and backward pumping which would minimize the PDG in a RFA.

High fibre PMD ($\sim 0.1 \text{ pskm}^{-1/2}$) reduces the Raman PDG substantially but at the expense of on-off gain and net gain. This is also a disadvantage in long haul applications because PMD accumulates as a function of square root of fibre length. In addition, the small Raman gain coefficient in SMFs requires a very long length of amplification fibre in order to compensate for signal losses. Thus even for a fibre of PMD coefficient of $0.1 \text{ pskm}^{-1/2}$, the length would contribute significantly to undesirable DGD of the signal.

The gain saturation is also dependent on the PMD coefficient of the fibre. Since low PMD results in high average gain, the RFA tends to saturate at a lower signal power than when a high PMD fibre is used. That is for a given pump power, the high gain fibre will start to deplete the pump at lower signal power, resulting in RFA saturation. On the other hand, when the input signal power is very low there is considerable interference with amplifier noise. Thus in an event where several channels are to be amplified simultaneously, their total power can take a range of values with the maximum determined by the power at saturation and the minimum defined by the power level of the amplifier noise.

The OSNR of a Raman amplified system is gain dependent and therefore influenced by the fibre PMD. As a result, OSNR increases with pump-signal wavelength shift with forward pumping having the highest OSNR. The performance of a Raman amplified system which is best evaluated using the BER improves with increasing OSNR at the receiver input. Spontaneous noise which is generated throughout the amplified transmission fibre degrades the OSNR at the fibre output end. At the same time the system BER is partly degraded when the dominant source of noise is due to signal-ASE beating. Forward pumping has superior ASE noise performance compared with backward pumping. The quality of a signal at the receiver is consequently determined by the Raman amplification process and PMD effects. A low OSNR manifests itself as high BER and decreases the eye opening. A fibre with high PMD would perform better in the case of backward pumping. However, in a high bit rate system ($>40 \text{ Gb/s}$), high PMD would cause inter-symbol interference thereby reducing the quality of the signal. It is important to point out here that system performance depends on data modulation formats and may show varying performances for other advance formats.

In chapter 5 it was shown that the statistics of Raman gain in single mode fibres depend on both the pumping scheme and PMD coefficient of the fibre. The length of the fibre plays an

important role and for short fibre where pump power remains high and signal losses are less, the gain is normally distributed for both high and low PMD fibres. For very low PMD coefficients, polarization mixing is poor even in long fibres and therefore when analysing the gain distributions, both the pump and signal should be scrambled at the input to provide full Poincaré sphere coverage. Backward pumping shows the lowest average gain and gain fluctuation for low and high PMD fibres, while forward pumping shows the highest PDG and gain fluctuation for fibres of PMD coefficient $< 0.03 \text{ pskm}^{-1/2}$. The three pumping configurations exhibit almost similar statistics when high PMD fibres are involved. Despite the requirement of two pumps bidirectional pumping configuration seems to be a good candidate for Raman amplification in fibres of PMD $> 0.03 \text{ pskm}^{-1/2}$. It was observed on a dB scale that there exists a linear relationship between PDG and signal on-off gain which is in agreement with the analytical model. Because of this linear dependence it is possible to extract the fibre PMD coefficient simply by measuring these two gain quantities in the forward pumping. The PMD values obtained by this method compare well with the standard JME measurements. Further analysis showed that for fibres of PMD coefficient between $0.01\text{-}0.1 \text{ pskm}^{-1/2}$, reliable results can be obtained by maintaining high SNR and low system PDL during the measurements. For values of PMD coefficient $< 0.01 \text{ pskm}^{-1/2}$, Raman techniques may excite nonlinear birefringence if the pump power is very high. Such high power should be avoided since linear and nonlinear birefringence interacts in a complex manner changing the overall fibre PMD.

In chapter 6 we showed that Raman PDG and PDL interact causing more severe effects than when only one of them is involved. However, this interaction depends on the PMD of the fibre and is less at low PMD. High PMD greatly reduce PDG such that when component PDL is large the effects of PDL dominate in the system. Similarly, when PMD is low PDG effects tend to dominate in the interaction with PDL. Optical components PDL not only reduce the gain of the signal but also interact with PMD resulting in gain tilting of the Raman spectrum.

A polarized RFA has unique characteristics which translate into its potential for new applications. Chapter 7 demonstrated the potential of RFAs in polarization control when the fibre PMD is very low. Raman PDG which is an inherent phenomenon of SRS in fibre is a cause of polarization pulling in RFA. In modern fibre the linear birefringence can be very small due to improved fabrication technology. When such fibre is used in the RFA configuration the pump SOP pulls the signal SOP to an extent that depends on the power of the pump. The PMD coefficient of the fibre and the fibre length are the two parameters that

play a vital role in enabling Raman polarization pulling. When the fibre PMD is $> 0.01 \text{ ps km}^{-1/2}$, pulling is not easily observed and would require very high power to be realized. On the other hand, the length of a fibre influences the pulling effect in that both the attenuation and PDG increase with length. When the fibre is very long, attenuation indirectly limits polarization pulling by reducing the power of the pump. For a short length of fibre, PDG is very small unless a special type of fibre is used. In a short SSMF fibre it would require very high pump power to achieve pulling. Again, polarization pulling is limited by gain saturation which occurs in RFA as a result of pump depletion. Thus low signal power is a requirement for effective pulling and can be achieved through optimization of the fibre length. Finally, we can conclude that polarization effects in RFA, though detrimental in optical communication, bear significant potential for future applications.

Appendix I

PDG-PDL interaction in the presence of PMD

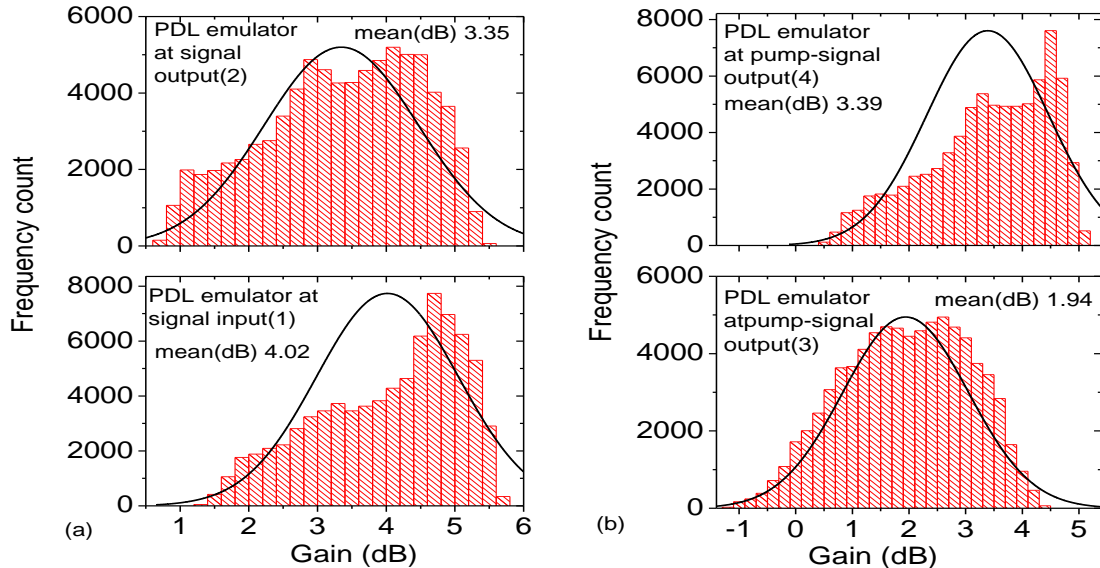


Fig AI.1 Raman on-off gain distribution in the presence of PDL. Fibre PMD (D_p) = 0.113 pskm^{-1/2}

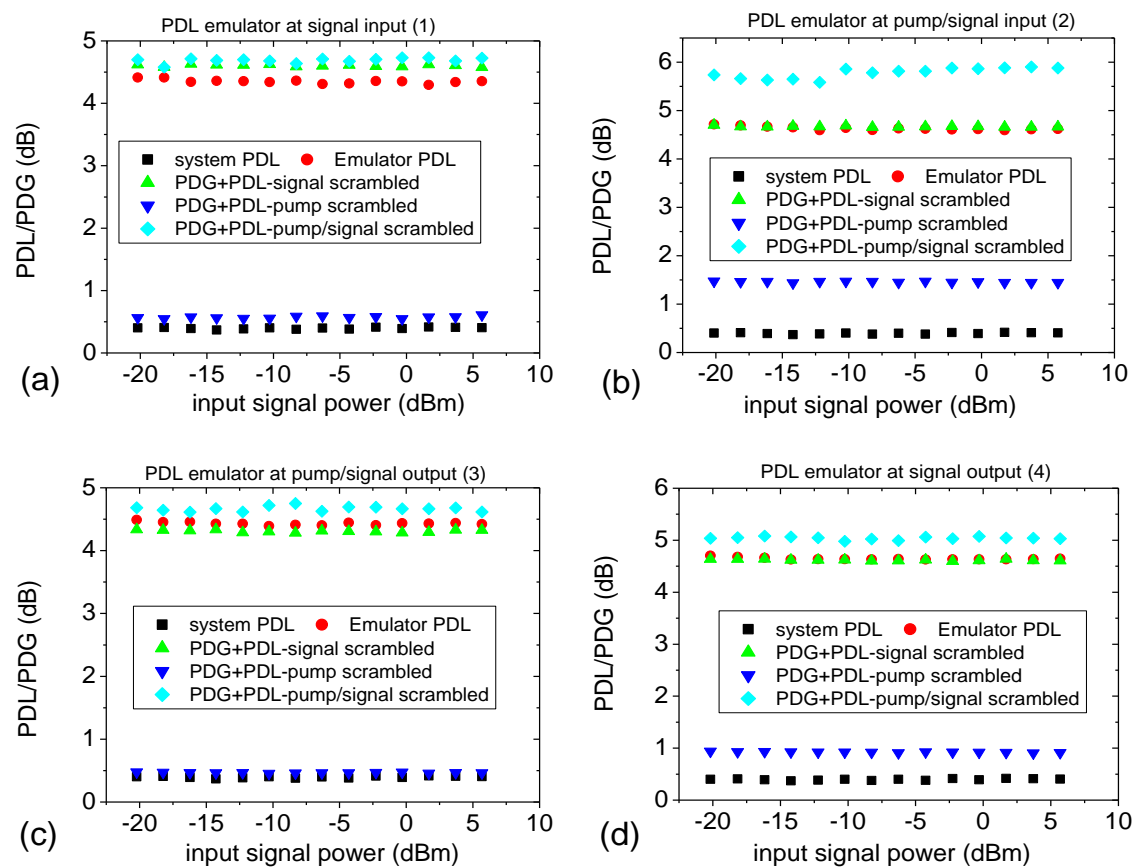


Figure AI.2: Raman PDG variation with input signal power in the presence of PDL

Appendix II

Pump and signal SOPs variation with pump power

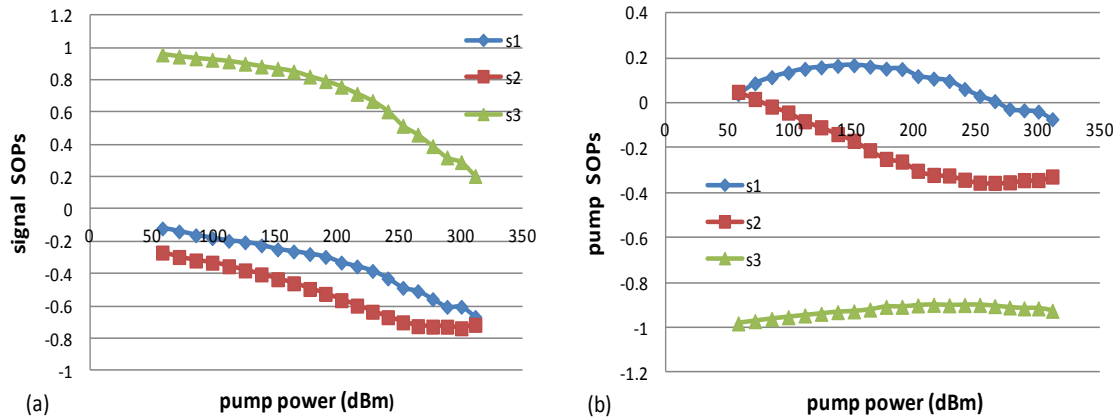


Figure AII.1: Experimental results showing the output signal and pump SOP as a function of input pump power. The length of fibre is 24.06 km and PMD (D_p) $0.011 \text{ ps km}^{-1/2}$. while the initial output SOP in (a) is RC and (b) LC

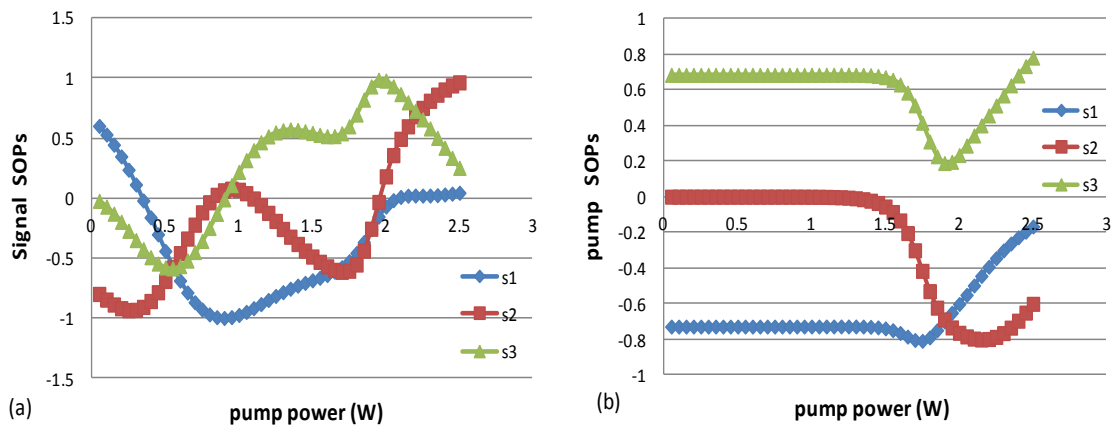


Figure AII.2: Simulations results showing the output SOPs of signal and pump as a function of pump power. The length of fibre is 25 km and PMD D_p $0.01 \text{ ps km}^{-1/2}$. In this case the SOPs were initialized at the input (a) RC and (b) LC

Appendix III

Equipment and components used in experimental work

Equipment/component	Specification
WDM laser source THORLABS Pro8000	Wavelength 1550 nm Optical power (max) 13 dBm
Tunable laser source	Agilent 8164A
Optical spectrum analyser (OSA)	Agilent 86142B
Laser Module (Raman pumps) 34-GVT074 and 34-GXW864	Power (max) 360 mW Peak wavelength (nm) 1449.1 and 1449.2
Power meter -EXFO IQS -1722X	Wavelength range (nm) 800 to 1660 Power range (dBm) 21 to -53
Polarization controller -Adaptif A3200	Insertion loss: <3 dB PDL: <0.3 dB DGD: <0.1ps Wavelength range 1520-1580 nm
Polarization scrambler -EXFO IQS 5100B	Wavelength 1260 nm to 1650 nm Activation dependent loss (dB) 0.006 (typ.) 0.01 (max.) Extinction ratio (dB) > 40 Insertion loss (dB) < 0.1 Scrambling (s) 1 to 99.9 s Poincaré sphere coverage 1 scrambling period: 98 % 2 scrambling periods: 99 % Max Optical power 1W
Polarimeter -Adaptif A1000	Wavelength 1460 nm to 1620 nm Optical Power(max) 7.5 dBm
Tunable filter	FWHM: 0.33 nm Tunable range 1520-1570 nm Insertion loss 4.12 dB PDL 0.07 dB
WDM coupler- ThorLabs 202C	Wavelength range(nm) 1480/1550 Bandwidth (nm): ± 5 nm PDL: <0.3 Insertion loss (dB) (0.12 /0.08 Directivity (dB) 50 dB Optical power (max) 500 mW
Filter based WDM coupler WDM-F-1415-1-FA oeMarket.com	Wavelength (nm) 1450-1490/1520-1580 Insertion loss 0.26 Isolation (dB) at 1550 nm > 15 Directivity (dB) > 50 PDL (dB) < 0.1 Optical power (max) 500 mW

Appendix IV

Polarization of light representation

Selected SOPs

Polarization state	Azimuth ψ	Ellipticity χ	Stokes vector $S_1 S_2 S_3$	Jones vector
LHP	0	0	$\begin{bmatrix} 1 \\ 0 \\ 0 \end{bmatrix}$	$\begin{bmatrix} 1 \\ 0 \end{bmatrix}$
LVP	$\pi/2$	0	$\begin{bmatrix} -1 \\ 0 \\ 0 \end{bmatrix}$	$\begin{bmatrix} 0 \\ 1 \end{bmatrix}$
L+45P	$\pi/4$	0	$\begin{bmatrix} 0 \\ 1 \\ 0 \end{bmatrix}$	$\frac{1}{\sqrt{2}} \begin{bmatrix} 0 \\ 1 \end{bmatrix}$
L-45P	$-\pi/4$ or $3\pi/4$	0	$\begin{bmatrix} 0 \\ -1 \\ 0 \end{bmatrix}$	$\frac{1}{\sqrt{2}} \begin{bmatrix} 0 \\ -1 \end{bmatrix}$
RCP	0	$\pi/4$	$\begin{bmatrix} 0 \\ 0 \\ 1 \end{bmatrix}$	$\frac{1}{\sqrt{2}} \begin{bmatrix} 1 \\ i \end{bmatrix}$
LCP	0	$-\pi/4$	$\begin{bmatrix} 0 \\ 0 \\ -1 \end{bmatrix}$	$\frac{1}{\sqrt{2}} \begin{bmatrix} 1 \\ -i \end{bmatrix}$
Elliptical			$\begin{bmatrix} \cos 2\psi \cos 2\chi \\ \cos 2\chi \sin 2\psi \\ \sin 2\chi \end{bmatrix}$	$\frac{1}{\sqrt{2}} \begin{bmatrix} \cos \psi e^{-i\delta/2} \\ \sin \psi e^{i\delta/2} \end{bmatrix}$

Where δ is the phase difference between the two components Comprehensive lists of Jones and Stokes vectors and the relationship between them is available in several text books.

Azimuth

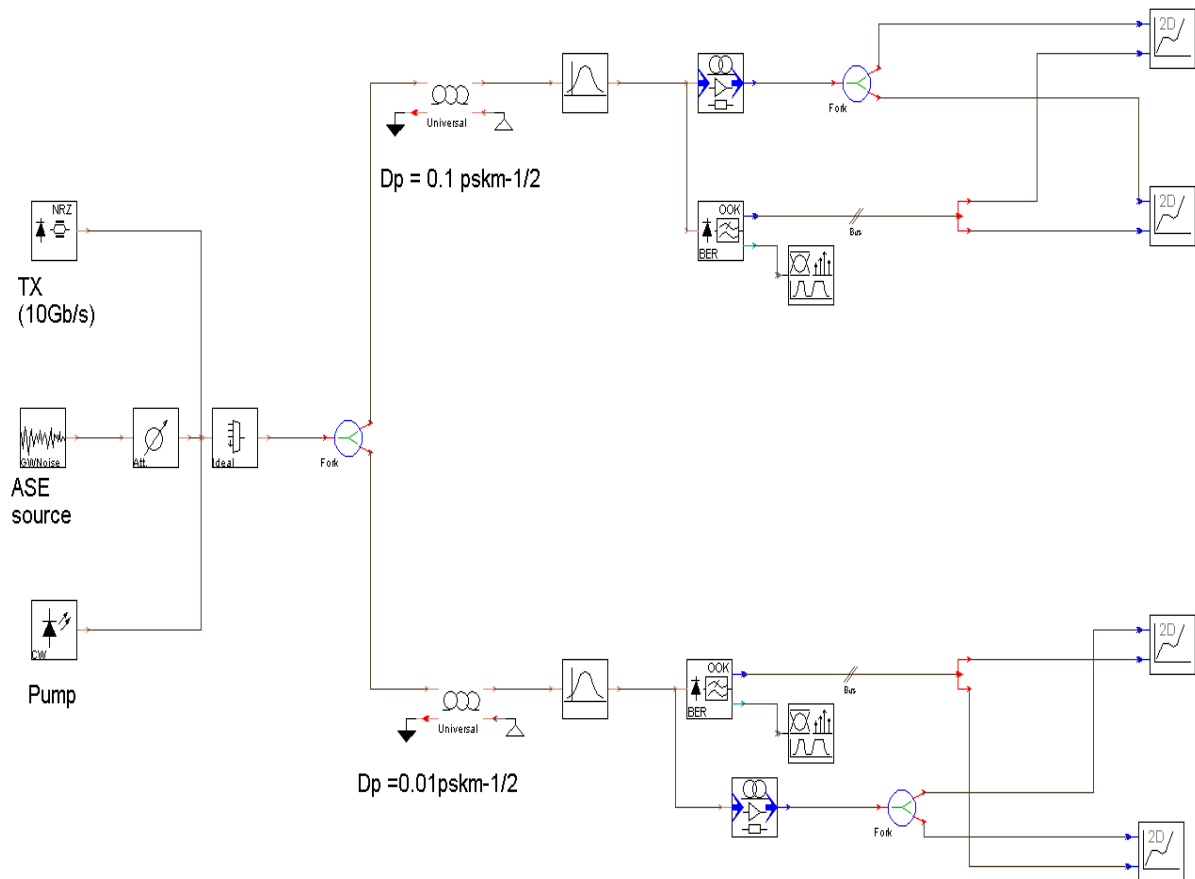
$$\psi = \frac{1}{2} \tan^{-1} \left(\frac{S_2}{S_1} \right)$$

Ellipticity

$$\chi = \frac{1}{2} \tan^{-1} \sqrt{\frac{S_3^2}{S_1^2 + S_2^2}}$$

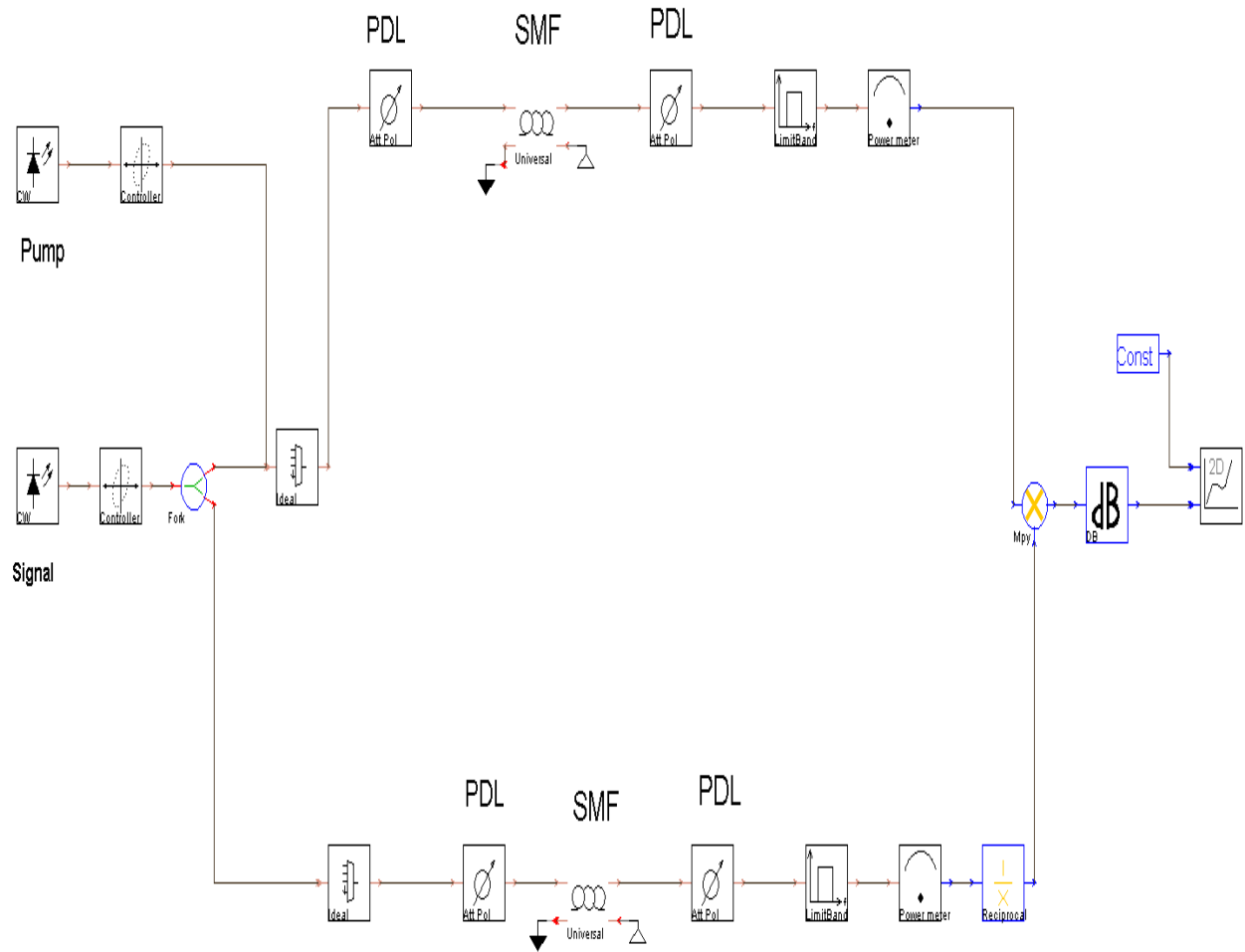
Appendix V

An enlarged version of the simulated schematic of a distributed Raman amplified fibre link used in the determination of the effects of ASE on the performance of the system.



Appendix VI

An enlarged version of simulation schematic used in the measurements of the effects of PDL in a distributed RFA.



Appendix VII

Research outputs of the author

2011:

Muguro K.M., Gibbon T.B., Leitch A.W.R., “*Polarization pulling during Raman distributed amplification in single mode fibres of low PMD*”, Poster presentation at the 4th African Laser centre (ALC) student Symposium, Zevenwacht wine estate, Stellenbosch, South Africa, Nov 9-13th 2011

Muguro K.M., Gibbon T.B., Waswa D.W., Leitch A.W.R. “*Impact of PMD on distributed Raman amplifiers using modern transmission fibres,*” Proc. Southern African Telecommunication Networks and Application conference (SATNAC), International conference centre (ICC) East London, South Africa Sept 4th -7th 2011

Rotich E.K., Waswa D., Muguro K., Leitch A.W.R., “*Dual pump fibre optical parametric amplifier based on four-wave mixing in a highly nonlinear fibre,*” AFRICON, 2011, vol., no., pp.1-3, 13-15 Sept. 2011

2010:

Muguro K.M. Leitch A.W.R. “*Characterisation of Raman Amplifier gain in optical single mode fibres with respect to polarisation mode dispersion*” Oral presentation at the 3rd African Laser Centre (ALC) Student Symposium, Zevenwacht wine estate, Stellenbosch, South Africa 23- 26 September 2010

Muguro K.M. Changundega J.M., Leitch A.W.R. “*Influence of input state of polarisation of a signal on Raman amplification gain in single mode fibres*” Poster presentation at the 55th South African Institute of Physics (SAIP) Conference, CSIR Pretoria, 27th Sept.-1st Oct. 2010

Muguro K.M., Waswa D., Changundega J.M., Leitch A.W.R. “*Comparison of gain statistics of different pumping configurations in distributed fibre Raman amplification*” Proc. Southern African Telecommunication Networks and Application conference SATNAC Spier Estate, Stellenbosch, South Africa 5th -8th September 2010

Changundega J.M., Muguro K.M., Leitch A.W.R. “*Investigating depolarization of the probe in a two channel WDM system,*” Poster presentation at Southern African Telecommunication Networks and Application conference (SATNAC) Spier Estate, Stellenbosch, South Africa 5th -8th September 2010

Changundega J.M., Muguro K.M., Leitch A.W.R. “*Dependence of the DOP of a probe signal on various system parameters in a WDM system*”, Poster presentation at the 55th South African Institute of Physics (SAIP) Conference, CSIR Pretoria, 27th Sept.-1st Oct. 2010

2009:

Muguro K.M., Wu L. and Leitch A.W.R “*Investigation of Signal Power Variation in low PMD Single Mode Fibres during Raman Application*” Poster presentation at the 54th South African Institute of Physics (SAIP) Conference, University of KwaZulu-Natal, 8 – 10 July 2009.

Muguro K.M., Wu L. and Leitch A.W.R “*Comparative investigation of NRZ and RZ data formats with respect to PMD in a Raman amplified system*” Poster presentation at the 2nd African Laser Centre (ALC) Student Symposium, Kariega Game Reserve, 2 – 5 May 2009.

References

- Agrawal G. P.**, Nonlinear Fiber Optics, 4th ed. San Diego, CA:Academic, 2007 chapter six.
- Agrawal G. P.**, “Applications of nonlinear fibre optics” vol 10 Academic press Elsevier, 2008.
- Angelis C. De**, Galtarossa A., Gianello G., Matera F. and Schiano M., “Time evolution of polarization mode dispersion in long terrestrial links”, *J. Lightwave Technology*, vol.10, pp. 552-555 (1992).
- Azami N.**, “Characterization of polarization-dependent gain in Raman fiber amplifier,” *Optics Communications*, vol. 230, pp. 181-184 (2004).
- Amari A. El.**, Gisin N., Zbinden B. H. and Zimmer C W., “Statistical Prediction and Experimental Verification of Concatenations of Fiber Optic Components with Polarization Dependent”, *J. Lightwave Technol.*, vol. 16, no. 3 (1998).
- Ashcroft N. W.** and Mermin N. D., “Solid State Physics”, Philadelphia, PA: Saunders College (1976).
- Aso O.**, “Measurement of a parameter limiting the analysis of the first-order polarization-mode dispersion effect”, *Optics Letters*, vol. 23, pp. 1102-1104 (1998).
- Betti S.**, Curti F., Daino B., De Marchis G., Lannone E. and Matera F., “Evolution of the bandwidth of the principal states of polarization in single-mode fibers”, *Opt. Letters.*, vol. 16, pp. 467-469 (1991).
- Boyd R. W.**, “Nonlinear Optics,” *Academic Press*, San Diego, CA, (1992).
- Bononi A.** and Vannucci A., “Degree of polarization degradation due to cross-phase modulation and its impact on polarization-Mode Dispersion compensators”, *J. Lightwave Technol.*, vol. 21, pp.1903-1913 (2003).
- Bromage J.**, “Raman amplification for fiber communications systems” *J. Lightwave Technol.*, vol. 22, pp. 79-93 (2004).
- Bromage J.**, Winzer P. J. and Essiambre R.J., “Multiple Path Interference and its impact on system design”, in “Raman amplifiers for Telecommunications”, M.N. Islam, Ed, *Springer*, New York (2003), Chap. 15.
- Bruyère F.** and Audouin O., “Penalties in long-haul optical amplifier systems due to polarization dependent loss and gain”, *IEEE Photon.Technol. Lett.*, vol. 6, pp. 654-656 (1994).
- Bruyère F.**, “Impact of First and Second-Order PMD in Optical Digital Transmission Systems” *Optical Fiber Technol.*, vol. 2, no. 3, pp. 269-280 (1996).

Burgmeijer J. W., de Vries W. J., Artiglia M., Di Vita P., Novak R. P., Sundberg E., Nykjoor K. L., Allen J., Pelayo J., de Zaragoza U. and Gisin N., “COST 217 interlaboratory comparison of optical measurements on single-mode fibre couplers”, Symposium on optical fiber measurements, *Technical digest*, pp 7-10 (1990).

Buck J. A., “Fundamentals of optical fiber” (Wiley, New York, 1995) chap 3.

Böhm K., Petermann K. and Weidel E., “Performance of Lyot depolarizers with birefringent single-mode fibers,” *J. Lightwave Technol.*, vol. LT-1, pp. 71–74 (1983).

Cameron J., Liang Chen; Xiaoyi B. and Stears J., “Time evolution of polarization mode dispersion in optical fibers”, *IEEE Photonics Technology Lett.*, vol.10, pp. 1265-1267 (1998).

Cordina K. J. and Fludger C. R. S., “Changes in Raman gain coefficient with pump wavelength in modern transmission fibers,” in *Proc. Optical Amplifiers and their Applications* (2002).

Collings B. C. and Boivin L., “Nonlinear polarization evolution induced by cross-phase modulation and its impact on transmission systems,” *IEEE Photonics Technology Letters*, vol. 12, pp. 1582–1584 (2000).

Chowdhury D., “PMD induced system impairments in long-haul optical communication system”, in *Proceedings of IEEE Lasers and Electro-Optics Society (LEOS)*. (IEEE, 1999), pp. 147-148.

Ciprut P., Gisin B., Gisin N., Passy R., Von der Weid J. P., Prieto F. and Zimmer C. W., “Second-order polarization mode dispersion: impact on analog and digital transmissions” *J. Lightwave Technology*, vol. 16, p. 757 (1998).

Collet E. “Polarized light in fibre optics”, SPIE Press (2003).

Damask J. N., “Polarization Optics in Telecommunications”, *Springer* (2005).

Derrickson D., “Fiber optic test and measurement”, Prentice Hall PTR (1998).

De Mesquita T. M. G., dos Santos A. B., von der Weid J. P., “Polarization dependent gain fluctuations due to PMD in Raman amplified optical transmissions”, *Microwave and Optoelectronics Conference, 2003, IMOC 2003. Proc. of SBMO/IEEE MTT-S International*, vol.2, pp. 559- 561; vol.2, pp. 20-23 (2003).

Desurvire E., Simpson J. R. and Becker P. C., “High-gain erbium-doped traveling-wave fiber amplifier”, *Opt. Lett.*, vol. 12. pp. 888-890 (1987).

Desurvire E., “Erbium Doped fiber Amplifiers, Principles and applications”, John Wiley & Sons, Inc. (1994).

Desurvire E., “Erbium-Doped Fiber Amplifiers, Principles and Applications”, Hoboken, New Jersey: Wiley-Interscience (2002).

Ding P., Wang J., Zhuang Q., Sun J. and Hou R., “Analysis on the definition of polarization-dependent loss”, *Opt. Eng.* Vol. 46(11), p. 115009 (2007).

Dong H., Shum P., Yan M., Zhou J. Q., Ning G. X., Gong Y. D. and Wu C. Q., “Generalized Mueller matrix method for polarization mode dispersion measurement in a system with polarization-dependent loss or gain”, *Optics Express*, vol. 14, pp. 5067-5072 (2006).

Dougherty D. J., Kartner F. X., Haus H. A and Ippen E. P., “Measurement of the Raman gain spectrum of optical fibers”, *Opt. Lett.*, vol. 20, pp. 31–33 (1995).

Ebrahimi P., Hauer M. C., Yu Q., Khosravani R., Gurkan D., Kim D. W., Lee D. W. and Willner A. E., “Statistics of polarization dependent gain in Raman fiber amplifiers due to PMD”, in *Proc. CLEO Tech. Dig.*, pp. 143 – 144 (2001).

Eldada L., “Advances in telecom and datacom optical components”, *Opt. Eng.*, vol. 40, pp. 1165 (2001).

Evans A., Gray S. and Muktoyuk M., “The unique measurement challenges of Raman amplifiers” (**invited**), *12th Symposium on Fibre Optic Measurement*, TechDigest (2002).

Ehrhardt A., Fritzsche D., Paul M., Schuerer L., Breuer D., Weiershausen W., Cyr N., Chen H. and Schinn G. W., “Characterisation of the PMD distribution along optical fibres by a POTDR”, *Transparent Optical Networks, 2008. ICTON 2008. 10th Anniversary International Conference*, vol.1, pp.173-177 (22-26 June 2008).

Emori Y., Akasaka Y. and Namiki S., “Broadband lossless DCF using Raman amplification pumped by multichannel WDM laser diodes”, *Electron. Lett.* vol. 34, pp. 2145–2146 (1998).

Emori Y. and Namiki S., “100nm bandwidth flat gain Raman amplifiers pumped and gain-equalized by 12-wavelength-channel WDM high power laser diodes”, in *Wavelength Division Multiplexing Components*, D. Nolan, ed., Vol. 29 of *OSA Trends in Optics and Photonics* 1999, paper 177.

Emori Y., Matsushita S. and Namiki S., “Cost-effective depolarized diode pump unit designed for C-band flat-gain Raman amplifiers to control EDFA gain profile”, presented at the *OFC Conf.*, pp. 106–108, Paper FF4. (2000).

Essiambre R-J., Winzer P. J. and Grosz D. F., “Impact of DCF properties on system design”, in “Fiber based dispersion compensation: optical and fiber communication reports 5”, S. Ramachandran, *Springer*, pp. 425-491 (2007).

Eyal A. and Tur M., “A modified Poincaré sphere technique for the determination of polarization-mode dispersion in the presence of differential gain/loss”, in *Tech. Dig., Optical Fiber Communications Conference (OFC’98)*, San Jose, CA, paper ThR1, p. 340 (Feb. 1998).

Fludger C., Maroney A., Jolley N. and Mears R., “An analysis of the improvements in OSNR from distributed Raman amplifiers using modern transmission fibres”, in *Optical*

Fiber Communication Conference, OSA Technical Digest Series (Optical Society of America, 2000), paper FF2.

Frigo N., “A generalized geometric representation of coupled mode theory”, *IEEE Journal of Quantum Electronics*, vol. QE-22, pp. 2131–2140 (1986).

Galtarossa A. and Palmieri L., “The exact statistics of polarization-dependent loss in fiber-optic links”, *IEEE Photonics Technology Letters*, vol. 15, pp. 57–59 (2003).

Galtarossa A., Jung Y., Kim M. J., Lee B. H., Oh K., Paek U., Palmieri L., Pizzinat A. and Schenato L., “Effects of spin inaccuracy on PMD reduction in spun fibers”, *J. Lightwave Technol.*, vol. 23, pp. 4184-4191 (2005).

Galtarossa A., Palmieri L., Santagiustina M. and Ursini L., “Polarized backward Raman amplification in randomly birefringent fibers”, *J. Lightwave Technol.*, vol. 24, pp. 4055 - 4062 (2006).

Gisin N., “Statistics of polarization dependent losses”, *Optics Communications*, vol. 114, pp. 399-405 (1995)

Gisin N. and Huttner B., “Combined effects of polarization mode dispersion and polarization dependent losses in optical fibers”, *Optics Communications*, vol. 142, pp. 119–125 (1997).

Goldstein D. H. and Collett E., “Polarized Light”, 2nd Ed CRS Press, New York (2003).

Gordon J. P. and Kogelnik H., “PMD fundamentals: polarization-mode dispersion in optical fibers”, *Proc. Nat. Acad. Sci.*, vol. 97, pp. 4541-4550, (2000).

Hansen S. L., Andreasen S. B., Thorsen P. and Dybdal K., “Experimental verification of new EDFA gain –tilt distortion theory”, *IEEE Photon. Technol. Lett.*, vol. 5, pp. 1433-1435 (1993).

Haunstein H. and Kallert H. M., “Influence of PMD on the performance of optical transmission systems in the presence of PDL”, in *Optical Fiber Communication Conference*, 2001 OSA Technical Digest Series (Optical Society of America, 2001), paper WT4.

Headley C. and Agrawal G. P., “Raman Amplification in Fiber Optical Communication Systems”, Elsevier Academic Press (2005).

Hecht J., “Understanding fiber optics”, 3rd Ed. Prentice Hall Inc (1999).

Hansen P. B., Eskildsen L., Grubb S. G., Stentz A. J., Strasser T. A., Judkins J., DeMarco J. J., Pedrazzani R. and DiGiovanni D. J., “Capacity upgrades of transmission systems by Raman amplification”, *IEEE Photonics Technology Letters*, vol. 9, pp. 262–264 (1997).

Heebner E., Bennink R. S., Boyd R. W. and Fisher R. A., “Conversion of unpolarized light to polarized light with greater than 50% efficiency by photorefractive two-beam coupling”, *Opt. Lett.*, vol. 25, pp. 257-259 (2000).

Hellwarth R. W., Cherlow J. and Yang T., “Origin and frequency dependence of nonlinear optical susceptibilities of glasses”, *Phys. Rev. B*, vol. 11, pp. 964–967 (1975).

Hellwarth R. W., “Third-order optical susceptibilities of liquid and solids”, *Prog. Quantum Electron.*, vol. 5, pp. 1–68 (1977).

Hernday P., “Dispersion measurements”, in *Fiber Optic Test and Measurements*, D. Derickson, ed. (Prentice-Hall, Inc, Upper Saddle River, New Jersey, 1998), pp. 475-518.

Heras C., Subias J., Pelayo J. and Villuendas F., “Analysis of the Raman gain distribution as a technique to determine longitudinal PMD distribution in optical fibers”, *Opt. Comm.*, vol. 265, pp. 336-341 (2006).

Heismann F., Fishman D. A. and Wilson D. L., “Automatic compensation of first-order polarization mode dispersion in a 10 Gb/s transmission system”, in *Proc. ECOC*, Madrid, Spain, 1998, vol. 1, pp. 529–530.

Hill P. M., Olshansky R. and Burns W. K., “Optical polarization division multiplexing at 4 Gb/s”, *IEEE Photon. Technol. Lett.*, vol. 4, pp. 500–502 (1992).

Huttner B. and Gisin N., “Anomalous pulse spreading in birefringent optical fibers with polarization-dependent loss”, *Optics Letters*, vol. 22, pp. 504–507 (1997).

Huttner B., Barros C. D., Gisin B. and Gisin N., “Polarization-induced pulse spreading in birefringent optical fibers with zero differential group delay”, *Optics Letters*, vol. 24, pp. 370–372 (1999).

Huttner B., Geiser C. and Gisin N., “Polarization-induced distortions in optical fiber networks with polarization-mode dispersion and polarization-dependent losses,” *IEEE Journal of Selected Topics in Quantum Electronics*, vol. 6, pp. 317–329 (2000).

Hui R., and O'Sullivan M. S., “Fibre optic measurement techniques”, Elsevier academic press, chapter 5 (2009).

Iannone E., Matera F., Mecozzi A. and Settembre M., “Nonlinear Optical Communication Networks”, (Wiley, New York, 1998).

Ikeda M., “Stimulated Raman amplification characteristics in long span single-mode silica fibers”, *Optics Communications*, vol. 39, pp 148-152 (1981).

Ip E., Lau A. P. T., Barros D.J.F. and Kahn J.M., “Coherent detection in optical fiber systems”, *Opt. Express*, vol. 16, pp. 753-791 (2008).

Islam M. N., “Raman amplifiers for telecommunications”, *IEEE J. Selected Topics Quantum Electron.*, vol. 8, pp. 548–559 (2002).

Islam M. N. “Raman Amplifiers in Telecommunications 2: Sub-Systems and Systems”, Springer-Verlag, New York (2004).

Jopson R. M., Nelson L. E. and Kogelnik H., “Measurement of second-order polarization-mode dispersion vectors in optical fibers”, *IEEE Photon. Technol. Lett.*, vol. 11, pp. 1153–1155 (1999).

Jordanova L. T. and Topchiev V. I., “Improvement of the Optical Channel Noise Characteristics Using Distributed Raman Amplifiers”, *ICEST Conference*, pp. 20-23 (2008).

Kang Y., “Calculations and Measurements of Raman Gain Coefficients of Different Fiber Types”, M.Sc. Thesis, Virginia Polytechnique Institute and State University, Blacksburg, Virginia, December, 2002.

Karlsson M., Brentel J. and Andrekson P. A., “Long-Term Measurement of PMD and Polarization Drift in Installed Fibers”, *J. Lightwave Technol.*, vol. 18, p. 941 (2000).

Kee H. H., Fludger C. R. S. and Handerek V., “Statistical properties of polarization dependent gain in fibre Raman amplifiers”, in *Proc. OFC Tech. Dig.*, pp. 180 – 181 (2002).

Keiser G., “Optical fiber communications”, McGraw-Hill (2000).

Kimsas A., Staubo P., Bjornstad S., Slagsvold B. and Sudbo A., “A dispersion compensating Raman amplifier with reduced double Rayleigh backscattering, employing standard DCF”, *Proc. Transparent Optical Networks, 6th International Conference* , vol.2, pp. 326- 329 (4-8 July 2004).

Kim C.H., Son E. S., Cho H-S., Han Y-G, Lee J. H and Lee S. B, “Experimental study on the effect of codirectional Raman gain on system’s performance”, *Opt. Express*, vol. 15, pp. 6146-6151 (2007).

Kjær R., Monroy I. T., Oxenlowe L. K. and Jeppesen P., “Impairments due to burst-mode transmission in a Raman-based long reach PON link”, *IEEE Photon. Technol. Lett.*, vol. 19, pp. 1490–1492 (2007).

Kogelnik H., Jopson R. M. and Nelson L. E., “Polarization-mode dispersion” in *Optical Fibre Telecommunications IVB, Systems and Impairments I*. Kaminow and Tingye Li, eds. (Academic press, San Diego, Calif., 2002), pp. 725-861.

Krummrich P. M., “Advanced modulation formats for more robust optical transmission systems”, in *J. Electron. Comm.*, (AEÜ) 61, pp 141-146 (2007).

Lewis S. A. E., Koch F., Chernikov S.V. and Taylor J.R., “Low-noise high gain dispersion compensating broadband Raman amplifier”, in *Proc. Optical Fiber Communications Conf.*, (2000).

Li L., Wei C. and Yang R., “Effect of cabling process and installation on Polarization Mode Dispersion”, *International Wire and Cable Symposium*, pp. 371-375 (2000).

Li Y., Lu F., Guo W. and Wei D., “High efficiency and low noise figure double-pass fibre Raman amplifier”, *J. Opt. A: Pure Appl. Opt.*, vol. 8, pp 1019–1022 (2006).

Lin Q. and Agrawal G. P., “Polarization mode dispersion-induced fluctuations during Raman amplifications in optical fibers”, *Opt. Lett.*, vol. 27, pp. 2194-2196 (2002).

Lin Q. and Agrawal G. P., “Statistics of polarization-dependent gain in fiber-based Raman amplifiers”, *Opt. Lett.*, vol. 28, pp. 227-229 (2003).

Lin Q. and Agrawal G. P., “Vector theory of stimulated Raman scattering and its application to fiber-based Raman amplifiers”, *J. Opt. Soc. Amer.*, vol. B20, pp. 1616– 1631 (2003).

Lichtman E., “Performance degradation due to polarization dependent gain and loss in lightwave systems with optical amplifiers”, *Electron. Lett.*, vol. 29, pp. 1971-1972 (1993).

Lichtman E., “Limitations imposed by polarization-dependent gain and loss on all-optical ultralong communication systems”, *J. Lightwave Technol.*, vol. 13, pp. 906–913 (May 1995).

Lu P., Chen L. and Bao X., “Statistical Distribution of Polarization-Dependent Loss in the Presence of Polarization- Mode Dispersion in Single-Mode Fibers”, *IEEE Photon. Technol. Lett.*, vol. 13, pp. 451-453 (2001).

Mahgerefteh D., Hao-Yun Yu, Butler D. L., Goldhar J., Ding Wang, Golovchenko E., Pilipetskii A. N, Menyuk C. R. and Joneckis L. J., “Effect of randomly varying birefringence on the Raman gain in optical fibers”, *Lasers and Electro-Optics, 1997. CLEO '97. Summaries of Papers Presented at the Conference*, vol. 11, p. 447, (18-23 May 1997).

Maker P. D., Terhune R. W. and Savage C. M., “Intensity-Dependent Changes in the Refractive Index of Liquids”, *Phys. Rev. Lett.*, vol. 12, pp. 507-509 (1964).

Martinelli M., Martelli P. and Pietralunga S. M., “Polarization stabilization in optical communications systems”, *J. Lightwave Technol.*, vol. 24, pp. 4172-4183 (2006).

Martinelli M., Cirigliano M., Ferrario M., Marazzi L. and Martelli P., “Evidence of Raman-induced polarization pulling”, *Optics Express*, vol. 17, pp. 947-955 (2009).

Masuda H., “Hybrid EDFA/Raman amplifiers”, in “Raman amplifiers for telecommunications 2: subsystems and systems”, by Islam M.N, *Springer series in optical sciences*, 2004, chap 13.

Matera F. and Settembre M., “Comparison of the performance of optically amplified transmission systems”, *J. Lightwave Technol.*, vol. 14, p.1 (1996).

McCurdy A. H., Sengupta A. and Glodis P., “Compact measurement of low-PMD optical telecommunication fibers”, *Opt. Express*, vol. 12, pp. 1109-1118 (2004).

Mecozi A. and Shtaif M., “The Statistics of Polarization-Dependent Loss in Optical Communication Systems”, *IEEE Photonics Technology Letters*, vol. 14, pp. 313-315 (2002).

Mecozi A. and Shtaif M., “Signal-to-Noise-Ratio Degradation Caused by Polarization-Dependent Loss and the Effect of Dynamic Gain Equalization,” *J. Lightwave Technol.*, vol. 22, p. 1856 (2004).

Menyuk C. R., “Application of multiple-length-scale methods to the study of optical fiber transmission”, *J. Eng. Math.*, vol. 36, pp. 113–136 (1999).

Monroy I. T., Kjær R., Öhman F., Yvind K. and Jeppesen P., “Distributed fiber Raman amplification in long reach PON bidirectional access links”, *Optical Fiber Technol.*, vol. 14, pp. 41- 44 (2008).

Mollenauer L. F., Gordon J. P. and Islam M. N., “Soliton propagation in long fibers with periodically compensated loss”, *IEEE J. Quantum Electron.*, vol. QE-22, pp. 157–173 (1986).

Namiki S. and Emori Y., “Ultrabroad-band Raman amplifiers pumped and gain-equalized by wavelength-division-multiplexed high-power laser diodes”, *IEEE J. Selected Topics in Quantum Electronics*, vol. 7, pp. 3-16 (2001).

Namiki S., Emori Y. and Oguri A., “Discrete Raman amplifier”, in “Raman amplification in fiber optics communication systems”, C. Headley and G. P. Agrawal, chapter 4, Elsevier academic press (2005).

Newbury N., “Full wavelength dependence of Raman gain in optical fibers: measurements using a single pump laser”, in *Proc. Optical Fiber Communications Conference*, (2003).

Noé R., Hinz S., Sandel D. and Wüst F., “Crosstalk detection schemes for polarization division multiplex transmission”, *J. Lightwave Technol.*, vol. 19, pp. 1469–1475 (2001).

O’Neill E. L. “Introduction to statistical optics”, Dover Publications (2004).

Olsson N. A., “Lightwave systems with optical amplifiers”, *J. Lightwave Technology*, vol. 7, pp. 1071–1082 (1989).

Papoulis A. “Probability, Random variables and stochastic processes, 3rd ed. WCB/Mcgraw-Hill, New york, 1991.

Pauer M. and Winzer P. J., “Impact of extinction ratio on return to zero coding gain in optical noise limited receivers,” *IEEE Photon Technology Letters*, vol. 15, pp 879-881 (2003).

Pitois S., Sauter A. and Millot G., “Simultaneous achievement of polarization attraction and Raman amplification in isotropic optical fibers”, *Opt. Lett.*, vol. 29, pp. 599-601 (2004).

Pitois S., Fatome J. and Millot G., “Polarization attraction using counter-propagating waves in optical fiber at telecommunication wavelengths”, *Opt. Express*, vol. 16, pp. 6646-6651 (2008).

Poole C. D. and Wagner R. E., “Phenomenological approach to polarization mode dispersion in long single-mode fibers”, *Electronics Letters*, vol. 22, pp. 1029–1030 (1986).

Poole C. D., “Statistical treatment of polarization dispersion in single-mode fiber,” *Opt. Lett.*, vol. 13, pp. 687-689 (1988).

Poole C. D., Tkach R. W., Chraplyvy A. R. and Fishman D. A., “Fading in lightwave systems due to polarization-mode dispersion,” *Photonics Technol. Letts.*, vol. 3, pp. 68-70 (1991).

Poole C. D., in *Optical Fiber Telecommunications III A*, I. P. Kaminov and T. L. Koch, eds. (Academic, San Diego, Calif., 1997), Chap. 6.

Popov S., Sergeyev S. and Friberg A. T., “The impact of pump polarization on the polarization dependence of Raman gain due to the breaking of a fibre’s circular symmetry”, *J. Opt A: Pure and Appl. Opt.*, vol. 6, pp. S72-S76 (2004).

Popov S., Vanin E. and Jacobsen G., “Influence of polarization mode dispersion value in dispersion-compensating fibers on the polarization dependence of Raman gain”, *Opt. Lett.*, vol. 27, pp. 848-850 (2002).

Raman C. V., “A new radiation”, *Indian J. Phys.*, vol. 2, p. 387 (1928).

Rashleigh S. C., “Wavelength dependence of birefringence in highly birefringent fibers”, *Opt. Lett.*, vol. 7, pp. 294-296 (1982).

Rashleigh S. C., “Origins and control of polarization effects in single-mode fibers,” *J. Lightwave Technol.*, vol. 1, pp. 312–331 (1983).

Rottwitt K., and Kidorf H. D., “A 92 nm Bandwidth Raman Amplifier,” *Optical fiber conference proceedings (OFC '98)*, pap. pd 6 (1998).

Rottwitt K. and Stentz A. J., “Raman amplification in lightwave communications systems”, in *Optical Fiber Telecommunications, IVA*, I. P. Kaminov and T. Li, Eds. San Diego, CA: Academic, pp. 213–257 (2002).

SATNAC Chronicle 2011, “Social communications- Challenging the limits of technology innovation”, in *Proc. of the 14th annual Southern African Telecommunication Networks and Applications Conference (SATNAC)*, East London, Eastern Cape, South Africa (2011).

Sergeyev S., Popov S. and Friberg A. T., “Fiber Raman Amplifiers with Suppressed Polarization Impairments”, *OSA/CLEO/IQEC* (2009).

Sergeyev S., Popov S. and Friberg A. T., “Characterization of Randomly Varying Birefringence in Long Single Mode Fibers”, in *Optical Fiber Communication Conference and Exposition and The National Fiber Optic Engineers Conference*, OSA Technical Digest (CD), paper OWG2 (2008).

Sergeyev S. V., Popov S. and Friberg A. T., “Modeling polarization-dependent gain in fiber Raman amplifiers with randomly varying birefringence”, *Optics Communications*, vol. 262, pp. 114-119 (2006).

Snitzer E. and Osterberg H., “Observed Dielectric Waveguide Modes in the Visible Spectrum”, *J. Opt. Soc. Am.*, vol. 51, pp. 499-505 (1961).

Sunnerud H., Xie C., Karlsson M., Samuelson R. and Andrekson P. A., “A comparison between different PMD compensation techniques”, *J. Lightwave Technol.*, vol. 20, pp. 368–378 (2002).

Son E. S., Lee J. H. and Chung Y. C., “Exact analysis for statistics of gain variation in counter-pumped Raman amplifier”, in *Optical Fiber Communication Conference*, Technical Digest (CD) (OSA, 2004), paper WJ3.

Son E. S., Lee J. H. and Chung Y. C., “Statistics of polarization-dependent gain in fiber Raman amplifiers”, *J. Lightwave Technol.*, vol. 23, pp. 1219–1226 (2005).

Spirit D. M., Ellis A. D. and Barnsley P. E., “Optical time division multiplexing: systems and networks”, *Communications Magazine, IEEE*, vol. 32, no.12, pp. 56–62 (Dec 1994).

Steinkamp A., Vorbeck S. and Voges E. I., “Polarization mode dispersion and polarization dependent loss in optical fiber systems”, *Optical Transmission Systems and Equipment for WDM Networking III, Proceedings of the SPIE*, pp. 243–254 (2004).

Srivastava A. K. and Sun Y. *Optical Fiber Telecommunications IVA*, Chapter 4. Advances in Erbium-Doped Fiber Amplifiers, pp. 174–212, *Academic Press* (2002).

Sun Y., Lima I., Lima A., Jiao H., Zweck J., Yan L., Menyuk C. and Carter G., “Effects of partially polarized noise in a receiver”, in *Proc. Optical Fiber Communications Conf.*, (2003).

Steele R. C., Walker G. R. and Walker N. G., “Sensitivity of optically preamplified receivers with optical filtering”, *IEEE Photon. Technol. Lett.*, vol. 3, pp. 545–547 (1991).

Stolen R. H., Ippen E. P. and Tynes A. R., “Raman Oscillation in Glass Optical Waveguide”, *Applied Physics Letters*, vol. 20, pp. 62–64 (1972).

Stolen R. H. and Ippen E. P., “Raman gain in glass optical waveguides”, *Applied Physics Letters*, vol. 22, no. 6, (1973).

Stolen R. H., “Polarization effects in fiber Raman and Brillouin lasers”, *IEEE J. Quantum Electron.*, vol. QE-15, pp. 1157–1159 (1979).

Stolen R. H., Gordon J. P., Tomlinson W. J. and Haus H. A., “Raman response function of silica-core fibers”, *J. Opt. Soc. Amer. B*, vol. 6, pp. 1159–1166 (1989).

Stolen R. H. “Issues in Raman gain measurements”, in tech. Digest. Symp. optical fiber measurements, *NIST special publication 953* (National Institute of Standards and Technology), Gaithersburg, MD, pp. 139–142, (2000).

Singh S. P., Gangwar R. and Singh N., “Nonlinear scattering effects in optical fibers”, *Progress in Electromagnetics Research, PIER 74*, pp. 379–405 (2007).

Thévenaz L., Zadok A., Eyal A. and Tur M., “All-optical polarization control through Brillouin amplification”, in *Optical Fiber Communication Conference*, 2008 OSA Technical Digest CD (2008), paper OML7.

Tokura T., Kogure T., Sugihara T., Shimizu K., Mizuochi T. and Motoshima K., “Pump light depolarization method for low PDG Raman amplification”, presented at the OFC Conf., pp. 645–646, Paper ThGG24 (2002).

Tokura T., Kogure T., Sugihara T., Shimizu K., Mizuochi T. and Motoshima K., “Efficient pump depolarizer Analysis for distributed Raman amplifier with low polarization Dependence of Gain”, *J. Lightwave Technol.*, vol.24, pp.3889-3896 (2006).

Toge K., Hogari K. and Horiguchi T., “Measurement of Raman gain distribution in optical fibers”, *IEEE Photon. Technol. Lett.*, vol. 14, pp. 974–976 (2002).

Tricker R., “Optoelectronics and fiber optic technology”, Newnes, (Elsevier Ltd), 1st ed., (2002).

Ursini L., Santagiustina M. and Palmieri L., “Raman Nonlinear Polarization Pulling in the Pump Depleted Regime in Randomly Birefringent Fibers”, *IEEE Photonics Technology Letters*, vol. 23, pp. 254-256 (2011).

Visser J., Leblanc M., Salmi R., Conibear A. B. and Leitch A. W. R., “Locating bad PMD sections with a polarization-OTDR”, *Proceedings of the 2003 SATNAC conference*, Fancourt, Southern Cape, vol. 2, pp. 195-200 (2003).

van Antwerpen U., Conibear A. B. and Leitch A. W. R., “The effect of cabling on the PMD of an optical fibre”, in *Proc. of South African Telecommunication Networks and Application Conference (SATNAC)*, Fancourt, Southern Cape, Vol. 2, pp. 191-194 (2003).

van Deventer M. O. and Boot A. J., “Polarization properties of stimulated Brillouin scattering in singlemode fibers”, *J. Lightwave Technology*, vol. 12, pp. 585-590 (1994).

Virtual Photonics, Inc. (VPI), version 8.6, software Available: <http://www.virtualphotonics.com>.

Wai P. K. A. and Menyuk C.R., “Polarization mode dispersion, decorrelation, and diffusion in optical fibers with randomly varying birefringence”, *J. Lightwave Technol.*, vol. 14, pp. 148-157 (1996).

Walker N. G. and G. R. Walker, “Polarization control for coherent communications”, *J. Lightwave Technology*, vol. 8, pp. 438–458 (1990).

Wang J. S., Costelloe J. R. and Stolen R. H., “Reduction of the degree of polarization of a laser diode with a fiber Lyot depolarizer”, *IEEE Photonics Technology Lett.*, vol. 11, pp. 1449–1451 (1999).

Williams P., “PMD measurement techniques and how to avoid the pitfalls”, *J. Opt. Fiber Commun.*, vol. 1, pp. 84-105 (2004).

Winzer P. J. and Essiambre R-J., “Advance optical modulation formats”, in *Optical Fiber communications 5*, Vol. 1, I.P Kaminow, T. Li and A.E.Willner, Elsevier Academic Press (2008), Chap. 2.

Woodbury E.J. and Ng W. K., “First demonstration of stimulated Raman scattering”, *Proc. IRE* 50, 2347 (1962).

Xie C., Mollenauer L. and Moller L., “Pulse Distortion Induced by Combined Effects of PMD and PDL in Optical Transmission Systems”, *Bell Labs, Lucent Technologies, Holmdel, NJ*.

Yamamoto S., Edagawa N., Taga H., Yoshida Y. and Wakabayashi H., “Observation of BER degradation due to fading in long-distance optical amplifier system”, *Electron. Lett.*, vol. 29, pp. 209–210 (1993).

Yaman F., Lin Q., Radic S. and Agrawal G. P., “Fiber-optic parametric amplifiers in the presence of polarization-mode dispersion and polarization-dependent loss”, *J. Lightwave Technol.*, vol. 24, pp. 3088-3096 (2006).

Yan L. S., Yu Q., Xie Y. and Willner A. E., “Experimental demonstration of the system performance degradation due to the combined effect of polarization-dependent loss with polarization-mode dispersion”, *IEEE Photonics Technology Letters*, vol. 14, pp. 224-226 (2002).

Yan L. S., Yu Q., Luo T., McGeehan J. E. and Willner A. E., “Deleterious system effects due to low-frequency polarization scrambling in the presence of non-negligible polarization-dependent loss”, *IEEE Photonics Technology Letters*, vol.15, pp. 464-466 (2003).

Yu M., Kan C., Lewis M. and Sizmann A., “Statistics of signal-to-noise ratio and path-accumulated power due to concatenation of polarization-dependent loss”, *IEEE Photonics Technology Letters*, vol.14, pp. 1418- 1420 (2002).

Zhou X. and Magill P., “Polarization dependent gain due to signal-signal Raman interaction: can fiber PMD be too low?” in *OFC 2004*, Paper WE6.

Zheng X., Feng F., Y. Ye, Zhang H. and Li Y., “Analysis in distributed Raman amplification”, *J. Optics Commun.* Vol. 207 pp. 321–326 (2002).

Zyskind J., Barry R., Pendock G., M. Cahill and Ranka J., “High-capacity, ultra long haul networks”, in *Optical Fiber Telecommunications, IVB*, I. P. Kaminov and T. Li, Eds. San Diego, CA: Academic, 2002, chapter 5.